MODELING OF IMPACT DYNAMICS OF A TENNIS BALL WITH A FLAT SURFACE

A Thesis

by

SYED MUHAMMAD MOHSIN JAFRI

Submitted to the Office of Graduate Studies of
Texas A&M University
in partial fulfillment of the requirements for the degree of

MASTER OF SCIENCE

May 2004

Major Subject: Mechanical Engineering

MODELING OF IMPACT DYNAMICS OF A TENNIS BALL WITH A FLAT SURFACE

A Thesis

by

SYED MUHAMMAD MOHSIN JAFRI

Submitted to the Office of Graduate Studies of
Texas A&M University
in partial fulfillment of the requirements for the degree of

MASTER OF SCIENCE

Approved as to style and content by:

John M. Vance (Chair of Committee)	Alan B.Palazzolo (Member)
Guy Battle (Member)	Dennis L.O'Neal (Head of Department)

May 2004

Major Subject: Mechanical Engineering

ABSTRACT

Modeling of Impact Dynamics of a Tennis Ball with a Flat Surface. (May 2004)
Syed Muhammad Mohsin Jafri, B.E., NED University, Pakistan
Chair of Advisory Committee: Dr. John M. Vance

A two-mass model with a spring and a damper in the vertical direction, accounting for vertical translational motion and a torsional spring and a damper connecting the rotational motion of two masses is used to simulate the dynamics of a tennis ball as it comes into contact with a flat surface. The model is supposed to behave as a rigid body in the horizontal direction. The model is used to predict contact of the ball with the ground and applies from start of contact to end of contact. The springs and dampers for both the vertical and the rotational direction are linear. Differential equations of motion for the two-mass system are formulated in a plane. Two scenarios of contact are considered: Slip and no-slip. In the slip case, Coulomb's law relates the tangential contact force acting on the outer mass with the normal contact force, whereas in the no-slip case, a kinematic constraint relates the horizontal coordinate of the center of mass of the system with the rotational coordinate of the outer mass. Incorporating these constraints in the differential equations of motion and applying initial conditions, the equations are solved for kinematics and kinetics of these two different scenarios by application of the methods for the solutions of second-order linear differential equations. Experimental data for incidence and rebound kinematics of the tennis ball with incidence zero spin, topspin and backspin is available. The incidence angles in the data range from 17 degrees up to 70 degrees. Simulations using the developed equations are performed and for some specific ratios of inner and outer mass and mass moments of inertia, along with the spring-damper coefficients, theoretical predictions for the

kinematics of rebound agree well with the experimental data. In many cases of incidence, the simulations predict transition from sliding to rolling during the contact, which is in accordance with the results obtained from available experimental measurements conducted on tennis balls. Thus the two-mass model provides a satisfactory approximation of the tennis ball dynamics during contact.

DEDICATION

To my

Family and Teachers

ACKNOWLEDGMENTS

I would like to express my earnest gratitude to Dr. John M.Vance, my advisor, who provided me with an opportunity to work on this interesting thesis topic. His broad knowledge and patience, with great insight and wisdom inspired me to work for the comprehensive formulation of this topic within the limitations of assumptions in the analysis. He has been an invaluable help to me and his great communication has been of enormous encouragement.

I will like to thank Dr. Alan Palazzolo and Dr. Guy Battle for serving on my thesis committee. I have benefited immensely from their teaching while attending classes under them. The concepts and analytical methods that I gathered from those classes have been extremely valuable and useful for the completion of my thesis.

Finally, I will like to thank all of my friends at the Turbomachinery lab and at home for their encouragement and help in many aspects. I am thankful to all of you.

NOMENCLATURE

X Axis	-	Horizontal coordinate direction
Y Axis	-	Vertical coordinate direction
V_1	-	Incident velocity of mass center of tennis ball [L/T]
V_2	-	Rebound velocity of mass center of tennis ball [L/T]
θ_i	-	Incident angle [-]
θ_r	-	Rebound angle [-]
ω_1	-	Incident spin [1/T]
ω_2	-	Rebound spin [1/T]
V_{y1}	-	Vertical component of incident velocity [L/T]
V_{x1}	-	Horizontal component of incident velocity [L/T]
V_{y2}	-	Vertical component of rebound velocity [L/T]
V_{x2}	-	Vertical component of rebound velocity [L/T]
t	-	Time [T]
t_c	-	Time of contact [T]
n	-	Dimensionless contact time [-]
$y(t)$	-	Vertical motion coordinate of mass M_1 [L]
$\dot{y}(t)$	-	Vertical velocity of mass M_1 [L/T]
$\ddot{y}(t)$	-	Vertical acceleration of mass M_1 [L/T^2]
$x(t)$	-	Horizontal motion coordinate of system [L]

$\dot{x}(t)$	-	Horizontal velocity of system [L/T]
$\ddot{x}(t)$	-	Horizontal acceleration of system [L/T^2]
R	-	Outer radius of tennis ball [L]
M	-	Mass of tennis ball [FT^2/L]
M_1	-	Mass of inner core [FT^2/L]
M_2	-	Mass of outer shell [FT^2/L]
K_y	-	Stiffness of the spring in vertical direction [F/L]
C_y	-	Damping coefficient of the vertical damper [FT/L]
ζ_y	-	Damping ratio of vibration in vertical direction [-]
ω_y	-	Natural frequency of vibration in vertical direction [1/T]
ω_{dy}	-	Damped natural frequency in vertical direction [1/T]
I	-	Mass moment of inertia of tennis ball [FLT^2]
I_1	-	Mass moment of inertia of inner core [FLT^2]
I_2	-	Mass moment of inertia of outer shell [FLT^2]
K_θ	-	Torsional stiffness [FL]
C_θ	-	Torsional damping coefficient [FLT]
ζ_θ	-	Torsional damping ratio [-]
ω_θ	-	Torsional natural frequency [1/T]
$\omega_{d\theta}$	-	Damped torsional natural frequency [1/T]
μ	-	Sliding coefficient of friction [-]
$\overline{\mu}$	-	Time-averaged coefficient of friction [-]

COR	-	Vertical coefficient of restitution [-]
$HCOR$	-	Horizontal coefficient of restitution [-]
$F_X(t)$	-	Tangential or frictional contact force [F]
$F_Y(t)$	-	Normal contact force [F]
$\theta_1(t)$	-	Rotational motion coordinate of inner core [-]
$\theta_2(t)$	-	Rotational motion coordinate of outer shell [-]
$\dot{\theta}_1(t)$	-	Rotational velocity of inner core [1/T]
$\dot{\theta}_2(t)$	-	Rotational velocity of outer shell [1/T]
$\ddot{\theta}_1(t)$	-	Angular acceleration of inner core [$1/T^2$]
$\ddot{\theta}_2(t)$	-	Angular acceleration of outer shell [$1/T^2$]
$\theta(t)$	-	Relative rotational coordinate [-]
$\dot{\theta}(t)$	-	Relative rotational velocity [1/T]
$\ddot{\theta}(t)$	-	Relative rotational acceleration [$1/T^2$]

TABLE OF CONTENTS

Page

CHAPTER Page

CHAPTER Page

LIST OF FIGURES

Page

Page

LIST OF TABLES

Page

CHAPTER I

INTRODUCTION

BACKGROUND OF IMPACT DYNAMICS

Historically, the topic of impact dynamics has been of both experimental and theoretical interest from the time of Newton to the present time. Impact dynamics has its importance in mechanical systems whenever two or more bodies, one of which is in motion with respect to the others, come into contact with each other for a short duration of time. This brief contact creates contact forces of significant magnitudes that can change dramatically the kinematics of the bodies involved in the contact. The impact can occur in mechanical systems, for instance, when a rotor supported on the magnetic bearings falls on its retainer bearings due to the failure of the magnetic bearings. In this situation, the rotor impacts the inside surface of the retainer bearings and hence upon its rebound from the bearing surface, its velocity and spin changes significantly from what it was when it came into contact with the bearing. Another important problem where impact dynamics plays an important part is the collision of a rotor with its stator, when the clearance between the rotor and the stator is very small and rotor contacts the stator due to the vibration induced by its imbalance. Contact forces of high magnitudes are usually developed when the rotating speeds are high, so that the contact forces have the destructive potential for both the rotor and the stator. Analysis of this and all such problems with the application of impact dynamics can help design the proper speeds and material selection for the moving parts, so as to devise some means of avoiding the contact and in case of contact, avoiding the failure of the parts involved. Also measurements made on the rotating machineries which show different vibration signatures can be compared with the theoretical predictions from an

---

This thesis follows the style and format of *ASME Journal of Applied Mechanics.*

impact dynamics model of such machineries and hence used to diagnose the root cause of the problem.

Impact can also be seen in a beneficial context, for the case of rotordynamic bumpers which are used to suppress vibration amplitudes in rotating machines operating near their critical speeds. In this case, the bumpers, which are mounted around the rotor, are impacted by the rotor near the critical speed and their frictional and damping properties allow the suppression of vibration amplitudes. The impact with the bumpers also provides damping to the system when properly designed. Improperly designed, bumpers can create violent dynamic instabilities, such as dry friction whip.

From a theoretical point of view, impact dynamics can be analyzed in two ways: Rigid-body collisions and deformable body collisions. The rigid-body collision approach is based on the classical Newtonian viewpoint of considering the impact as an instantaneous phenomena and describing the loss of kinetic energy of the colliding bodies in terms of a parameter called as coefficient of restitution. Newton's laws of motion are applied to the body before and after collision, and then the kinematics is solved for the rebound in terms of the incidence kinematics. There is no description of whatever happens during the collision, nor any description of the duration of contact, because these parameters are simply eliminated from the equations of motions while solving for the rebound kinematics in terms of a coefficient of restitution. From the flexible-body point of view, which is credited to Hertz for its development, the impact is not considered as an instantaneous phenomenon but rather a phenomenon involving a finite duration of time, no matter however small. The colliding bodies involved are considered to be deformable in a small region around the point of contact. During this contact time, the contact forces are developed and the bodies change their kinematic and kinetic properties gradually, usually in form of continuous mathematical functions. Newton's laws are applied during the contact based on the assumed form of contact force, which in turn is usually dependent on the geometric and elastic properties of the

bodies involved in the collision. The equations of motion are solved and the kinematics during the contact and at rebound is determined.

The application of this concept of finite contact duration and the assumption of the contact force can then be applied to a problem where the experimental measurements are available regarding the rebound kinematics given the incident kinematics such as incident translational velocities and angular spins, so that the developed impact model can be implemented and the results developed thereof can be compared against the measurements to ascertain the accuracy of the model. If such a problem can be modeled with a linear model of contact force, then it will definitely provide an efficient method of computation in terms of time and effort. One such problem of impact found in the literature is the incidence and rebound of tennis ball with flat surfaces of varying properties, the modeling and simulation of which is the objective of this thesis. The next section describes the relevant theoretical and experimental research appropriate to this objective.

LITERATURE REVIEW

Wang **[1]** conducted experiments on the impacts of tennis balls with acrylic surface, with varying incident conditions. In his experiments, he varied the angles of incidence from 17 degrees up to 70 degrees, and for all incident angles, the tennis ball was thrown on the surface with zero spin, topspin and backspin. The average incident translational speeds were around 17 m/s. From the measurements, he concludes that the tennis ball incident with backspin rebounds at a higher rebound angle than the ball with zero spin, which in turn rebounds at a higher rebound angle than the ball thrown with topspin. He also proposes a damped contact force model to predict the velocities at rebound, for only one case of incidence angle.

Smith **[2]** conducted experiments on the tennis balls in order to study the effect of the angle of incidence, the velocity of incidence and the spin of incidence on the angle of rebound. He projected the tennis balls on a Laykold court surface and the angles of projections were 15, 30, 45, 60 and 75 degrees. The tennis ball was incident with the zero spin, the topspin and the backspin. He concludes that in general, a ball thrown with the backspin will rebound at a high angle than with either the zero spin or the topspin. Further more, he concludes that the angle of rebound for the backspin and the zero spin will be greater than the corresponding angles of incidences for these incident spins. For the topspin, the angle of rebound, in general, will be either equal to or less than the angle of incidence. Considering the effects of incident velocity on the angle of rebound, he concludes that the rebound angles for the balls incident with the topspin will be higher for higher incident translational velocities. For backspin, the opposite is concluded. From zero spin results, the conclusion for the backspin holds that the higher the incident velocity, the higher is the rebound angle.

Cross **[3]** conducted measurements on the vertical bounce of various sports balls with no spin, including tennis balls, with the help of piezo disks. From his experiments on different balls, he obtained the time varying form of normal contact forces during impact, which generally showed asymmetry about the time axis. He estimated the time of contact for various balls and curve fitted the force wave-forms into mathematical functions to obtain the displacements and velocities as functions of time during contact. He concludes that the impact of tennis balls can be approximated as the one in which the vertical coefficient of restitution can be treated as independent of incident velocity and also that the contact force for tennis ball contact can be modeled as linear force model. Cross **[4]** conducted further measurements on the tennis ball with oblique incidences with various flat surfaces but zero incident spin in all cases. He employs Brody's **[5]** model of tennis ball impact and shows from his measurements that the model reasonably well predicts the rebound kinematics, including rebound spin. He concludes from the measurements of tangential to normal impulses during the contact that for higher angles

of incidences and rougher surfaces, the tennis ball during its contact with the surface does not continue to slide, but that there is a transition in the motion from sliding to rolling mode during the contact. Due to this occurrence of rolling mode in the motion during contact, the ball leaves at a higher rebound horizontal velocity and lower spin, then will be expected if it were sliding throughout the contact. He verifies this by modifying Brody's equations to account for this transition and shows that the theoretical results agree well with the observations. He defines another parameter analogous to the vertical coefficient of restitution, called the horizontal coefficient of restitution. Horizontal coefficient of restitution is defined as the ratio of rebound horizontal velocity of contact point to incident horizontal velocity of contact point. For the rolling mode, it will be expected that the horizontal coefficient of restitution will be equal to zero(because the contact point has no relative motion with respect to the ground in rolling mode), whereas his measurements reveal it does not when it should, as per Brody's model. This forms some deviation between Brody's model and his measurements. He concludes that the deviation can be explained if the tennis ball is considered as flexible in horizontal direction of motion as well.

Brody **[5]** presented a model for the bounce of a tennis ball from a flat surface, in which the incident vertical velocity component is not too high. He models the tennis ball as a hollow sphere, with certain thickness. He considers the separate scenarios of sliding and rolling throughout the motion. His model for both cases is based upon the application of Newton's impulse and momentum laws applied at incidence and rebound and incorporates the vertical coefficient of restitution and sliding coefficient of friction in the formulations. He concludes that for the sliding mode, the rebound horizontal velocity is dependent upon incident vertical velocity as well as coefficients of friction and restitution, whereas for the rolling mode, the horizontal rebound velocity is dependent only on the incident horizontal velocity. He develops a relation for transition between sliding to rolling and concludes that the transition will occur depending strictly upon the coefficient of sliding friction and the angle of incidence of the tennis ball.

Hubbard and Stronge **[6]** consider the analysis and experiments of the bounce of hollow balls on flat surfaces. They consider various dynamic properties of the table tennis balls such as the elastic deformation under the action of the interaction force, the contact force itself and the velocity of rebound. They consider in detail the geometry of the ball and conduct their analysis using a finite element method.

Hubbard **[7]** considers the impact phenomena of the ball with both the classic point of view considering both no duration of contact as well as finite duration of contact by using spring-damper models to model the impact of solids with each other. From these later simplified models, he develops the idea of the coefficient of restitution for the central as well as oblique impacts and explains the velocities of rebound. He also considers a number of contact models to model the normal contact force. His methods represent the nonlinear models of the contact; he accordingly solves most of the contact problems with the help of numerical techniques.

Stevenson, Bacon and Baines **[8]** describe the measurements of the normal contact forces using the piezo disks. They show the inelasticity of the vertical incident collisions for the cases of collisions of steel ball bearings and plumber's putty balls with pads made of different surfaces. They derived the relationship between the voltage output obtained from the measurements and the normal contact force. They vary the height of drop as well the types of surface to determine the normal contact force. Also they estimate the duration of contact for various vertical incident collisions. Their experiments indicate that the normal contact force can not be described as perfectly symmetrical about the time axis, rather it has some asymmetry. They concluded that the impulse imparted to the colliding ball with a surface is dependent on the type of surface as well as the height from which it is dropped.

Malcolm **[9]** describes the properties of piezoelectric films for measurements and shows an example of impact. Minnix and Carpenter **[10]** use the piezoelectric film to perform experiments on different balls and obtain the impact force as a function of time.

The International Tennis Federation (ITF) **[11]** provides the standards of some of the parameters for the tennis balls that need to be met for them to give the level of performance expected to be met out of them. In their standards, they mention the procedures for the testing of the balls as well as the forward and return deformations values for the testing of the balls. They mention the range of the deformation values for the balls. Also they mention the coefficient of restitution range values to be expected out of the tennis balls. They also mention the construction of tennis balls and how the internal pressure is maintained inside some of the designs, and what must be the values of the internal pressures under different conditions.

Lankarani and Nikravesh **[12]** employ the Hertz theory of contact to model the two-body and multi-body impact, neglecting the effect of friction. They elaborate the idea that the kinetic energy loss during an impact can be interpreted as the damping term in the contact force equation. Thus the contact force will consist not only of the elastic term, but also a damping term. The form of the normal contact force in their analysis is non-linear. They apply the Newton's impulse and momentum laws, and express the deformation of the colliding bodies, which they call indentation, and the indentation velocities in terms of the initial approach velocities, normal coefficient of restitution and the masses of the bodies. Thus they derive a contact force equation and thence investigate the kinematics occurring during and at the end of contact. They apply this theory to multi-body impact.

Stronge **[13]** performs a theoretical analysis of impact problem and calculates how friction does mechanical work to dissipate energy. Sonderbaarg **[14]** conducted

measurements on the rebound of solid spheres made of steel and pyrex glass from various surfaces of varying dimensions. He concludes that the vertical coefficient of restitution is dependent on both the incident surface and the bounce surface. The vertical coefficient is more or less a constant, varying initially with some geometric parameters of the system. The horizontal coefficient of restitution, in his paper defined as the ratio of rebound horizontal velocity of center of mass to incident horizontal velocity of center of mass, is not a constant value and varies significantly with the incident angles

Keller **[15]** considers the problem of impact of two bodies with friction. He derives the equations of motion for the bodies and considers the impact as a phenomenon involving a finite duration of contact. He shows in the analysis that if the slip velocity between two bodies changes direction, the friction force reverses in direction, so that the energy at rebound is lesser than at incidence.

Hudnut and Flansburg **[16]** have modeled the collision problem of gliders on air tracks as masses connected by linear springs. Gliders are specially shaped metal objects that are used for experiments on air tracks and they levitate on the air tracks when air is passed through the track. They have performed the experiments on the collisions of gliders with various initial separations and they show that the elastic modeling of the collisions of gliders provides a more comprehensive and realistic picture of the rebound phenomenon as compared to the classical approach, employing the impulse and momentum equations applied to the impact and rebound.

Bayman **[17]** derives the wave equation for the contact modeling of two bodies which collide elastically and which can be modeled as linear Hooke's springs. He considers the wave propagation through the bodies and estimates the duration of contact during collision. He also concludes that the elastic wave reflections from both bodies play an important role in determining the time of contact.

Johnson **[18]** applies the theory of elasticity at the contact point of the super ball to explain the unusual bounce phenomenon it shows when it is thrown with backspin. He shows that these phenomenon can not at all be explained by the rigid-body impact theory. He concludes that it is the tangential flexibility at the interface of super ball and the flat surface which imparts the super ball its unusual properties of bounce. Hunt and Crossley **[19]** consider a non-linear force model based on Hertz theory of contact to the case of solids impacting at low speeds. From energy considerations and the work done by the contact force, they conclude that the velocity -dependent coefficient of restitution can be regarded as damping in a second-order, non-linear differential equation describing the contact motion of two bodies.

RESEARCH OBJECTIVE

The objective is to develop a computationally efficient model and method of analysis to predict impact dynamics and kinematics of a tennis ball.

RESEARCH METHOD

The method investigated is to apply a piecemeal theory of linear vibrations and impact dynamics to the phenomena of the impact, contact and rebound of a tennis ball striking ground or any other flat surface. The main predictions of interest are going to be the rebound spin and translational velocities, the contact forces during contact, the translational and spin velocity variations with time during contact and the identification of an important dynamic parameter called coefficient of restitution that relates the velocities before and after impact, given the mass, stiffness (translational and torsional) of the ball, amount of damping, incoming spin and translational velocities and angles of impact.

CHAPTER II

MODELING AND ANALYSIS OF A TENNIS BALL IMPACT

IMPACT MODEL FOR A TENNIS BALL

Impact of a tennis ball with a surface is considered in detail with the dynamic parameters taken into account. Consider a tennis ball striking a surface, as shown in the following figure:

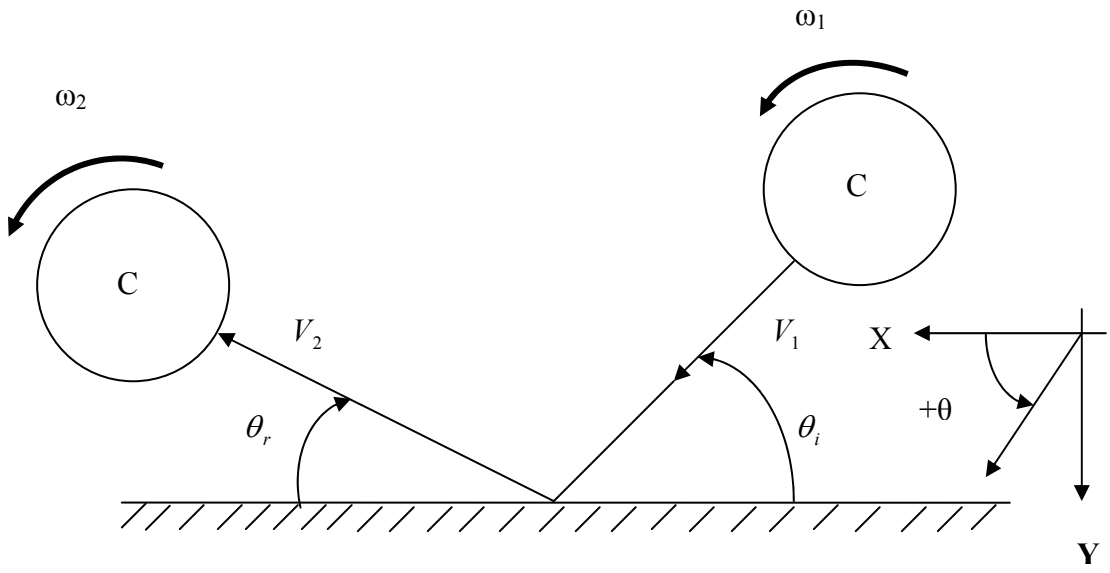

Fig. 1 Kinematic parameters of the tennis ball striking the non-smooth surface.

Kinematic parameters of the tennis ball incident on ground surface are shown in figure 1. The incident parameters are:

1. Translational speed of the center of mass, V_1
2. Angle of the velocity vector with respect to ground (incident angle of the ball),θ_1

3. Spin of the ball about its centroidal axis, ω_1

Similarly, rebound parameters of the ball are:

4. Translational speed of the center of mass, V_2
5. Angle of the velocity vector with respect to ground (rebound angle of the ball), θ_2
6. Spin of the ball about its centroidal axis perpendicular to plane of the page, ω_2

The kinematics on rebound is related to the kinematics at impact with the help of dynamics, or Newton-Euler equations of motion.

Physical modeling of the impact phenomena of the ball with the ground and the derivation of the equations of motion consists in modeling the ball as a linear spring-damper system as soon as it contacts the ground. This linear spring-damper system is for modeling the vertical translation motion as well as rotational motion of the ball. The motions before and after impact are determined by two physical possibilities during impact:

(a) No Slip or Rolling condition
(b) Sliding or slipping condition

For modeling of spin of the ball, the ball is modeled as a two-mass system connected by torsional spring and damper. This torsional spring-damper is also considered as a linear pair. From these modeling elements, equations of motion for the ball during the impact are derived and then the results are compared with the available experimental data. In this thesis, by incident conditions is meant the kinematics of the ball before it contacts the ground, whereas initial conditions will be the values of the kinematic parameters as soon as it comes into contact with ground.

MOTION IN Y-DIRECTION

Physical model for the impact of the ball with the ground is illustrated in figure 2:

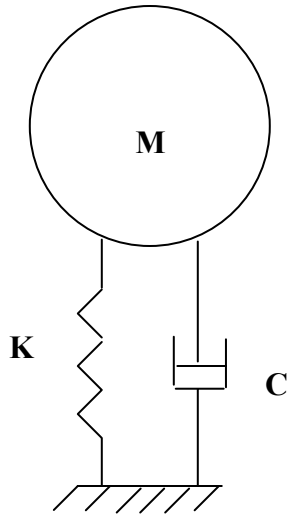

Fig. 2 Linear spring-damper-mass model for vertical impact.

For physical description of the problem, the ball is modeled as having an inner core and an outer core. As soon as the ball touches the ground, the outer core comes into contact with the ground and is stopped whereas the inner core continues to move down. The outer and the inner core are connected with a linear spring-damper as shown in following figure on next page:

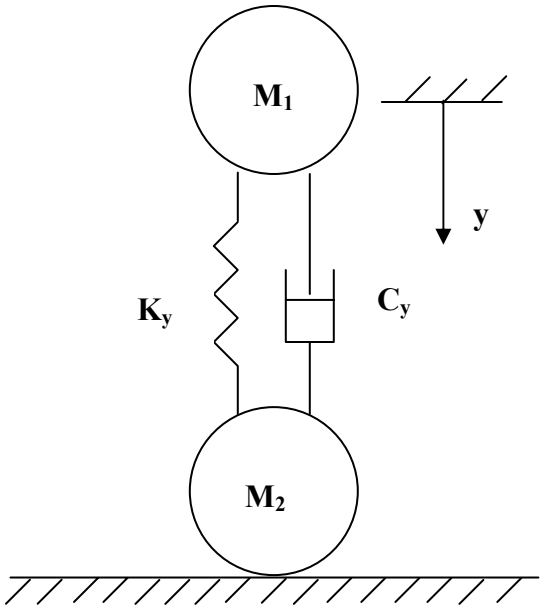

Fig. 3 Inner core (mass M_1) and outer shell (mass M_2) connected by linear spring-damper elements.

Initial conditions of the kinematics can be expressed as follows:

$$y(0) = 0$$
$$\dot{y}(0) = V_{y1}$$

i.e., measured from the position of the inner core as soon as outer core touches the ground, initial displacement of the inner core is zero whereas it carries the vertical velocity component indicated above. This vertical component of velocity is vertical velocity of the ball seen as a whole just before impact. The above two relations are initial conditions for vertical motion during the contact.

Equation of motion in the vertical direction is:

$$M_1 \ddot{y}(t) + C_y \dot{y}(t) + K_y y(t) = 0 \qquad (1)$$

Equation (1) describes motion of the inner core of the ball and it helps to model contact duration time when the ball is going to be rebounded, as well as the velocity of the ball at rebound.

Solution of equation (1) is given as follows:

$$y(t) = \frac{V_{y1}}{\omega_{dy}} e^{-\zeta_y \omega_y t} \sin(\omega_{dy} t) \qquad (2)$$

after applying the initial conditions of velocity and displacement. Definitions of the symbols are given as:

$$\zeta_y = \frac{C_y}{2M_1\omega_y} \qquad \omega_y = \sqrt{\frac{K_y}{M_1}} \qquad \omega_{dy} = \omega_y \sqrt{1-\zeta_y{}^2}$$

It can be seen from equations (1) and (2) how the spring-damper approach is employed to model a collision, or impact problem to one of the vibration problem.

The physical significance of the above model can be explored by observing that the time of rebound for the ball, i.e., the time in which downward motion is completely reversed, inner core mass M_1 reaches its original position and with negative velocity in the Y-direction is simply half of the period of this simple vertical spring-mass-damper system.

The time of contact is given as follows:

$$t_C = \frac{\pi}{\omega_{dy}} \tag{3}$$

Differentiating equation (2) with respect to time, it is seen that:

$$\dot{y}(t) = \frac{-\zeta\omega_y V_{y1}}{\omega_{dy}} e^{-\zeta\omega_y t} \sin(\omega_{dy} t) + V_{y1} e^{-\zeta\omega_y t} \cos(\omega_{dy} t) \tag{4}$$

It can be immediately seen that this approach used to describe the collision process is not only applicable in finding out the rebound vertical velocity component but also the variation of the vertical velocity with time *during* the contact.

For evaluating the vertical velocity at rebound for inner mass, simply substituting the value of contact time in equation (4), it can be seen that:

$$\dot{y}(t_c) = -e^{-\frac{\zeta_y \pi}{\sqrt{1-\zeta_y{}^2}}} V_{y1} \tag{5}$$

Now for finding out the vertical velocity at rebound of the tennis ball, or in other words, of the two-mass system, it is necessary to apply the conservation of linear momentum between the time the contact ends (at which the inner mass moves with the rebound velocity given by equation (5)) and some time after the ball has left the ground such that the inner and outer mass are moving with some common value of vertical velocity. Expressing it in mathematical form:

$$M_1 \dot{y}(t_c) = (M_1 + M_2) V_{y2} \tag{6}$$

In equation (6), v_{y2} is the velocity of rebound and is related to the vertical coefficient of restitution as follows:

$$V_{y2} = -(COR)V_{y1} \tag{7}$$

Combining equations (5), (6) and (7), the following equation is obtained which can be used to determine the damping ratio and damping coefficient of the two-mass model in vertical direction:

$$e^{\frac{-\xi_y \pi}{\sqrt{1-\xi_y{}^2}}} = \frac{(M_1 + M_2)}{M_1}(COR) \tag{8}$$

It can be seen that the coefficient of restitution is dependent on the system dynamic parameters such as mass, stiffness and damping and these parameters determine as to what fraction the velocity of rebound is of the incoming velocity in Y-direction.

MOTION IN THE HORIZONTAL DIRECTION

Motion in the x-direction presents two possible scenarios of impact for the ball, that is, rolling and slipping. For either case, the basic equation of motion in the x-direction is given as:

$$\sum F_X = (M_1 + M_2)\ddot{x}(t) \tag{9}$$

The model can be presented in Figure 4 below:

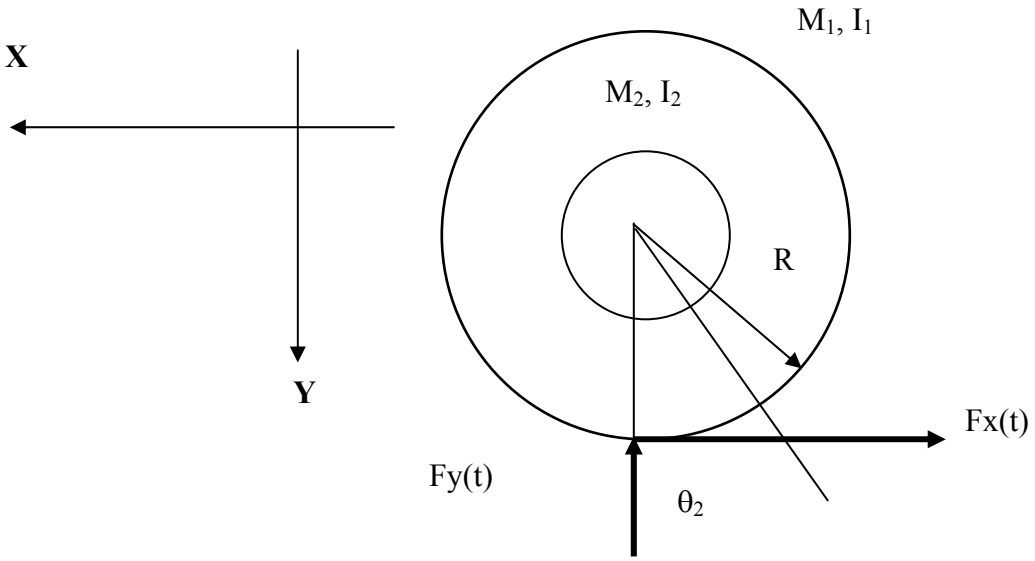

Fig. 4 The model, motion and force in x-direction.

Depending on whether there is rolling or slipping condition, we accordingly have the following equations:

Kinematical constraint- rolling

$$x(t) = R\theta_2(t) \tag{10}$$

Kinetic constraint- sliding

$$F_X(t) = \mu F_Y(t)\,\mathrm{sgn}(\dot{x}(0) - R\dot{\theta}_2(0)) \tag{11}$$

Equation (8) represents the rolling condition-it relates the kinematic parameters, namely the translational displacement of the inner core with the rotational displacement or coordinate of the outer core, as soon as the ball contacts the ground.

Equation (9), on the other hand, expresses the relationship between the horizontal force acting on the outer shell and the normal reaction on the outer core as soon as contact is made. It is the statement of Coulomb's law of sliding friction, with 'μ' as the coefficient of sliding friction. In equation (9), "sgn" represents sign function, which is defined as follows:

$$\text{sgn}(A) = +1 \ , \ A>0$$
$$\text{sgn}(A) = -1 \ , \ A<0 \qquad (12)$$

Equations in (A) above indicate that when this function acts on an argument, which in turn itself can be a function, then it either attaches +1 or –1 with the argument. Physically, its use in equation (9) means that the friction force during the sliding motion can be either in the positive coordinate direction or in the negative coordinate direction, depending upon the velocity of point of contact with the ground. The velocity of the point of contact is not only determined by the translational velocity but also the incoming spin velocity and will be discussed later in this chapter.

Once the rotational equation of motion for the ball is formulated, these conditions can be used in conjunction with the vertical motion to describe the dynamics of the ball during contact with ground in either of the two modes of motion i.e., sliding or rolling.

ROTATIONAL EQUATIONS OF MOTION

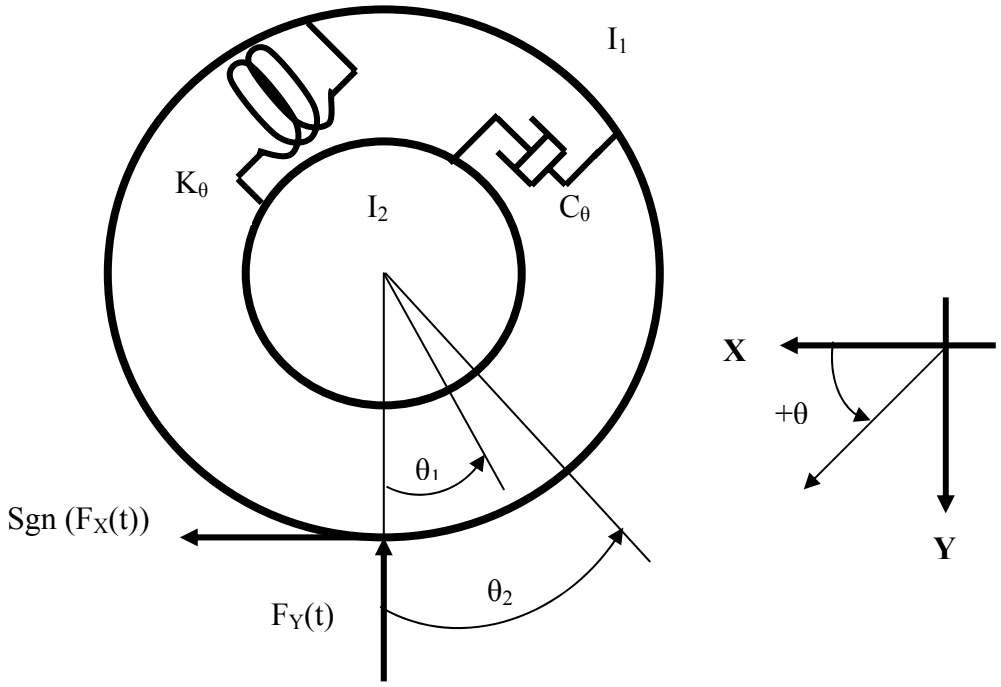

Fig. 5 Model and coordinates of the rotational motion.

Figure 5 shows the model and the coordinates used for the formulation of the rotational equations of motion. In this figure, it is seen that a torsional spring and damper connect the inner and outer core. As in the case of vertical motion, these elements are considered as linear. As can be guessed, the damping element will give rise to the concept of rotational coefficient of restitution.

Applying Newton-Euler equations of motion, the rotational equations of motions are written as follows:

$$I_G \ddot{\theta}(t) = M_G \tag{13}$$

Applying equation (10) to the inner and the outer core, considering the torsional spring, damper and finally, the horizontal friction force acting on the outer shell, the equations of motion are derived as follows in Figure 6:

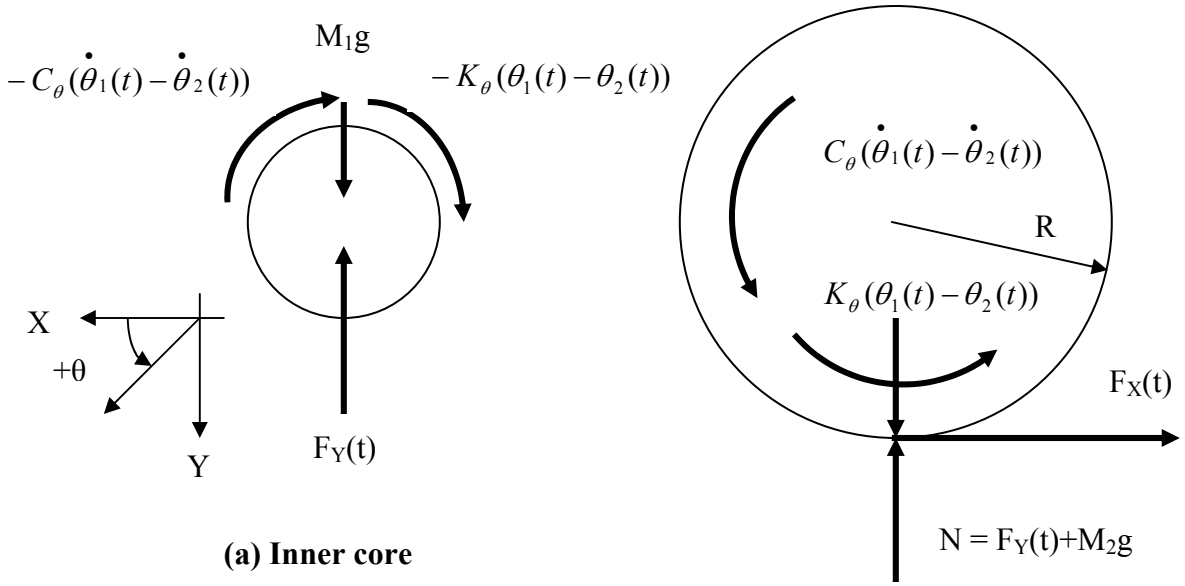

(a) Inner core

(b) Outer shell

Fig. 6 Free body diagrams of the inner core and the outer core.

Inner core

$$I_1\ddot{\theta}_1(t)+C_\theta(\dot{\theta}_1(t)-\dot{\theta}_2(t))+K_\theta(\theta_1(t)-\theta_2(t))=0 \qquad (14)$$

Outer core

$$I_2 \ddot{\theta}_2(t) + C_\theta(\dot{\theta}_2(t) - \dot{\theta}_1(t)) + K_\theta(\theta_2(t) - \theta_1(t)) - F_X(t)R = 0 \qquad (15)$$

In order to solve equations (11) and (12) completely, we need one more equation, that relates $F_x(t)$ to one of the other parameters, namely $\theta_2(t)$ or the vertical motion. These are the conditions of rolling and sliding, respectively.

First, consider the case of rolling.

Rolling motion

Using equation (7) and equation (8), it can be seen that:

$$F_X(t) = -(M_1 + M_2)R\ddot{\theta}_2(t) \qquad (16)$$

The negative sign is due to the reason that in the rolling motion, velocity of the contact point is zero at all instants, and hence the friction force then becomes dependent only on the sign of the incident horizontal velocity. Since in the chosen coordinate system, the incident horizontal velocity is always positive, accordingly the direction of the rolling friction force is always in the negative x-direction. This is not necessarily so, however, for the sliding friction force.

Using equations (12) and (13), it can be seen that the resulting differential equation of rotational motion is:

$$(I_2 + (M_1 + M_2)R^2)\ddot{\theta}_2(t) + C_\theta(\dot{\theta}_2(t) - \dot{\theta}_1(t)) + K_\theta(\theta_2(t) - \theta_1(t)) = 0 \qquad (17)$$

Now it is possible to solve equations (11) and (14) completely.

Defining:

$$\theta(t) = \theta_1(t) - \theta_2(t) \tag{18}$$

Dividing equations (11) and (14) by their respective coefficients of the first terms, and then subtracting from each other, using equation (15), the following rotational equation of motion in one single coordinate is obtained:

$$\ddot{\theta}(t) + C_\theta\left(\frac{1}{I_1} + \frac{1}{I_2 + (M_1 + M_2)R^2}\right)\dot{\theta}(t) + K_\theta\left(\frac{1}{I_1} + \frac{1}{I_2 + (M_1 + M_2)R^2}\right)\theta(t) = 0 \tag{19}$$

It is obvious that the term M_1+M_2 is the total mass of the ball.

This is a second-order linear differential equation and it can be solved analytically. The initial conditions are given as follows:

$\theta(0) = 0$ i.e., no relative motion between the inner and outer core at instant of contact

In order to determine the initial condition regarding velocity, it is first necessary to determine the initial spin of the outer shell upon contacting the ground. It can be determined by applying the conservation of kinetic energy between the incident and initial impact of the two-mass model as follows:

$$T_0 = \frac{1}{2}MV_1^2 + \frac{1}{2}I\omega_1^2 = \frac{1}{2}M(\dot{x}(0))^2 + \frac{1}{2}M(\dot{y}(0))^2 + \frac{1}{2}I_1\omega_1^2 + \frac{1}{2}I_2(\dot{\theta}_2(0))^2 \tag{20}$$

In equation (17) above, T_0 is the total incident kinetic energy of the ball. This energy can be expressed in terms of the ball as a whole, as well as in terms of the two-mass model, as expressed by the terms on right hand side.

During the no slip case, from equation (8), the initial conditions are related as:

$$\dot{x}(0) = R\dot{\theta}_2(0)$$

Hence the energy equation can be solved for the initial spin of the outer core as follows:

$$\dot{\theta}_2(0) = \sqrt{\frac{MV_1^{\,2} + I\omega_1^{\,2} - I_1\omega_1^{\,2} - M(\dot{y}(0))^2}{I_2 + MR^2}} \qquad (21)$$

where $\omega_1 = \omega(0)$

The initial condition for θ related to spin velocity will be:

$$\dot{\theta}(0) = \omega(0) - \sqrt{\frac{MV_{X1}^{\,2} + I(\omega(0))^2 - I_1(\omega(0))^2}{I_2 + MR^2}}$$

Thus the solution of equation (16) is given as follows:

$$\theta(t) = \frac{\dot{\theta}(0)}{\omega_{d\theta}} e^{-\zeta_\theta \omega_{n\theta} t} \sin(\omega_{d\theta} t) \qquad (22)$$

where the following definitions are given:

$$\omega_{n\theta} = \sqrt{K_\theta (\frac{1}{I_1} + \frac{1}{I_2 + MR^2})}$$

$$\zeta_\theta = \frac{C_\theta}{2\omega_{n\theta}}$$

$$\omega_{d\theta} = \omega_{n\theta}\sqrt{1-\zeta_\theta^{\,2}}$$

As can be seen from equation (17), this equation has a similar form as the one for the case of vertical motion with a linear spring-mass-damper.

Differentiating equation (17) with respect to time, the relative spin velocity is obtained i.e.,

$$\dot{\theta}(t) = \frac{-\zeta_\theta \omega_{n\theta}\,\dot{\theta}(0)}{\omega_{d\theta}} e^{-\zeta_\theta \omega_{n\theta} t} \sin(\omega_{d\theta} t) + \dot{\theta}(0) e^{-\zeta_\theta \omega_{n\theta} t} \cos(\omega_{d\theta} t) \qquad (23)$$

So the spin velocity at rebound can be determined by substituting for 't' the value of t_c from equation (3). This is an based on assumption that the spin velocities of both the inner and the outer masses attain the same values well before the contact is over and hence the spin velocities at rebound can be determined by using the contact time of vertical motion.

Sliding motion

In the sliding scenario, as indicated by equation (9), the tangential force (friction) and the normal contact force are related by the coefficient of dynamic friction. Using this equation in equation 12, the following equation for the spin of the outer core is obtained:

$$I_2 \ddot{\theta}_2(t) + C_\theta(\dot{\theta}_2(t) - \dot{\theta_1}(t)) + K_\theta(\theta_2(t) - \theta_1(t)) + \mathrm{sgn}(\mu F_Y(t))R = 0 \qquad (24)$$

During contact between the ball and the ground, the normal contact force can be expressed as follows:

$$F_Y(t) = -C\dot{y}(t) - Ky(t) \tag{25}$$

Substituting equation 20 into equation 19, the following differential equation results:

$$I_2\ddot{\theta}_2(t) + C_\theta(\dot{\theta}_2(t) - \dot{\theta}_1(t)) + K_\theta(\theta_2(t) - \theta_1(t)) = \text{sgn}(\mu R[C\dot{y}(t) + Ky(t)]) \tag{26}$$

VELOCITY OF CONTACT POINT AND SIGN OF CONTACT FORCE

In the two-mass model of the tennis ball, the ball moves as a rigid body in the x-direction. The direction of the sliding friction force from the ground to the outer core of the ball depends upon the direction of the velocity of the contact point on the ball at the instant the outer core comes into contact with the ground; i.e. the sliding friction force acts opposite to the initial contact point velocity.

The contact point initial velocity can be determined as follows:

$$\vec{V}_A = V_{X1}\hat{i} + \vec{V}_{A/C} \tag{27}$$

In equation (23), the first term on the right hand side is the velocity of the center of mass of the ball in x-direction, as soon as it contacts the ground, whereas the second term is the relative velocity of the contact point with respect to the center of mass, considering center of mass as fixed and the contact point moving about point C with angular spin ω.

However, this computation of the contact point velocity requires careful consideration with regards to the possibilities of incoming angular spin as topspin, backspin or zero spin. Consequently, each one is considered on the next pages:

Topspin

In topspin, the direction of spin is such that the surface velocity of the bottom point due to angular spin alone is in opposition to the center of mass velocity. Consequently, from equation (22), the contact point velocity can be evaluated as follows:

$$\vec{V}_A = (V_{X1} - R\omega_1)\hat{i} \tag{28}$$

Hence the direction determination of sliding friction force is now strictly a matter of whether the center of mass translational velocity is greater than or less than the rotational surface velocity, which is the $R\omega_1$ term (In case they are equal at the very onset of impact, then V_A is zero and it is then a case of rolling motion).

Based on equation (23), then the sign function relevant to the sliding friction force as described in equation (9) can be evaluated as follows:

$$V_{X1} > R\omega_1 \text{, sgn} = +1$$
$$V_{X1} < R\omega_1 \text{, sgn} = -1$$

Backspin

From equation (23), the contact point velocity can be determined for the case of incident backspin as follows (ω_1 is positive for backspin in the chosen coordinate system):

$$\vec{V}_A = (V_{X1} + R\omega_1)\hat{i} \tag{29}$$

Physically, in backspin, the direction of incoming angular spin is such that the velocity of the bottom point of the ball due to spin alone is in the same direction as the center of mass velocity at the moment of impact.

Inspecting equation (24), it can be immediately concluded that the sign of the sliding friction force acting on the ball for the case of incoming backspin can be determined as follows:

$$\text{Sgn} = +1$$

Zero spin

For incident zero spin, equation (22) indicates that:

$$\vec{V}_A = V_{X1}\hat{i} \tag{30}$$

Consequently, sign of the sliding friction force in this case can be determined as follows:

$$\text{Sgn} = +1$$

Now, in equation 21, results of equation 2 and equation 4 can be substituted to yield an equation of motion for the relative spin, which is a non-homogenous differential equation and hence must be solved for transient and forced response (forced response is in the form of the normal force which is also a function of time).

With the same procedure as used for the rolling motion and using the notation developed in equation 15, the equation of motion for the relative spin becomes:

$$\ddot{\theta}(t) + C_\theta(\frac{1}{I_G} + \frac{1}{I_2})\dot{\theta}(t) + K_\theta(\frac{1}{I_G} + \frac{1}{I_2})\theta(t) = \\ \text{sgn}(\frac{R\mu}{I_2}[e^{-\zeta_y\omega_{oy}t}\sin(\omega_{dy}t)(\frac{C_y\xi_y\omega_{oy}V_y}{\omega_{dy}} - \frac{K_yV_y}{\omega_{dy}}) - C_yV_ye^{-\xi_y\omega_{oy}t}\cos(\omega_{dy}t)]) \tag{31}$$

Equation 22 is of the following form:

$$a\ddot{\theta}(t) + b\dot{\theta}(t) + c\theta(t) = \gamma_1 e^{\alpha t}\sin(\beta t) + \gamma_2 e^{\alpha t}\cos(\beta t) \tag{32}$$

where the following notation has been used:

$$a = 1 \qquad b = C_\theta(\frac{1}{I_G} + \frac{1}{I_2}) \qquad c = K_\theta(\frac{1}{I_G} + \frac{1}{I_2})$$

$$\gamma_1 = \text{sgn}(\frac{\mu R}{I_2}[\frac{K_yV_y}{\omega_{dy}} - \frac{C_y\xi_y\omega_yV_y}{\omega_{dy}}]) \qquad \gamma_2 = \text{sgn}(\frac{\mu R}{I_2}C_yV_y)$$

$$\alpha = -\xi_y\omega_y \qquad \beta = \omega_{dy}$$

The particular solution of equation 26 is as follows:

$$\theta_p(t) = Ae^{\alpha t}\sin(\beta t) + Be^{\alpha t}\cos(\beta t) \tag{33}$$

where:

$$A = \frac{(2a\alpha\beta + b\beta)}{[\{a(\alpha^2 - \beta^2) + b\alpha + c\}^2 + (2a\alpha\beta + b\beta)^2]}[\gamma_2 + \frac{\gamma_1(a\alpha^2 - a\beta^2 + b\alpha + c)}{(2a\alpha\beta + b\beta)}] \tag{34}$$

$$B = \frac{A(a\alpha^2 - a\beta^2 + b\alpha + c) - \gamma_1}{(2a\alpha\beta + b\beta)} \tag{35}$$

The homogenous solution of equation 26 is as follows:

$$\theta_h(t) = 0 \tag{36}$$

since:

$$\dot{\theta}(0) = \omega(0) - \omega(0) = 0 \qquad \text{for sliding motion.}$$

The complete solution to equation (22) is, therefore,

$$\theta(t) = \theta_h(t) + \theta_p(t) = \theta_p(t) \tag{37}$$

MOTION IN X-DIRECTION

Rolling

From equation 14, it is seen that:

$$(I_2 + (M_1 + M_2)R^2)\ddot{\theta}_2(t) = -C_\theta(\dot{\theta}_2(t) - \dot{\theta}_1(t)) - K_\theta(\theta_2(t) - \theta_1(t)) = -C_\theta \dot{\theta}(t) - K_\theta\theta(t) \quad (38)$$

From equation (18) and equation (19), the solution for the relative spin has already been determined. This can be substituted in equation (34) above to obtain a differential equation for outer shell, which can then be solved for angular spin and displacement by successive integrations. Once the angular spin velocity of the outer shell is obtained, it can be related to the translational velocity of the center of mass of the ball in X-direction using equation (8). Hence a complete solution for rebound is obtained in the no-slip case, with the solution for vertical velocity already determined earlier on.

Sliding

From equations 21, 22 and 28, it is seen that:

$$I_2\ddot{\theta}_2(t) = -C_\theta \dot{\theta}(t) - K_\theta\theta(t) + \text{sgn}(\frac{R\mu}{I_2}[e^{-\zeta_y\omega_{oy}t}\sin(\omega_{dy}t)(\frac{C_y\xi_y\omega_y V_y}{\omega_{dy}} - \frac{K_y V_y}{\omega_{dy}}) - C_y V_y e^{-\xi_y\omega_{oy}t}\cos(\omega_{dy}t)]) \quad (39)$$

Hence from equations 21, 26 and 28, angular acceleration of the outer shell is determined and thus by successive integrations, its angular velocity as well as displacement as a function of time during contact can be determined.

For the sliding motion, motion in the X direction is independent of the spin velocity of the outer shell. Using equations 7, 9 and 20, it can be seen that the acceleration in X direction can be simply expressed for the sliding case as follows:

$$\ddot{x}(t) = -\frac{\mu}{M}(C\dot{y}(t) + ky(t))\,\mathrm{sgn}(\dot{x}(0) - R\dot{\theta}_2(0)) \qquad (40)$$

Then by utilizing equations 2 and 4, and substituting the results in equation 31, the acceleration of the ball in X direction during sliding, as a function of time, is obtained.

Then successive integrations lead to the velocity and displacement of the ball in the X direction.

Equations developed thus for the tennis ball in both scenarios i.e., slip and no-slip, then represent the two dimensional model and the motion during the contact with the ground. With the knowledge of the motion, the contact forces can be formulated and the contact problem completely solved.

EFECT OF HIGH INCIDENT VERTICAL VELOCITY COMPONENT ON ROLLING MOTION

In rolling motion, when there is high incident vertical velocity, it is possible that the ball squashes asymmetrically and as a result, the normal force of contact does not pass through the center of the ball but has some x-eccentricity about the center, as shown in the figure below:

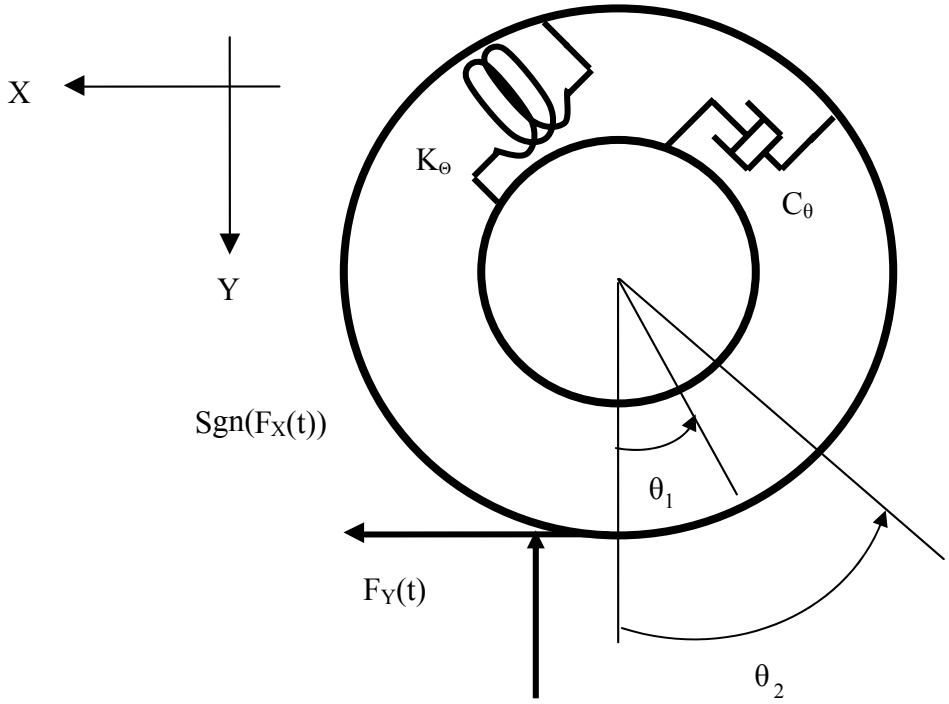

Fig. 7 Effect of high incident velocity on the ball during rolling.

As shown in figure 7, the way in which this effect is taken into account in the present model is simply that since the ball is considered as a rigid body in the horizontal motion (x-direction), the normal contact force $F_Y(t)$ is offset from the common center of mass X-coordinate by a distance 'ε'. This results in a moment about the center of outer shell. Accordingly, the equations of rotational motion for the outer core need to be re-formulated and then the coupled rotational equations of motion need to be solved to get the solution considering this effect.

Equations (1), (2), (4) and (8) still hold. Equation of motion for the outer shell can be re-written as follows:

$$I_2 \ddot{\theta}_2(t) + C_\theta(\dot{\theta}_2(t) - \dot{\theta}_1(t)) + K_\theta(\theta_2(t) - \theta_1(t)) - F_X(t)R + F_Y(t)\varepsilon = 0 \tag{41}$$

Equation (36) is same as equation (12) except for the moment term due to normal contact force $F_Y(t)$. Utilizing equations (13) and (20), equation (36) can be written as:

$$(I_2 + MR^2)\ddot{\theta}_2(t) + C_\theta(\dot{\theta}_2(t) - \dot{\theta}_1(t)) + K_\theta(\theta_2(t) - \theta_1(t)) = \varepsilon(C_y \dot{y}(t) + K_y y(t)) \tag{42}$$

Adopting the same procedure as in analysis of rolling without the eccentric force, the two rotational equations of motion can be written as:

$$\ddot{\theta}_1(t) = -\frac{C_\theta}{I_1}\dot{\theta}(t) - \frac{K_\theta}{I_1}\theta(t) \tag{43}$$

$$\ddot{\theta}_2(t) = \frac{C_\theta}{I_2 + MR^2}\dot{\theta}(t) + \frac{K_\theta}{I_2 + MR^2}\theta(t) + \frac{\varepsilon}{I_2 + MR^2}(C_y \dot{y}(t) + K_y y(t)) \tag{44}$$

where

$$\theta(t) = \theta_1(t) - \theta_2(t)$$

Subtracting equation (39) from (38), the following equation of relative rotational motion between the inner core and the outer shell is obtained:

$$\ddot{\theta}(t) + C_\theta\left(\frac{1}{I_1} + \frac{1}{I_2 + MR^2}\right)\dot{\theta}(t) + K_\theta\left(\frac{1}{I_1} + \frac{1}{I_2 + MR^2}\right)\theta(t) = -\frac{\varepsilon}{I_2 + MR^2}\left((K_y - C_y\zeta_y\omega_y)\frac{V_{y1}}{\omega_{dy}}e^{-\zeta_y\omega_y t}\sin(\omega_{dy}t) + C_y V_{y1}e^{-\zeta_y\omega_y t}\cos(\omega_{dy}t)\right) \quad (45)$$

Equation (40) is a second-order, non-homogenous, linear differential equation with constant coefficients. Solution to (40) consists of complementary function plus particular integral. Complementary solution to equation (40) is identical to that of equation (16) and is given by equation (17).

In order to obtain the particular integral, equation (40) is written in the following notation to facilitate the description of solution:

$$a\ddot{\theta}(t) + b\dot{\theta}(t) + c\theta(t) = \gamma_1 e^{\alpha t}\sin(\beta t) + \gamma_2 e^{\alpha t}\cos(\beta t) \quad (46)$$

In equation (41), upon comparison with equation (40), the coefficients are defined as follows:

$$a = 1 \qquad b = C_\theta\left(\frac{1}{I_1} + \frac{1}{I_2 + MR^2}\right) \qquad c = K_\theta\left(\frac{1}{I_1} + \frac{1}{I_2 + MR^2}\right)$$

$$\gamma_1 = \frac{-\varepsilon}{I_2 + MR^2}\frac{V_{y1}}{\omega_{dy}}(K_y - C_y\zeta_y\omega_y) \qquad \gamma_2 = \frac{-\varepsilon}{I_2 + MR^2}C_y V_{y1} \qquad \alpha = -\zeta_y\omega_y$$

$$\beta = \omega_{dy}$$

Then the particular solution to equation (41) is given as follows:

$$\theta_p(t) = Ae^{\alpha t}\sin(\beta t) + Be^{\alpha t}\cos(\beta t) \quad (47)$$

where:

$$A = \frac{(2a\alpha\beta + b\beta)}{[\{a(\alpha^2 - \beta^2) + b\alpha + c\}^2 + (2a\alpha\beta + b\beta)^2]}[\gamma_2 + \frac{\gamma_1(a\alpha^2 - a\beta^2 + b\alpha + c)}{(2a\alpha\beta + b\beta)}] \quad (48)$$

$$B = \frac{A(a\alpha^2 - a\beta^2 + b\alpha + c) - \gamma_1}{(2a\alpha\beta + b\beta)} \quad (49)$$

Hence, complete solution to the rolling problem then becomes:

$$\theta(t) = \frac{\dot{\theta}(0)}{\omega_{d\theta}} e^{-\zeta_\theta \omega_{n\theta} t} \sin(\omega_{d\theta} t) + Ae^{\alpha t} \sin(\beta t) + Be^{\alpha t} \cos(\beta t) \quad (50)$$

with A and B given by equations (44) and (45) above.

OFFSET DISTANCE AS A FUNCTION OF VERTICAL IMPACT VELOCITY

As the vertical component of impact velocity increases, the flatness becomes more pronounced in the tennis ball [1,5]. It can be assumed that the offset distance ‘ε’ of the normal reaction from center of mass of the tennis ball during rolling is a function of the vertical component of impact velocity. If a linear functional relationship is assumed, this can be expressed as:

$$\varepsilon(V_y) = C_1 V_y + C_2 \quad (51)$$

While performing the simulations (Chapter V) for the tennis ball , it was observed that ‘ε’ varies from 0.02 to 0.5 for vertical component velocities of 5 m/s and

16 m/s, respectively. These values are selected based on good agreement with experimental observations. It is then possible to calculate the values of coefficients C_1 and C_2 using these extreme values. Thus, the following linear equations in C_1 and C_2 result:

$$\begin{aligned} 0.02 &= C_1(5) + C_2 \\ 0.5 &= C_1(16) + C_2 \end{aligned} \tag{52}$$

Solving these two equations:

$$\begin{aligned} C_1 &= 0.0431 \\ C_2 &= -0.189 \end{aligned}$$

Thus the offset distance as a linear function of vertical component of impact velocity is expressed as:

$$\varepsilon(V_y) = 0.0431V_y - 0.189 \tag{53}$$

Using equation (49), the offset distance can now be obtained at any value of vertical componet of impact velocity between 5 m/s and 16 m/s or beyond 16 m/s. Equation (49) has been utilized in Chapter V in simulations whenever the ball's motion changes from sliding to rolling. Then the 'ε' value is needed and can be calculated using equation (49) to use in rolling motion simulation.

TRANSITION BETWEEN SLIDING AND ROLLING: TIME-AVERAGED COEFFICIENT OF FRICTION

Recall from the moment equation written for the outer shell in pure rolling (equation (42) in Chapter II), that due to the eccentricity of the normal force with respect to the center of mass of the two-mass system, there is a counter-clockwise moment, which is expressed as:

$$M_E = -\varepsilon F_Y(t) \tag{54}$$

In tennis ball dynamics, the moment expressed in equation (54) corresponds to the opposing moment that tends to retard the ball while it is in rolling motion. The opposing moment given by equation (54) can be converted to an equivalent "rolling friction force F_R", as follows:

$$F_R = \frac{-\int_0^{t_c} \varepsilon F_Y(t)dt}{R\int_0^{t_c} dt} \tag{55}$$

Equation (55) represents the average opposing moment acting on the tennis ball during contact. The radius used to evaluate the average friction force is the radius of the outer shell,'R'. In a similar way, the average sliding friction force can be expressed as:

$$F_S = \mu_S \frac{\int_0^{t_c} F_Y(t)dt}{\int_0^{t_c} dt} \tag{56}$$

Since the rolling friction defined by equation (55) is less than sliding friction,

$$|F_R| < |F_S|$$

It follows from equations (55) and (56) that:

$$\frac{\varepsilon}{R} < \mu_S \tag{57}$$

Or:

$$\mu_R < \mu_S \tag{58}$$

In (57), μ_R can be defined as rolling friction coefficient and is given as the ratio of the eccentricity distance from the center of mass to the radius of the ball. The inequality (56) is obtained because 'ε' is not a function of time (equation (55)) and hence the remaining terms in equations (54) and (55) simply cancel out.

Recall from equation (53) that 'ε' is a function of the vertical component of incident velocity. From inequality (57), it can be seen that for the values of coefficient of sliding friction 0.55 and radius of the tennis ball 1.3 in., the offset distance must satisfy the following constraint:

$$\varepsilon < 0.715 in$$

From equation (53), the maximum value of 'ε' for the simulations in case of maximum value of vertical component of incident velocity of arounf 16 m/s turns out to be 0.500 in. Thus constraint (58) is satisfied in all the simulations whenever the rolling takes place during motion of the tennis ball with the ground.

In tennis ball dynamics, collision problems that involve rolling during contact always start from pure sliding contact and then during contact, the motion of the tennis ball changes from sliding to pure rolling. In such problems , an expression for a time-averaged coefficient of friction, can be defined as follows:

$$\overline{\mu} = \frac{\int_0^{t_c} F_X(t)dt}{\int_0^{t_c} F_Y(t)dt} \tag{59}$$

Thus, a problem that involves transition from sliding to the pure rolling during contact can be identified or its accuracy of solution can be checked by evaluating the time-averaged coefficient of friction in equation (59) and comparing its value against the coefficient if kinetic friction in pure sliding. If there is a motion transition during contact, then the value evaluated from equation (59) will be appreciably less than the coefficient of kinetic friction of the surface involved in contact. Hence the time-averaged value calculated using equation (59) serves as a check that shows if $\overline{\mu} < \mu_s$,then rolling probably occurs .

Equation (59) can be simplified, since the integrals in numerator and denominator on the right hand side can be expressed in terms of the mass and velocities of the ball in the two coordinate directions, using Newton's second law of motion as follows:

$$F_X(t) = -m\frac{dv_X}{dt} \tag{60}$$

$$F_Y(t) = -m\frac{dv_Y}{dt} \tag{61}$$

Integrating equations (60)and (61) from start of collision (t = 0) to the end of collision ($t = t_c$), following expressions are obtained:

$$\int_0^{t_c} F_X(t)dt = -m(V_{X2} - V_{X1}) \tag{62}$$

$$\int_0^{t_c} F_Y(t)dt = -m(V_{Y2} - V_{Y1}) \tag{63}$$

In equation (61), the rebound component of velocity in the vertical direction can be related to the incident component of velocity in the vertical direction by an experimentally determined coefficient of restitution as follows:

$$V_{Y2} = -(COR)V_{Y1} \tag{64}$$

When equations (62) to (64) are inserted in equation (59), the following expression for the time-averaged coefficient of friction results:

$$\overline{\mu} = \frac{V_{X1} - V_{X2}}{(1 + COR)V_{Y1}} \tag{65}$$

Thus, if a tennis ball impact problem is solved with transition of motion from pure sliding to pure rolling during the contact (as determined by the condition when the contact point velocity goes to zero as motion changes from pure sliding to pure rolling), the solution of the velocities can be incorporated in equation (65) to calculate the time-averaged coefficient of friction during the contact. If transition occurs during the contact, then the value calculated from equation (65) will be less than the coefficient of kinetic

friction for the pure sliding. If no rolling occurs during contact and there is only sliding motion, the value calculated from equation (65) will then be almost equal to the value of the coefficient of kinetic friction.

Equation (65) can also be applied to experimentally determined data for the tennis ball dynamics to find out whether transition from sliding to pure rolling occurs during particular cases of impact. Equation (65) is used in Chapter IV to calculate the time-averaged coefficient of friction for an experimental data on tennis ball impact **[1]**, for estimates of transition from sliding to pure rolling during contact.

INNER AND OUTER CORE DYNAMIC PARAMETERS

In order to perform dynamic simulation of the tennis ball using the two-mass model, it is first necessary to ascertain physically feasible values of the inner and outer core dynamic parameters. These parameters include masses, mass moments of inertia, and radii of the two masses in the model.

There are various possibilities as regards to the feasible dynamic parameters. First of all, it is necessary to describe the equations for various dynamic parameters which are interrelated to each other. After that, it is possible to derive various combinations of dynamic parameters for the two masses.

Inner core

Mass of the inner core can be written in terms of its weight density and volume as follows:

$$M_1 = \frac{\gamma_1 V_1}{g} = \frac{\gamma_1 (\frac{4}{3}\pi R_1^{\,3})}{g} \tag{66}$$

Mass moment of inertia of the inner core can be described by the following equations:

$$I_1 = \frac{2}{3} M_1 R_1^{\ 2} \tag{67}$$

Outer core

In a similar manner, mass of the outer shell can be described as:

$$M_2 = \frac{\gamma_2 V_2}{g} = \frac{\gamma_2 (\frac{4}{3}\pi (R_i^{\ 3} - R_2^{\ 3}))}{g} \tag{68}$$

And its mass moment of inertia can be expressed as:

$$I_2 = \frac{2}{5} M_2 R_2^{\ 2} \tag{69}$$

In order that this model truly represents a tennis ball, there are simple constraints on the inner and outer cores' masses and mass moments of inertia and these are that the sum of the inner and outer core masses and mass moments of inertia should equal, respectively, to the mass and mass moment of inertia of a real tennis ball.

These constraints can be expressed as follows:

$$M_1 + M_2 = M \tag{70}$$

$$I_1 + I_2 = I \tag{71}$$

For a tennis ball, the average mass is about 0.000329 lb-s^2/in whereas its mass moment of inertia about its centroidal axes is 0.00028 lb-s^2-in (Chapter IV).

Final constraints to be placed are dimensional constraints on the radii of inner and outer core. For a tennis ball, maximum radius of outer shell is 1.3 in. **[11]** and for inner core, the radius must be less than the outer shell.

Mathematically, this can be expressed as:

$$R_2 = 1.3 \text{ in.} \qquad (72)$$
$$R_1 < R_2$$

Based on equations (66) to (72), the following physically possible sets of dynamic parameters can be obtained:

(a)

$M_1 = M_2 = M/2$

$I_1 = 0.0001008$ lb-s^2-in $= 0.353I$

$I_2 = 0.0001853$ lb-s^2-in $= 0.647I$

$I = 0.00028$ lb-s^2-in

$R_1 = 1.24$ in.

$\gamma_1 = 0.008$ lb/in^3

$\gamma_2 = 0.06$ lb/in^3

(b)

$M_1 = 2M/3$

$M_2 = M/3$

$I_1 = 0.0001403$ lb-s^2-in $= 0.532I$

$I_2 = 0.0001235$ lb-s^2-in $= 0.468I$

$I = 0.000264$ lb-s^2-in

$R_1 = 1.26$ in.

$\gamma_1 = 0.01$ lb/in^3

$\gamma_2 = 0.07$ lb/in^3

(c)

$M_1 = 3M/4$

$M_2 = M/4$

$I_1 = 0.000165$ lb-s^2-in $= 0.641I$

$I_2 = 0.00009267$ lb-s^2-in $= 0.359I$

$I = 0.000257$ lb-s^2-in

$R_1 = 1.29$ in.

$\gamma_1 = 0.0105$ lb/in^3

$\gamma_2 = 0.300$ lb/in^3

In calculating the weight density for the outer shell in case (a), the inside radius of the shell has been taken as 1.25 in. For cases (b) and (c), this value has been taken as 1.27 in. and 1.295 in., respectively.

In Chapter III and Chapter V, simulations of the tennis ball have been performed using these dynamic parameters. It should be noticed that in cases (b) and (c), the sum total of mass moments of inertia of inner and outer masses are not equal to 0.00028 lb-s^2-in, but instead these values turn out to be 0.000264 and 0.000257 lb-s^2-in, respectively. These values obtained for total mass moment of inertia are not very far off the experimentally determined value of 0.00028 lb-s^2-in (Chapter IV), with percentage difference as 6 % and 7%, respectively. This might as well be the uncertainty in experimental measurements. The reason these dynamic parameters have been used in Chapter III and Chapter V is that these parameters give good agreements with experimental rebound motion of the tennis ball, and the error in mass moment of inertia is not large.

CHAPTER III

GRAPHICAL RESULTS OF SOLUTIONS OF EQUATIONS OF MOTION

In the previous chapter, the equations of motion for the tennis ball impact with the ground have been derived and their solutions formulated for the cases of the tennis ball's motion as the slip and the no- slip scenarios during its contact with the ground. Kinematic and kinetic parameters of importance during the contact, as found from the analysis of the equations of motion for both cases of the slip and the no-slip are described below:

(a) Vertical displacement of the ball as a function of time (y(t))

(b) Vertical velocity of the ball as a function of time ($\dot{y}(t)$)

(c) Horizontal velocity of the ball as a function of time ($\dot{x}(t)$)

(d) Angular spin of the ball as a function of time ($\dot{\theta}_2(t)$)

(e) Normal contact force as a function of time ($F_Y(t)$)

(f) Tangential contact force (friction force) as a function of time ($F_X(t)$)

Solutions for the equations of motion with regards to the above mentioned kinematic and kinetic parameters are described as follows:

SLIDING THROUGHOUT THE CONTACT

For reference, solutions of the equations of motion for the sliding case are repeated below:

$$y(t) = \frac{V_{y1}}{\omega_{dy}} e^{-\zeta_y \omega_y t} \sin(\omega_{dy} t) \tag{2}$$

$$\dot{y}(t) = \frac{-\zeta_y \omega_y V_{y1}}{\omega_{dy}} e^{-\zeta_y \omega_y t} \sin(\omega_{dy} t) + V_{y1} e^{-\zeta_y \omega_y t} \cos(\omega_{dy} t) \tag{4}$$

Equations (2) and (4) are equally valid for the no-slip case, since the y-motion, according to the two-mass elastic model as well as per Newton's second law of motion, is not affected by either scenario.

$$\dot{x}(t) = V_{X1} - \text{sgn}(\frac{\mu}{M}[C_y \frac{V_{y1}}{\omega_{dy}} e^{-\xi_y \omega_y t} \sin(\omega_{dy} t) + K_y \frac{V_{y1}}{\omega_{dy}} (\frac{-\xi_y \omega_y}{(\xi_y \omega_y)^2 + (\omega_{dy})^2} e^{-\xi_y \omega_y t} \sin(\omega_{dy} t) - \frac{\omega_{dy}}{(\xi_y \omega_y)^2 + (\omega_{dy})^2} e^{-\xi_y \omega_y t} \cos(\omega_{dy} t) + \frac{\omega_{dy}}{(\xi_y \omega_y)^2 + (\omega_{dy})^2})]) \tag{73}$$

$$\dot{\theta}_2(t) = \dot{\theta}_2(0) + \frac{C_\theta}{I_2}(A e^{-\xi_y \omega_y t} \sin(\omega_{dy} t) + B e^{-\xi_y \omega_y t} \cos(\omega_{dy} t) - B) + \frac{K_\theta}{I_2} \int_0^t (A e^{-\xi_y \omega_y t} \sin(\omega_{dy} t) + B e^{-\xi_y \omega_y t} \cos(\omega_{dy} t)) dt + \int_0^t [(\gamma_1 e^{-\xi_y \omega_y t} \sin(\omega_{dy} t) + (\gamma_2 e^{-\xi_y \omega_y t} \cos(\omega_{dy} t)] dt \tag{74}$$

$$F_Y(t) = -C_y \dot{y}(t) - K_y y(t) = e^{-\zeta_y \omega_y t} \sin(\omega_{dy} t)(\frac{C_y \xi_y \omega_y V_{y1}}{\omega_{dy}} - \frac{K_y V_{y1}}{\omega_{dy}}) - C_y V_{y1} e^{-\xi_y \omega_y t} \cos(\omega_{dy} t) \tag{75}$$

$$F_X(t) = \mu F_Y(t) \text{sgn}(\dot{x}(0) - R\dot{\theta}_2(0)) \tag{11}$$

These equations are plotted in MathCAD using the codes shown in Appendix B. For each physical variable, the curves are plotted parametrically in MathCAD. The results and their descriptions are described on the following pages.

Vertical displacement as a function of time

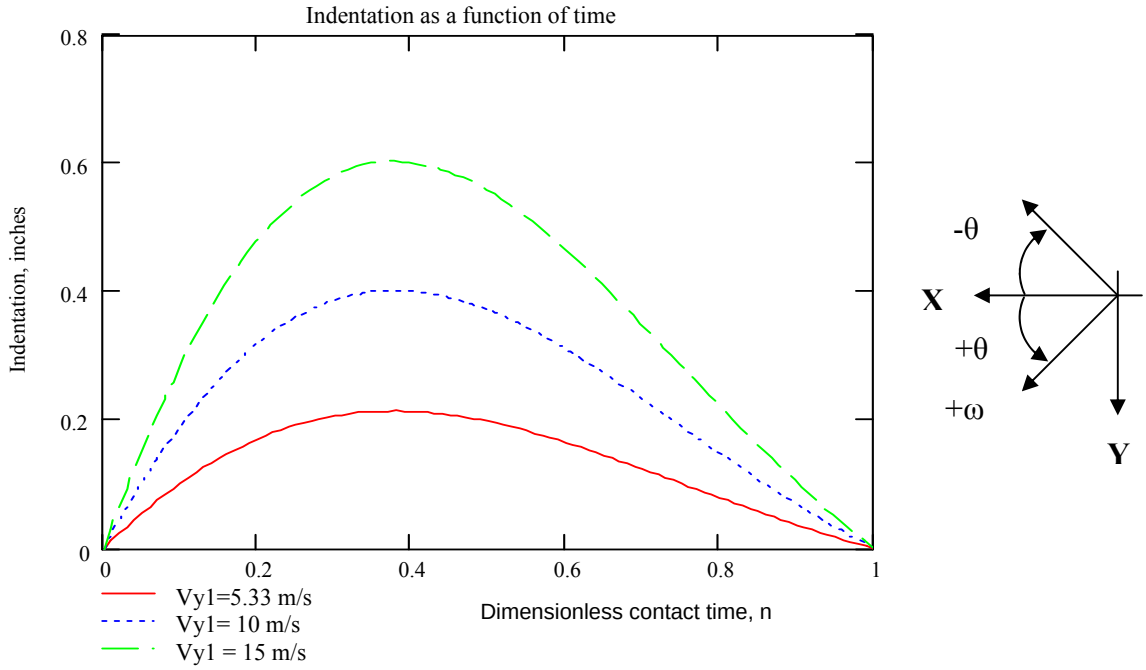

Fig. 8 Vertical displacement during contact as a function of time.

Figure 8 shows the predicted vertical displacement of the inner core mass as a function of time, during the contact of the outer core with the ground. The graphs are plotted for certain values of the inner core mass, a damping coefficient of the vertical

damper, and a stiffness coefficient of the vertical damper. The three curves correspond to three different incident vertical velocity components. It can be seen that maximum displacement of the inner core mass, corresponding to maximum compression of the tennis ball during contact, increases as the incident vertical velocity increases. Also it can be observed from figure 8 that due to presence of the damper in the model, the curves are not symmetrical but are rather asymmetrical. This agrees well with the physical measurements of the tennis ball displacements **[3].**

Vertical velocity as a function of time

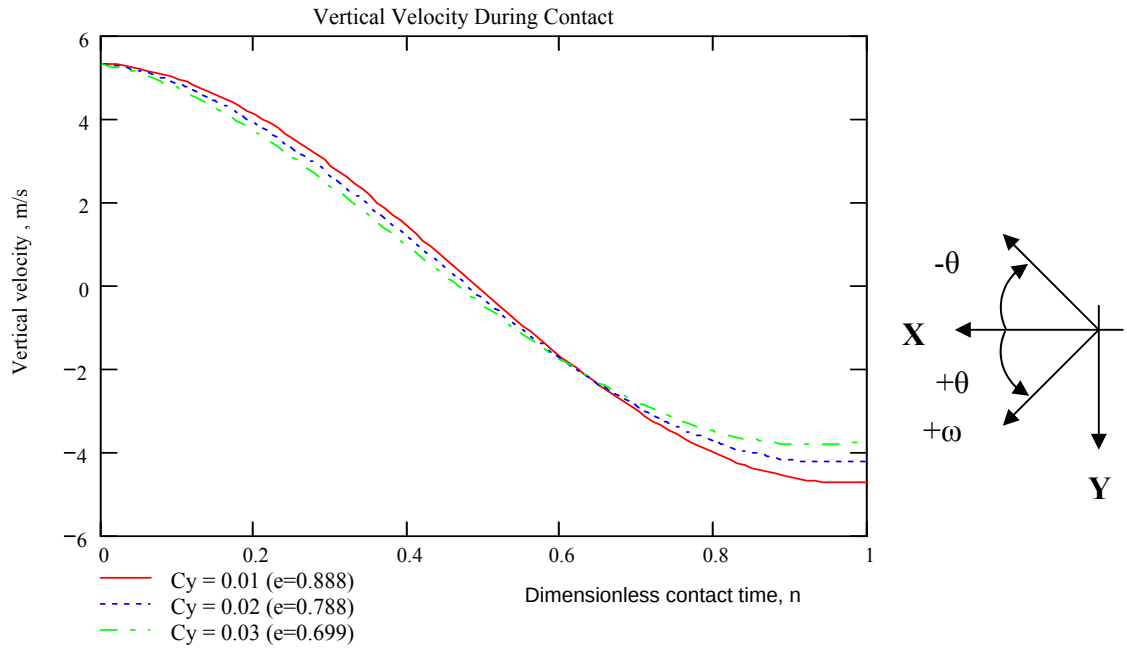

Fig. 9 Vertical velocity during contact as a function of time.

Figure 9 shows the curves of the vertical velocity during the contact as a function of time. The three curves correspond to different coefficients of restitution, which in turn is determined by a combination of the inner core mass, the stiffness of the spring and the

vertical damping coefficient, as can be seen from equation (6). The mass and stiffness are the same in the curves in figure 9, only the damping coefficients are different. Figure 9 indicates that the higher the coefficient of restitution in the vertical direction, the higher is the value of the rebound velocity in the same direction and vice versa. If the coefficient of restitution approaches unity, the rebound velocity in the vertical direction will be almost the same as the incident velocity in vertical direction.

Horizontal velocity as a function of time

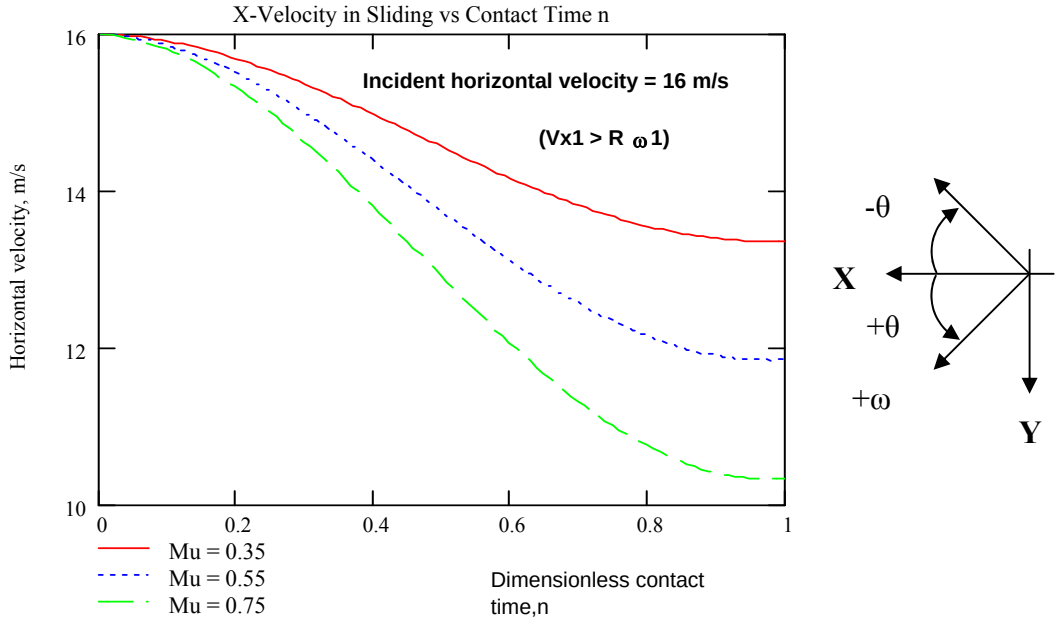

Fig. 10 Horizontal velocity during contact as a function of time.

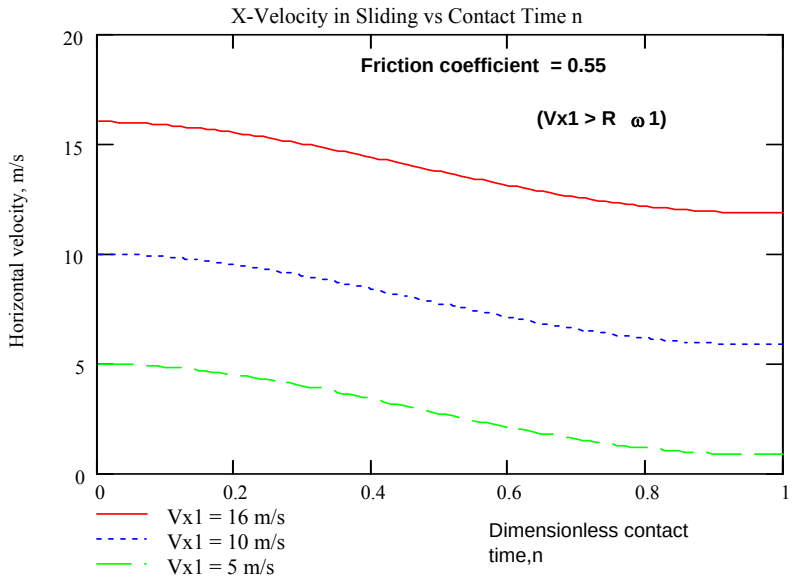

Fig. 11 Horizontal velocity during contact as a function of time(effect of initial velocity).

Figures 10 and 11 show the horizontal velocity of the center of mass of the ball during the sliding scenario as a function of time. There are two graphs for the horizontal velocity during the contact. In figure 10, the incident horizontal velocity is a constant whereas the coefficient of sliding friction is different for the three curves. In figure 11, the coefficient of sliding friction is same, whereas the incident horizontal velocities are different.

In figure 10, it can be seen that the horizontal velocity is decreasing during the contact. This is due to the direction of friction force which is acting in an opposite direction to the incident horizontal velocity for this particular case considered. This is always the case with the zero spin or backspin incidences, but not always for the topspin. The higher the coefficient of sliding friction, the greater is the decline in the horizontal velocity during the contact and subsequently the rebound horizontal velocity. From figure 11, it can be seen that the friction slows down the ball as expected.

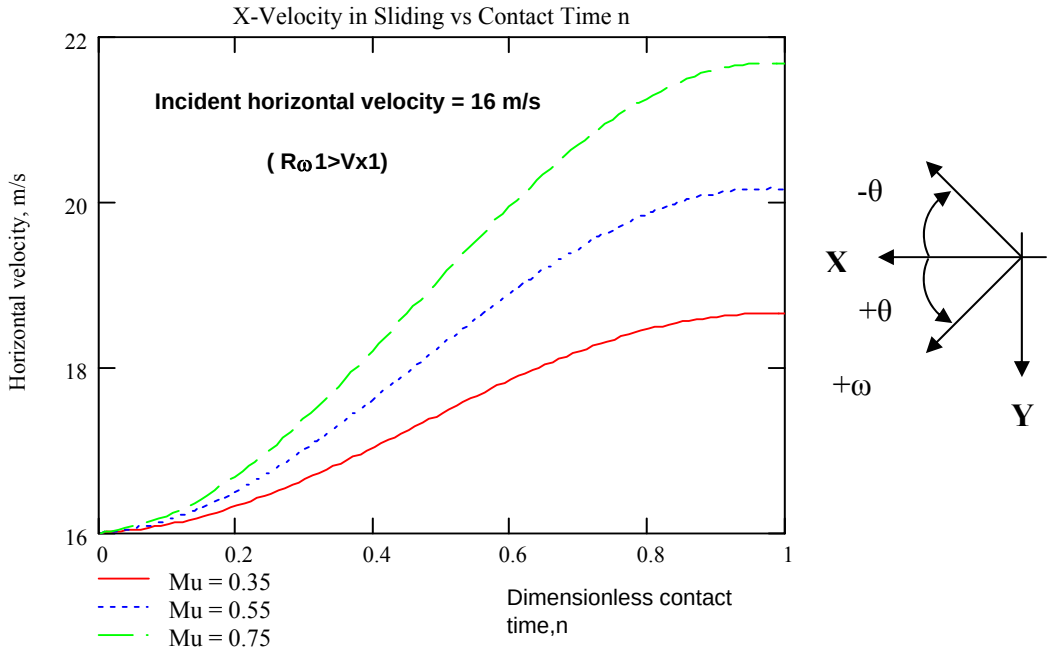

Fig. 12 Horizontal velocity during contact as a function of time(high topspin).

The horizontal velocity during the sliding scenario can also increase during the contact, as shown by figure 12. This can happen only when the ball is incident with a high topspin so that the initial surface velocity due to the spin is greater than the incident horizontal velocity. In this case, the physical situation is reverse of the other cases presented in the other graphs. From figure 12, the higher the friction (corresponding to a higher sliding coefficient of friction), the greater the rebound horizontal velocity.

Angular velocity as a function of time

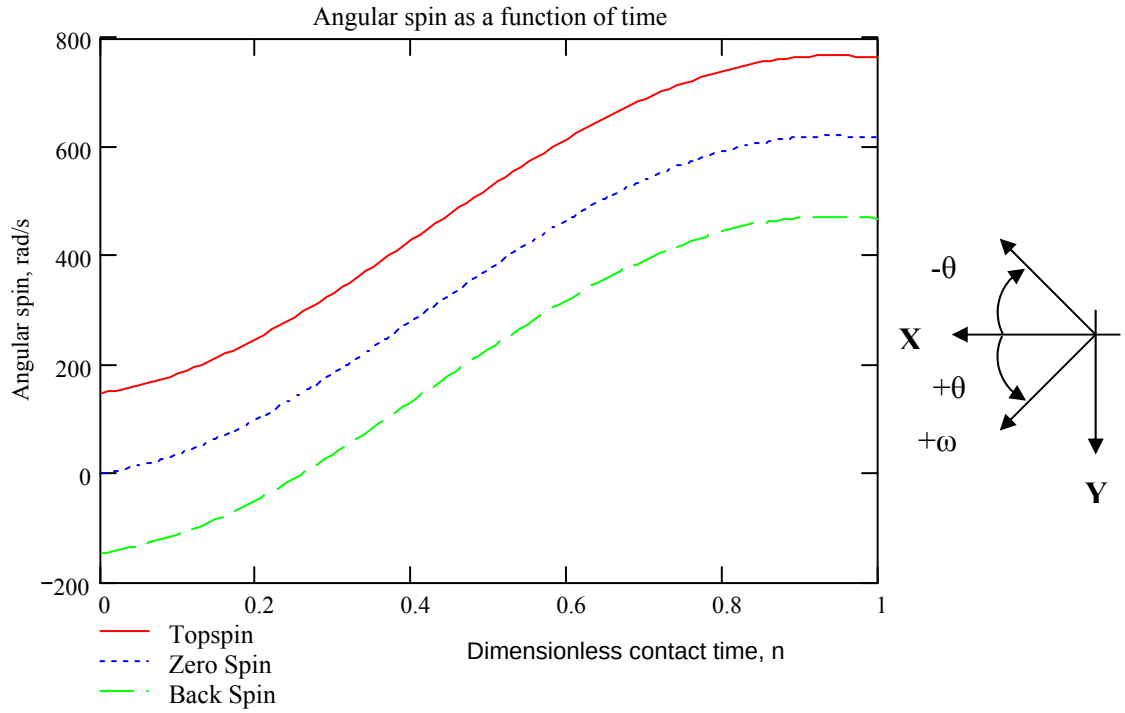

Fig. 13 Angular spin during contact as a function of time.

The angular spin of the outer shell, interpreted as the angular velocity of the ball, is shown in figure 13 for three different incident cases, namely the zero spin, the top spin and the back spin. It can be seen that the angular spin during the contact is increasing as a function of time for all the three cases. The angular spin decreases to zero and then reverses its direction for the back spin, in this particular case considered. For the top spin, the increase in the angular spin occurs when the surface velocity due to the incident spin is less than the incident horizontal velocity, but the angular velocity decelerates for the top spin if the rotational surface velocity at the incidence is greater than the incident horizontal velocity of the center of mass. The reason for the increment of the angular velocity during the contact for all the cases considered here is that the

torque exerted on the outer shell of the model due to the friction force is acting in an anti-clockwise direction (the positive direction as per the coordinate system selected for the analysis of the model) and due to this torque, the outer shell moves in the positive rotational direction and this is the reason that the angular spin increases with time.

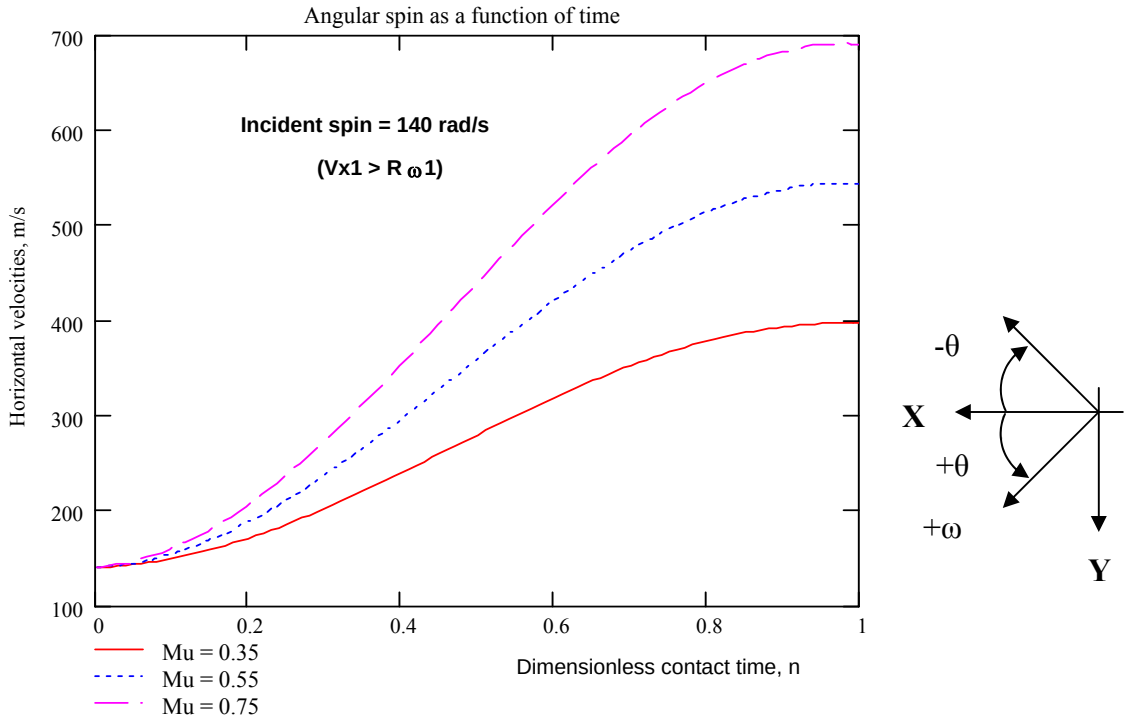

Fig. 14 Angular spin as a function of time.

Figure 14 shows the angular spin as a function of time with an incident top spin. The three curves in figure 14 correspond to three different sliding friction coefficients and indicate that the higher the friction, the more spin the ball will acquire during the contact. This argument always holds true for the zero spin and the back spin cases, but not always necessarily for the op spin incidence. In the top spin case, if the incident

surface velocity due to the spin is greater than the incident horizontal velocity, the friction force acts in a direction opposite to the surface velocity and due to the frictional torque, the angular spin decreases as a function of time, whereas the horizontal velocity increases as a function of time. In that case, then the higher the friction, the lower the rebound angular spin and vice versa.

Normal contact force as a function of time

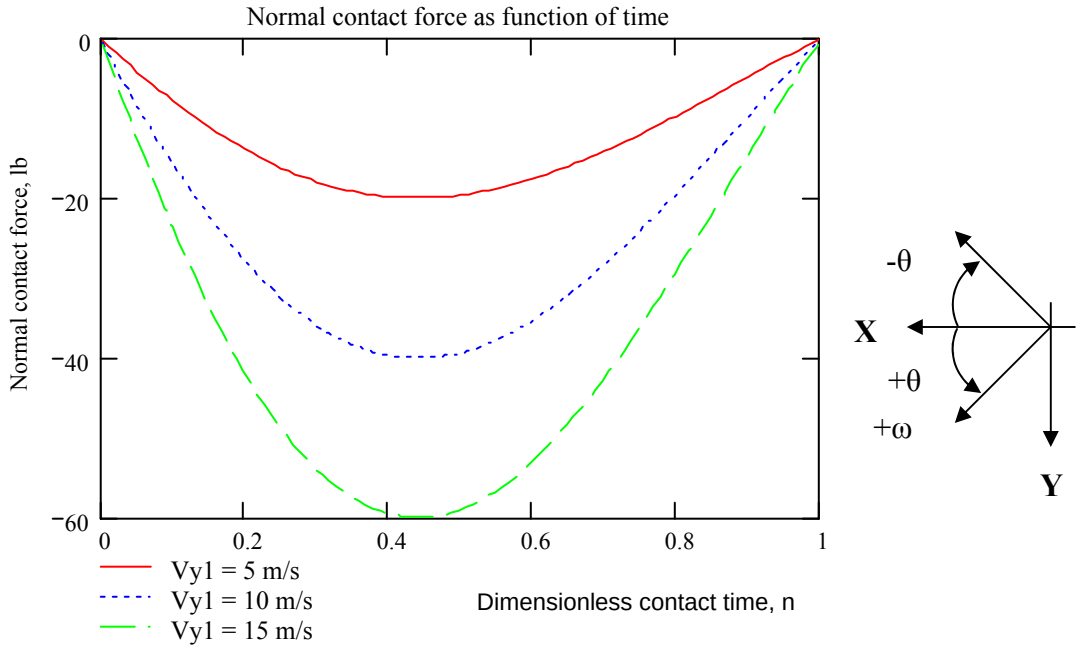

Fig. 15 Normal contact force as a function of time.

Figure 15 shows the normal contact force as a function of time. The three curves correspond to different incident vertical velocities. It can be seen from the curves that the higher the incident vertical velocity, the larger the magnitude of the compressive normal force developed in the spring-damper combination. Physically, it will correspond to a

greater magnitude of normal force exerted on the ball's surface as it comes in contact with the ground. The three curves all correspond to fixed inner core mass, stiffness and damping coefficients. Also, it should be observed from the curves that due to the presence of a finite amount of the damping in the vertical direction in the system, the normal force curves are not symmetrical and their maxima do not occur at n = 0.5, but rather they occur before n = 0.5. This prediction is consistent with the physical measurements of the normal contact forces conducted on the tennis balls **[3,8,10].**

Tangential (frictional) contact force as a function of time

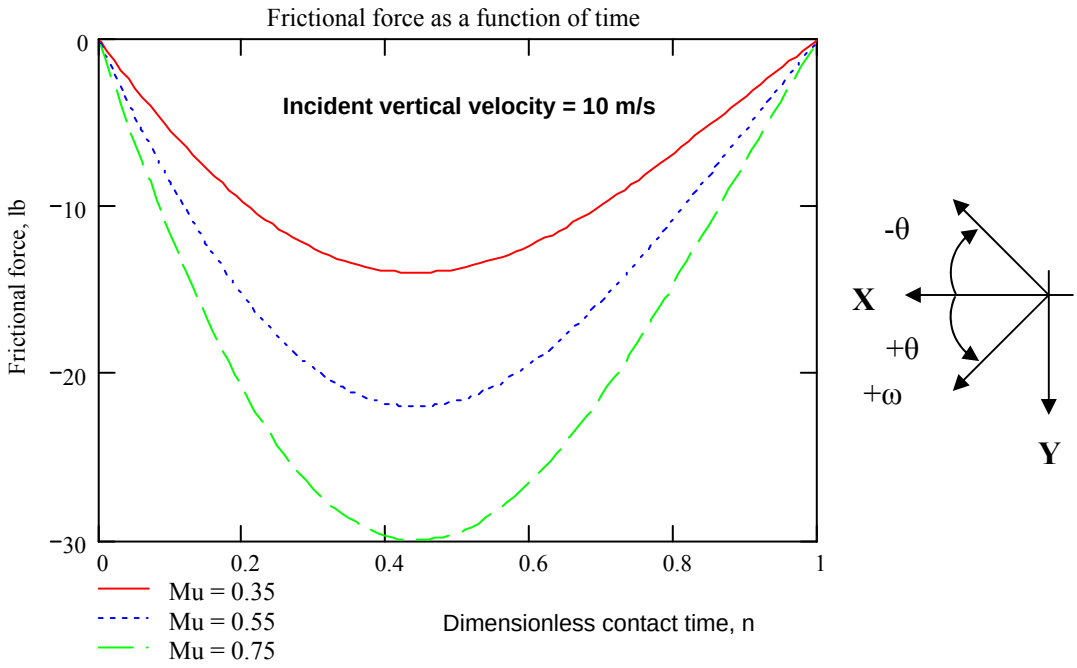

Fig. 16 Frictional force as a function of time.

Figure 16 shows the tangential contact force as a function of time for three different values of the sliding friction coefficients. Due to the direct relationship between the tangential force and the normal force as implied by Coulomb's law for sliding friction, it can be seen that the shape of the tangential force curve during the sliding is the same as the normal contact force curve, only that it is scaled by the friction coefficient factor. The higher the value of the sliding friction coefficient, the greater the magnitude of tangential force during the contact and vice versa. It should be noted that the sliding friction force can also be in the positive coordinate direction, as opposed to the curves shown in figure 16. This can happen when the relative tangential velocity at the point of contact is directed in the negative x-direction. This itself is possible only for the topspin incident, when the surface velocity due to the spin is higher than the incident horizontal component of the translational velocity of the center of mass of the ball.

NO-SLIP THROUGHOUT THE CONTACT

In the no-slip case, the equations for the horizontal velocity, angular spin of outer shell (and the inner core) and the tangential contact force are different from the ones presented for the sliding case. These are presented as follows:

$$\theta(t) = \frac{(\omega(0) - \dot{\theta}_2(0))}{\omega_{d\theta}} e^{-\zeta_\theta \omega_{n\theta} t} \sin(\omega_{d\theta} t) + Ae^{\alpha t} \sin(\beta t) + Be^{\alpha t} \cos(\beta t)$$

$$\dot{\theta}(t) = \frac{-\zeta_\theta \omega_{n\theta}(\omega(0) - \dot{\theta}_2(0))}{\omega_{d\theta}} e^{-\zeta_\theta \omega_{n\theta} t} \sin(\omega_{d\theta} t) + (\omega(0) - \dot{\theta}_2(0)) e^{-\zeta_\theta \omega_{n\theta} t} \cos(\omega_{d\theta} t) + \alpha A e^{\alpha t} \sin(\beta t)$$
$$+ \beta A e^{\alpha t} \cos(\beta t) + \alpha B e^{\alpha t} \cos(\beta t) - \beta B e^{\alpha t} \sin(\beta t)$$

$$\ddot{\theta}_2(t) = \frac{C_\theta}{I_2 + MR^2} \dot{\theta}(t) + \frac{K_\theta}{I_2 + MR^2} \theta(t) + \frac{\varepsilon}{I_2 + MR^2} (C_y \dot{y}(t) + K_y y(t))$$

$$\dot{\theta}_2(t) = \dot{\theta_2}(0) + \frac{C_\theta}{I_2 + MR^2} \int_0^t \dot{\theta}(t) dt + \frac{K_\theta}{I_2 + MR^2} \int_0^t \theta(t) dt$$

$$\dot{x}(t) = R \dot{\theta}_2(t)$$

$$F_X(t) = MR \ddot{\theta}_2(t)$$

The expressions for the vertical displacement, vertical velocity, and the normal contact force remain the same as in the sliding case. The above solutions are implemented in MathCAD software using the code given in Appendix B. These equations are plotted on the following pages:

Angular velocity as a function of time

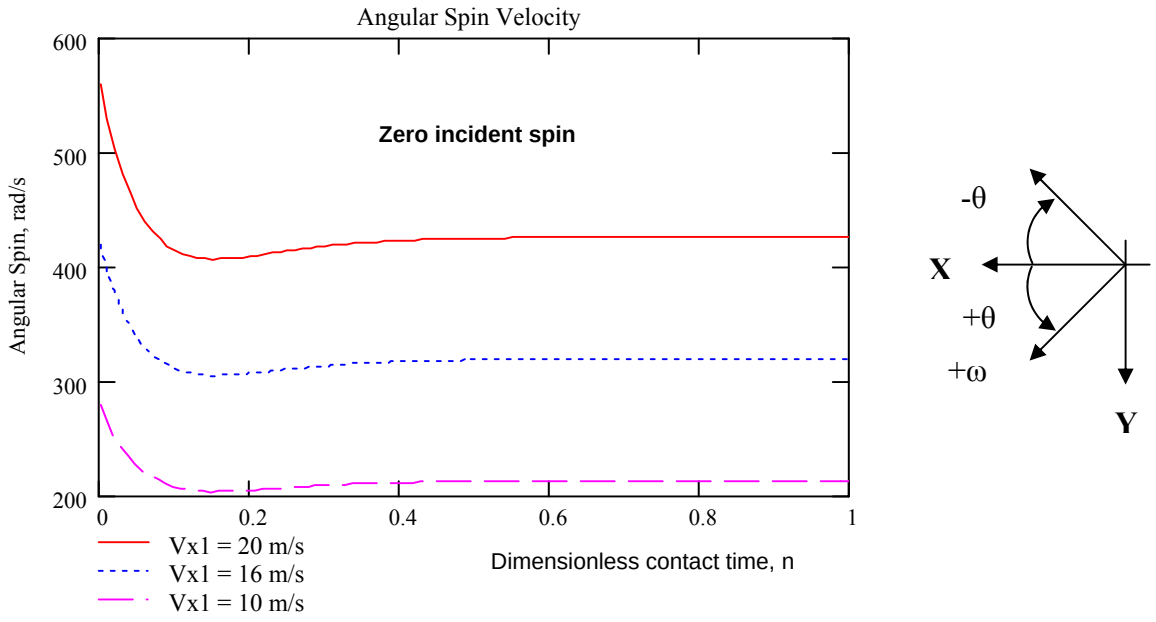

Fig. 17 Rolling angular velocity as a function of time.

Figure 17 shows the rolling angular velocity curves as a function of time, corresponding to three different incident horizontal velocity components and neglecting the effect of the eccentricity of the normal force through the center of the ball. All the curves correspond to the case of zero spin. The curves indicate that the higher the incident horizontal component of the translational velocity, the larger will be the rolling angular velocity. Initial conditions of the spins as shown on n = 0 correspond to the initial condition obtained for the outer shell as indicated on page 20, Chapter II. Thus the curves simply do not start from the initial condition of Vx1/R, but rather from the initial condition as defined in equation (18) for the outer shell. From the curves in figure 17, it is also observed that the spin decreases and well before the contact is over (which occurs at n =1), the angular spin increases and then attains a steady state value. An explanation of this behavior in terms of the model is that since the inner and the outer cores, as far as

the rotational motion is concerned, are connected with a linear torsional spring –damper system, then as soon as the half-period of vibration of the outer core is completed, it is acted upon by torques from the torsional spring and the damper and this causes acceleration of its angular velocity. After this, the angular spin attains the steady-state value. This is due to the high damping of the torsional damper as well as the reason that the frictional force keeps on decreasing in magnitude so that frictional torque is balanced by the internal torques, namely from the spring and the damper. As a result, any further vibrations die out and the outer core rotates as a rigid body with almost a constant value of the angular spin, towards the end of the contact. This initial deceleration of the spin and attainment of a steady-state value is always the case with the zero spin and backspin impacts, but not always necessarily for the topspin impacts.

It should be noticed that the curves as shown in figure 17are not the only possibility of the motion of the outer shell. If the initial angular spin of inner core is higher than the initial spin velocity of the outer shell compatible with the rolling, which is determined in Chapter II, only for the case of the topspin, then in that case, the outer shell will be accelerated instead of being retarded, because the initial torque acting on the outer shell from the torsional damper will be acting in the positive rotational direction. The graphs for such a case of topspin are presented in figure 18 on the next page.

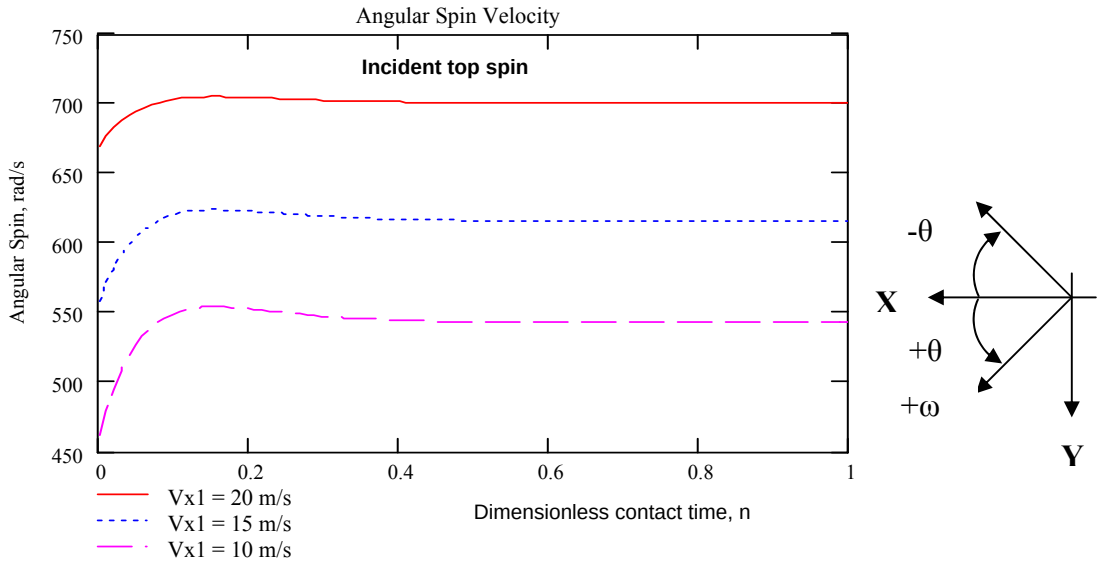

Fig. 18 Angular spin of outer shell as a function of time (Special case of topspin).

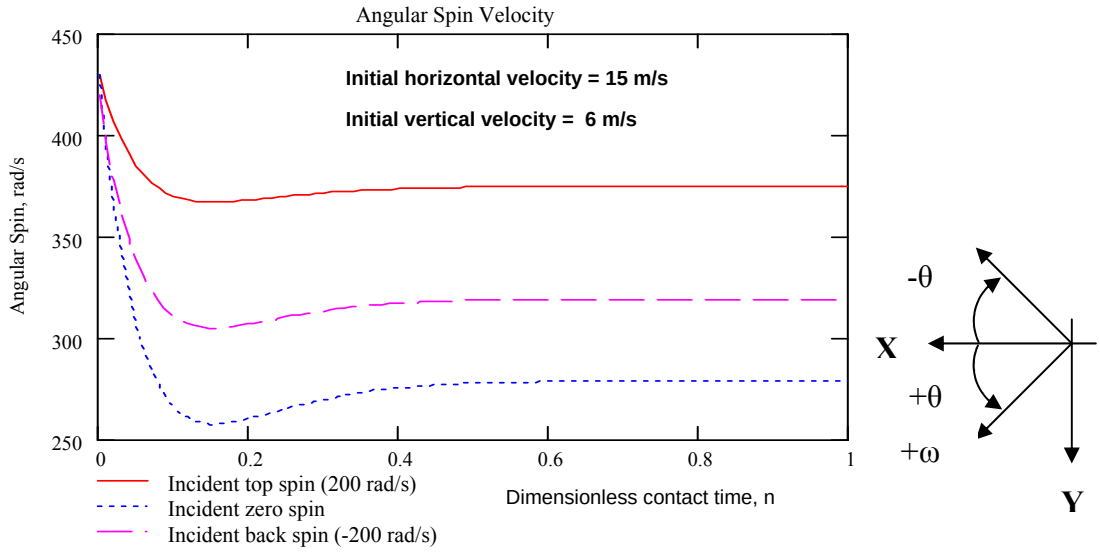

Fig. 19 Angular spin of outer shell as a function of time.

In Figure 19 are shown the angular spin curves of the outer shell corresponding to three different incident spins of the ball. The curves correspond to the zero spin, the topspin and the backspin impact, when the angles of incidence and the incidence translational velocities are the same for all the three cases. The curves indicate that the outer shell will rotate at a higher spin for the topspin impact as compared to the zero spin and the backspin. The backspin yields the lowest value of the rolling angular spin. This is due to the reason that in the model considered, the initial torque opposing the spin of the outer shell will be highest for the backspin, due to its spin direction as compared to either of the zero spin or the topspin. For the top spin, the initial torque will be lower than the zero spin, because this torque is proportional to the difference in initial angular spins of the inner mass and the outer mass. Since the difference in initial angular spins is less for the topspin case and hence the value of the initial torque opposing the spin of the outer shell is less as compared to the zero spin, the outer shell will spin faster as compared to the zero spin. As the outer shell rotates, the torsional spring connecting the inner and the outer masses starts winding. When it is unwinded, it starts exerting a torque on the two masses causing an acceleration for the outer shell and deceleration for the inner core. In figure 19, this acceleration of the outer shell is indicated as a hump in the curves of the angular spin velocities.

Finally, the effect of offset distance from the horizontal coordinate of the center of mass of the system to the normal reaction force, neglecting the weight of the outer shell, can be observed on the angular spin of the outer shell as shown in figure 20 on the next page. From figure 20 on the next page, it can be seen that the higher the offset distance, the lower the rolling spin, keeping the rest of the dynamic parameters as same. The effect of the offset is often referred to as “rolling friction”.

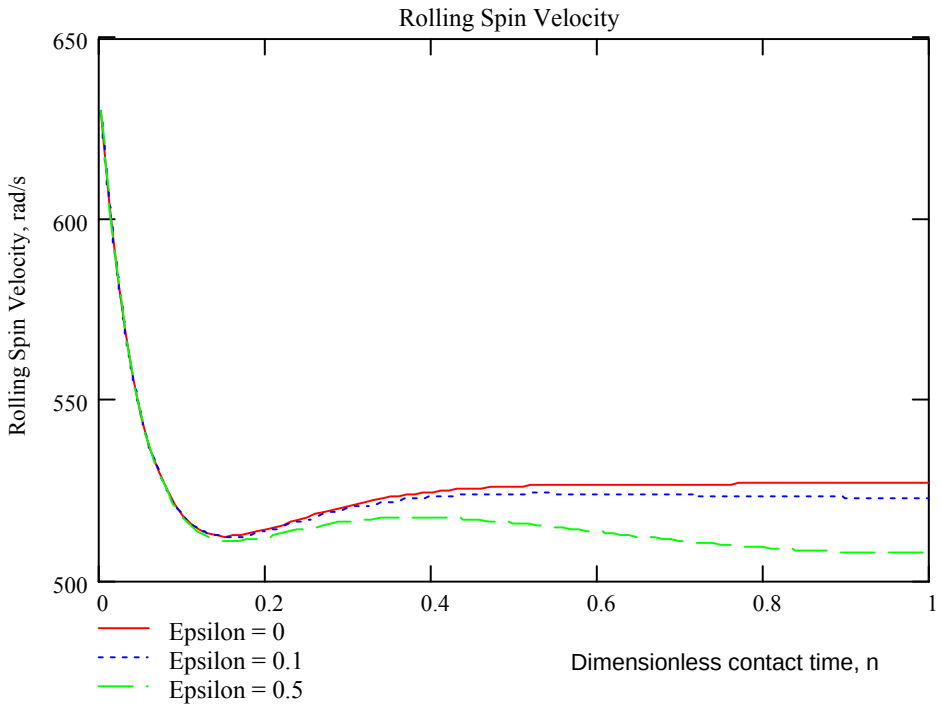

Fig. 20 Angular spin velocity as a function of time (effect of offset distances).

Figure 20 shows curves corresponding to three different offset distances. The graphs indicate clearly that the torque developed by the normal force due to the offset (which happens pronouncedly when the incident vertical component of the velocity gets higher and higher) slows down the angular spin during the rolling motion. It develops a torque which acts on the outer shell and opposes its angular spin. This is true for the cases of zero spin, topspin and backspin. For the zero offset distance, it can be seen that the rolling angular velocity attains almost a steady-state value well before the contact ends.

Horizontal velocity as a function of time

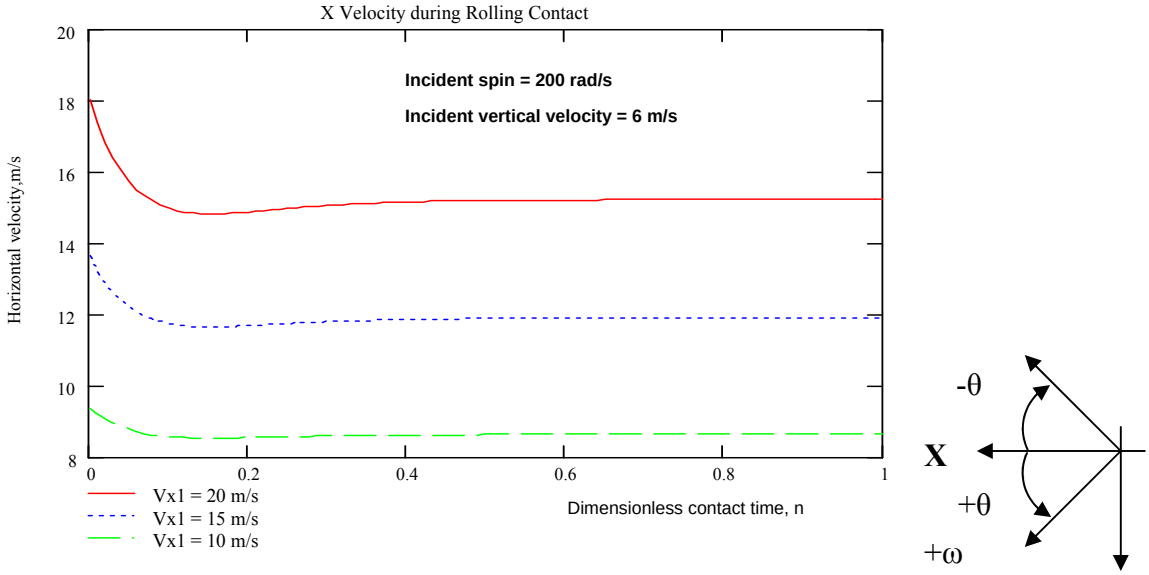

Fig. 21 Horizontal velocity as a function of time (effect of initial conditions).

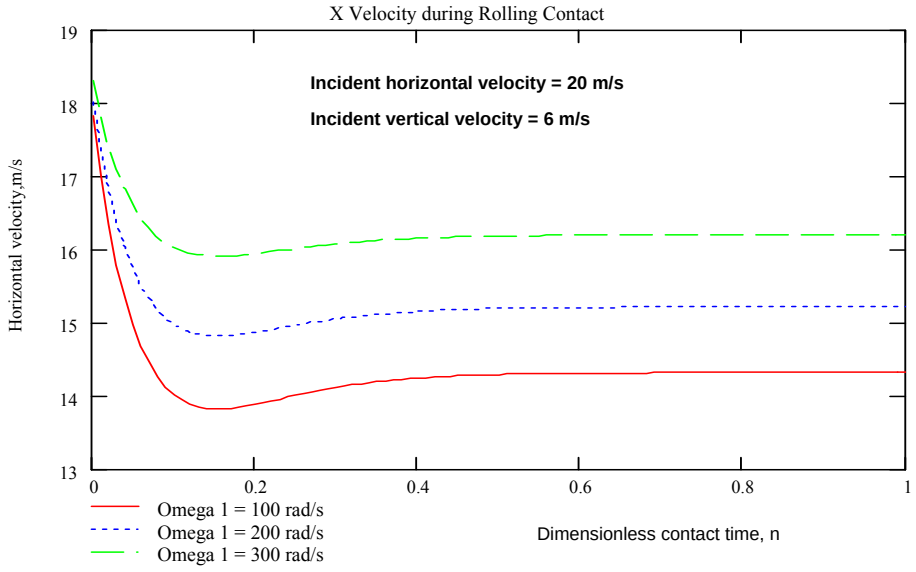

Fig. 22 Horizontal velocity as a function of time (effect of spin).

Figures 21 and 22 on the previous page (figures 21 and 22) show the horizontal velocity of the center of mass of the two-mass elastic system as a function of time during the no-slip case. Figure 21 corresponds to three different incident horizontal velocities of the center of mass. Figure 22 corresponds to three different incident spins. All cases are for the topspins. For the zero spin and backspin, trends of the curves will be the same.

From figure 21, it can be seen that the horizontal velocity during the contact decreases as a function of time. The higher the initial incident horizontal velocity, the larger will be the rebound value of the horizontal velocity. In this graph, only the incident horizontal speeds are different; the rest of the parameters used to generate the curves are identical. From figure 22, it can be seen that the ball incident at a higher spin but with the same value of incident horizontal velocity, will rebound at a higher horizontal velocity. Thus its angle of rebound will be lower for higher incident spin, if its starts rolling.

Tangential contact force as a function of time

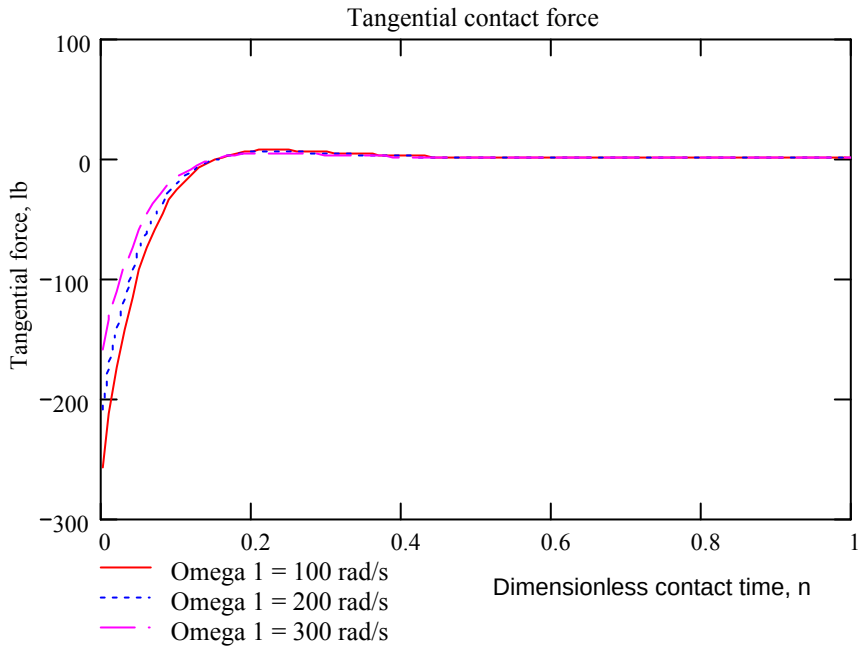

Fig. 23 Tangential friction force as a function of time.

The tangential friction force(maintaining the no-slip constraint) as a function of time for three different incident spins is shown in figure 23. From the graphs in figure 23 it can be seen that the tangential force magnitude increases with less spin and vice versa. It can be seen that the frictional force starts from negative values, thus validating that it will retard the horizontal velocity during the contact, as can be seen from the previous graphs. The force graph eventually attains the steady value very near to zero. Thus the friction force decreases with time to such an extent that its magnitude becomes almost equal to zero and then the outer shell starts rotating as a rigid body subjected to no torques (either from the spring-damper or the friction).

TRANSITION BETWEEN SLIDING AND ROLLING DURING CONTACT

Based on kinematic parameters presented for the cases of the sliding and the rolling, it is now possible to determine transition from the sliding to the rolling motion during the contact of the ball with the ground. This transition usually takes place when the ball is incident at large angles of incidence. The transition from the sliding to the rolling motion during the contact can occur for all of the zero spin, the topspin and the backspin impacts.

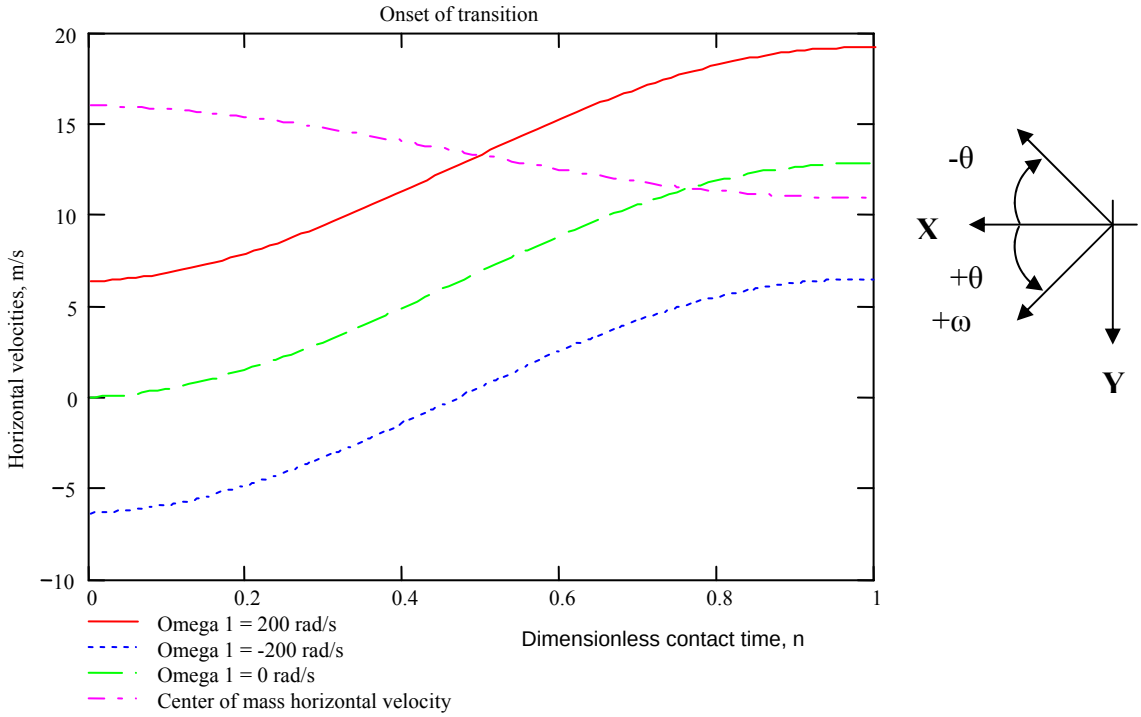

Fig. 24 Transition from sliding to rolling motion.

Figure 24 shows curves of the angular spin during the sliding scenario, multiplied by R corresponding to three different incident spins and the horizontal velocity of the

center of mass of the system. The curves correspond to a specific sliding friction coefficient and the other parameters are the same for each curve. It can be seen from the curves that the horizontal velocity curve intersects the topspin curve at a smaller value of 'n' as compared to the zero spin. For this particular case, it does not intersect the backspin curve at all. The intersection point of the curves physically implies the introduction of the kinematic no-slip constraint, due to which the sliding motion ceases and the ball starts rolling during the contact for remainder of the contact. It can be seen that the topspin actually helps in getting to the rolling mode earlier than either of the zero spin or the backspin. The rolling can occur for the backspin case, but then it is a strong function of the sliding friction coefficient of the surface, the horizontal component of incident velocity as well as the vertical component (angle of incidence) and the magnitude of the incident backspin itself. If the ball is incident at a high value of backspin and the angle of incidence is low with a high value of the incident horizontal velocity, it will keep on sliding throughout the contact, unless the sliding friction coefficient is very high (around 0.7 to 0.9). This is all easily deducible from the velocity and the angular spin curves. In the sliding, it has been observed that the rebound horizontal velocity decreases as the coefficient of friction increases and the incident horizontal velocity is decreases. This physically means a rough surface with a high friction force and a lesser initial velocity (high incidence angle). Due to the high friction force, the velocity reduces at a higher rate (more deceleration) and a stage is reached when the horizontal velocity of the center of mass and the surface velocity due to spin become equal (the angular spin is accelerating at the same time due to the friction torque acting on it). When this stage is reached, as shown by the intersection points of the curves, the relative velocity of the contact point with respect to the ground becomes zero and it starts rolling. This can be taken into account in the solutions of the equations of motion for the spin of the outer shell and the horizontal velocity of the center of mass by using in the solutions for the rolling the limits from the instant '$n_r tc$' to t_c, instead of from 0 to 't_c' where 'n_r' corresponds to the fraction of time of the total contact time where the curves intersect. When the two solutions are combined in this piecewise

manner, this will represent a complete solution including the transition from the sliding to the rolling mode of motion.

EXAMPLES FOR ILLUSTRATING THE APPLICATION OF EQUATIONS

In order to illustrate the application of the equations of motion and their solutions as outlined in Chapters II and the beginning of Chapter III, two examples of impact of the tennis ball with the ground are considered, which are simulated by the two-mass model. The examples will be the impact of the ball with the ground having friction at a low angle of incidence and a high angle of incidence with the topspin in each case, such that the incident horizontal velocity component is greater than the surface velocity due to the spin. Thus in both cases, the initial contact point velocity will be in the positive direction.

For the first case of impact simulation, consider the case of a ball incident with translational velocity of 17 m/s of the center of mass, with the topspin of 100 rad/s and an angle of incidence of around 18 degrees, measured with respect to surface of the ground. This is a really shallow angle of incidence. The initial conditions for impact are calculated as follows:

$$V_{X1} = V\cos\theta_i = 17\cos(18^0) = 16.13 \text{ m/s}$$

$$V_{Y1} = V\sin\theta_i = 17\sin(18^0) = 5.33 \text{ m/s}$$

The values calculated are the initial conditions for the motion in X and Y directions, respectively. The given value of the topspin of 100 rad/s is the initial condition for the spin motion. Suppose further that the surface with which the ball strikes is acrylic surface for which the coefficient of sliding friction is around 0.55. Also, the vertical coefficient of restitution on this surface can be taken as around 0.76.

In order to simulate the above impact problem with the help of the two mass model, first of all, a selection of the dynamic parameters for the two-mass model is required such that their combination makes the vertical coefficient of restitution as 0.76.

Accordingly, the dynamic parameters are selected as follows: Inner core mass, 2M/3, outer shell mass M/3. Stiffness coefficient , 80 lb/in (14040 N/m). However, in order to determine the damping coefficient C_y, equation (6) must be used. Using equation (8) in Chapter II, the value of C_y that gives the vertical coefficient of restitution as 0.76 is found out as:

$$C_y = 0.0113 \text{ lb-s/in (1.984 N-s/m)}$$

For selecting the rotational parameters, the inner and outer core mass moments of inertia are selected as 0.532I and 0.468I, respectively (Chapter II). The torsional stiffness coefficient of the torsional spring is selected as 1000 lb-in/rad (113.26 N-m/rad).

On the basis of assumption that the damped periods of the relative spin and the vertical motion are equal, the damping ratio in the rotational motion can be calculated as follows:

$$\omega_{d\theta} = \omega_{dy}$$

$$\omega_{n\theta}\sqrt{1-\xi_{\theta}^{\ 2}} = \omega_{ny}\sqrt{1-\xi_{y}^{\ 2}}$$

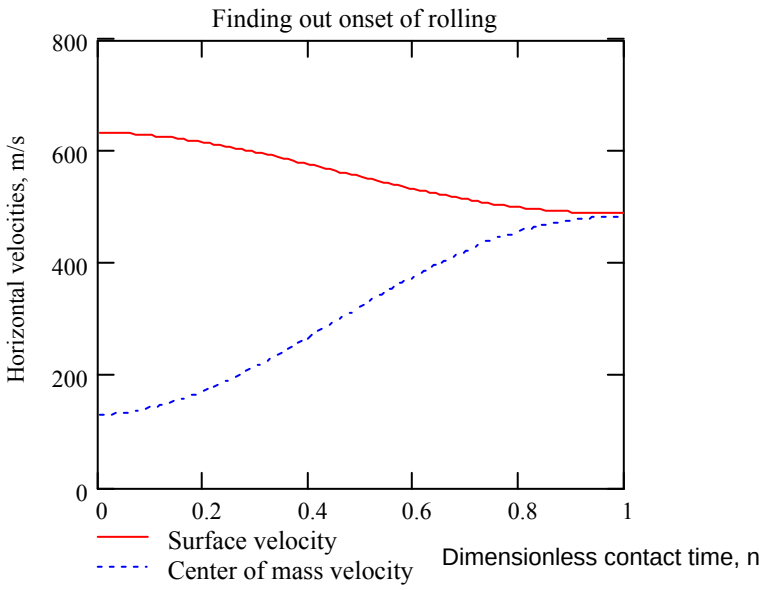

Fig. 25 Surface and center of mass velocities during contact.

Next, the horizontal velocities of the center of mass of the two-mass system and surface velocity of the outer shell are plotted on the same graph as shown in figure 25. This is done to find out if with the choice of the selected parameters, there is an onset of the rolling motion during the contact or that there is simply the sliding motion right till the end of contact. From figure 25, it can be seen that the graphs do not intersect during the contact time, indicating that the rolling does not occur and the ball keeps on sliding during the contact. Hence there is no need for the piecewise solution during the contact in this scenario, since there is no rolling.

Thus in this case, the horizontal component of the velocity at rebound is 12.667 m/s, as read from the graph, at n=1 and found out from MathCAD software.

$$V_{X2} = 12.461 \text{ m/s}$$

The rebound value of the spin of the outer shell is:

$$\omega_2 = 371.586 \text{ rad/s}$$

Positive sign of the spin velocity indicates that the rebound spin will be an increase of topspin. Comparing the value of the rebound with the incident spin, it can be seen that the spin value increases by more than twice, due to the friction torque acting on the outer shell which accelerates the spin.

The value of rebound angle is:

$$\theta_r = a\tan(\frac{V_{Y2}}{V_{X2}}) = a\tan(-\frac{4.053}{12.461}) = -16.644^0$$

The contact force graphs are plotted as follows:

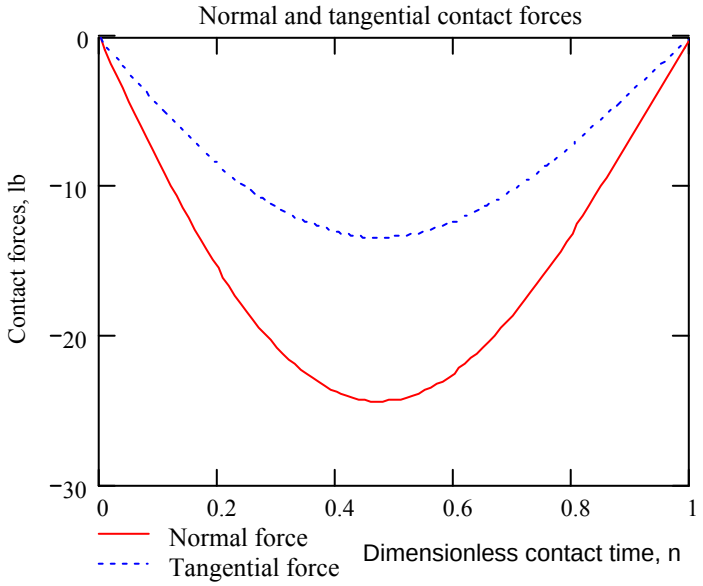

Fig. 26 Normal and tangential contact forces.

Figure 26 predicts the variation of the normal and the tangential contact forces with the contact time.

The value of the time-averaged coefficient of friction for this case can be calculated using equation (63) in Chapter II as follows:

$$\overline{\mu} = 0.400$$

This value is not greatly less than the value of the coefficient of sliding friction, which is 0.5. This shows that indeed in this case, the sliding occurs throughout the motion of the ball. This is also verified from figure 25, which shows that the ball does not start pure rolling during contact.

Consider the next case of impact simulation, in which the incident angle is increased from 18 degrees to 42 degrees, measured with respect to the ground surface. The incident topspin is 100 rad/s, whereas the incident translational velocity is 17 m/s. Thus the initial conditions for impact are calculated as follows:

$$V_{X1} = V\cos(\theta_i) = 17\cos(42^0) = 12.63 \text{ m/s}$$
$$V_{Y1} = V\sin(\theta_i) = 17\sin(42^0) = 11.37 \text{ m/s}$$

Values of the dynamic parameters for both the vertical as well as the rotational parameters are the same as for the first case.

The vertical component of the velocity at the rebound can be evaluated from the value of vertical coefficient of restitution as:

$$\therefore V_{Y2} = -8.646 \text{ m/s}$$

Next, the center of mass velocity and the surface velocity, both in the X direction, are plotted on the same graph to ascertain whether there is an onset of the rolling during the ball's contact with the ground:

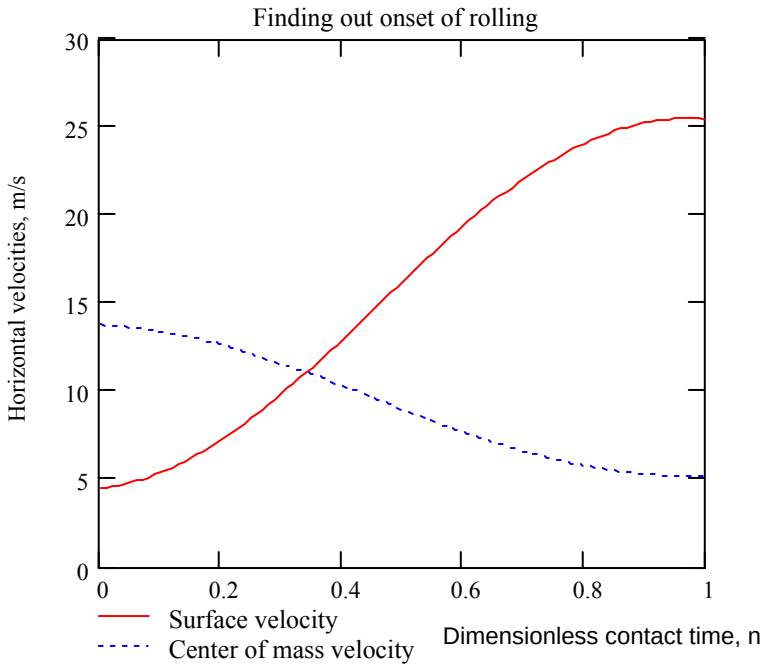

Fig. 27 Horizontal velocities of the two-mass model.

From figure 27, it can be seen that unlike the first case, the graphs intersect at around n = 0.35 (exact value is n = 0.342 as found from MathCAD code). Hence the rolling motion begins during the contact time as early as before half of the contact time is elapsed.

This indicates that the ball will not keep on sliding during the contact: more than 50 % of its contact time is spent in the rolling or the no-slip mode, in this particular case.

It is important to accommodate this transition and then connect the piecewise solutions of the sliding and the rolling to form a complete solution.

In order to complete the solution, the solution for the sliding velocities for both the horizontal velocity of the center of mass of the model as well as the angular spin of the outer shell should start from time n = 0 to n = 0.342. At n = 0.342, the rolling or the no-slip solution takes over from the sliding solution. The values of the horizontal velocity of mass center as well as the spin, at this particular intersecting point of the graphs, form the initial conditions for the rolling equations, as well as the value n = 0.342 which becomes the lower limit of integration for the solutions of the angular spin in the rolling contact. Applying these conditions and using the code in MathCAD, the graphs of the horizontal velocity of the mass center and the angular spin of the outer core are depicted in figure 28 on next page.

As can be seen from figure 28, the solutions are piecewise. The break in the graphs indicates the instant of time during the contact at which the sliding motion ceased and the rolling took place.

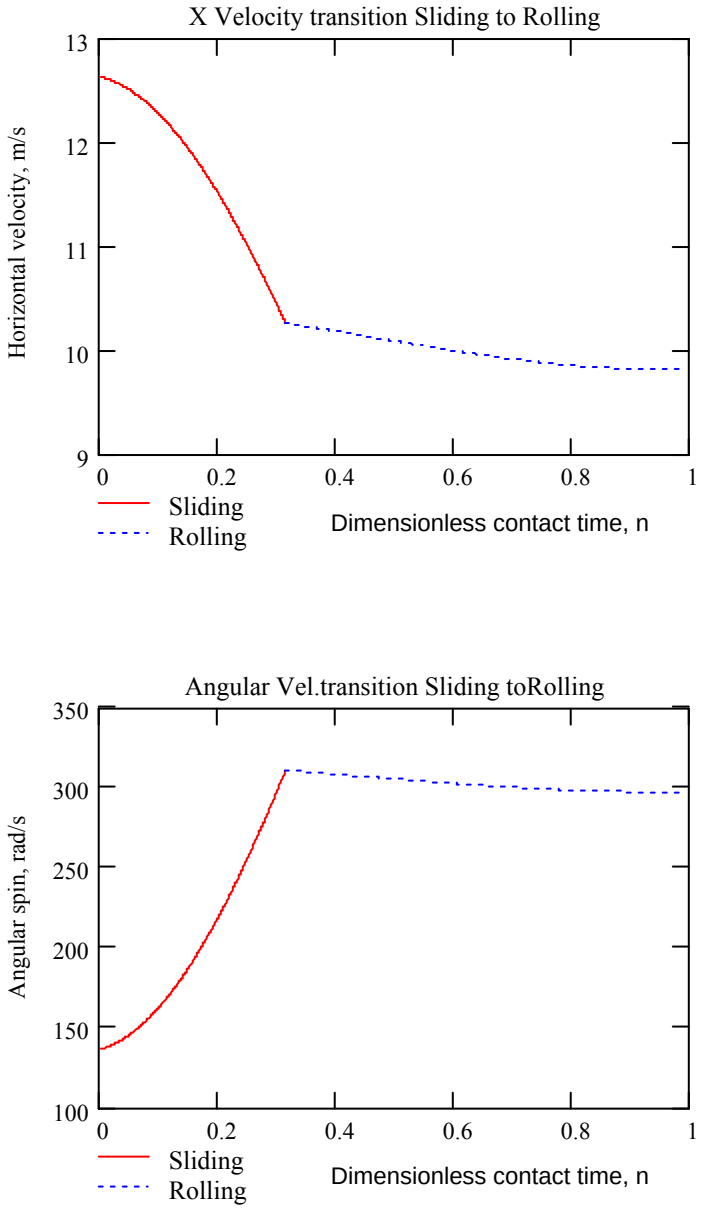

Fig.28 Horizontal and spin velocities during contact.

The rebound values can be obtained from the MathCAD code (as well as less accurately from end points of the graphs) as:

$$V_{X2} = 9.813 \text{ m/s}$$
$$\omega_2 = 297.181 \text{ rad/s}$$

The angle of rebound with respect to the surface is thus:

$$\theta_r = a\tan(\frac{V_{Y2}}{V_{X2}}) = a\tan(-\frac{8.646}{9.813}) = -41.38^0$$

The magnitude of rebound velocity is:

$$V_2 = \sqrt{{V_{X2}}^2 + {V_{Y2}}^2} = 15.99 \text{ m/s}$$

The value of average coefficient of friction, as calculated from equation (63), is:

$$\overline{\mu} = 0.127$$

The value is appreciably less than the coefficient of sliding friction, which is 0.55. This shows that the transition indeed takes place and hence the motion changes from sliding to rolling as indicated by figure 28.

This completes the rebound motion predictions for both the cases.

CHAPTER IV

EXPERIMENTAL DATA

In this chapter, two major experimental measurements for the tennis ball are described: the impact and rebound kinematics for three spin options, namely the zero spin, the topspin and the backspin **[1]**. These results are taken from the doctoral thesis of J.C.Wang, 1989, who conducted the experiments on the dynamics of the tennis balls and evaluated the rebound kinematics of the tennis balls given varying conditions of incident kinematics. The second experimental measurement is that of the mass moment of inertia of the tennis ball using a simple setup. This second measurement has been conducted by the author to determine an estimate of the numerical value of mass moment of inertia of the tennis ball, in order to use this value for the simulations of the tennis ball (Chapter V).

EXPERIMENTAL PROCEDURE

As mentioned in Wang **[1]**, the experimental procedure used to conduct the study of the incident and the rebound kinematics consists of an experimental design, test equipment, and apparatus. Following this, the data obtained is digitized and analyzed to convert the experimental results into the numerical values. The experimental test equipment consists of a ball pitching machine, an acrylic test surface, a camera in a single frame mode, two strobotacs for providing flashes of light at the impact point, operating at 20,000 flashes per minute, a function generator used to control the time period between the flashes of the strobotacs and a counter-timer, which is used to check the period of the flashes of the strobotac lights and check if there is any error in the period.

The stroboscopic photography is a relatively modern technique for understanding and analyzing the motion of bodies. Since a camera usually can not take many pictures in a short duration of time, for example, of an impact (the impact duration is of the order of milliseconds), the strobotacts provide basis of what is called as stroboscopic photography. As soon as the ball hits the impact point on the surface, the camera shutter is opened for around one second and at the same time, a picture is taken. However, the strobotact lights are also flashing at the object of interest, in this case, a tennis ball, for as short as duration of 1 microsecond and about 20,000 times per minute. This illuminates the object for a very short duration and hence in a sense, divides 1 second picture of the camera, which otherwise would be a still picture, in a sequence of images due to the strobotac flash images. This produces the perception of a continuous motion as a sequential motion in one single picture of the camera. This produces what is called as the stroboscopic effect. The schematic of the arrangement is shown in Figure 29.

Based on this procedure, the tennis ball's images before, during and after the contact were developed. The images were then transferred into a digitizing board and a coordinate system was established there, that marked coordinates of the center of mass of the ball, point where the ball touches the test surface, and two-cross points across the diameter of the ball (that were marked before the experiment to ascertain the angular spin). Once the coordinates were located, the incident and the rebound velocities were calculated using the sequential images from the stroboscopes and dividing the difference of the respective X and Y coordinates by the strobe period, which was 0.003 seconds.

However, there is a possibility of an error in analysis of the data in a sense that for the impact and the rebound kinematics, the coordinates were located for the tennis balls that were slightly before impact and slightly after impact, not at the exact point where the incidence and rebound occurred [1].

In order to get to the impact points and the rebound points, the linear curve fit based on the images before the impact and after the impact was utilized. This may introduce some error in the estimation of the horizontal and vertical velocities, because even if the force in X direction is neglected, the ball will follow a parabolic trajectory, instead of a linear path, as is assumed in the data analysis.

This in turn affects the angle of incidence and the rebound, and based on the equations mentioned in [1], this as well affects the incident and the rebound spin. This might be a source of error in the data analysis as shown in **[1]** by the values of standard deviation in the experimental values of the kinematics.

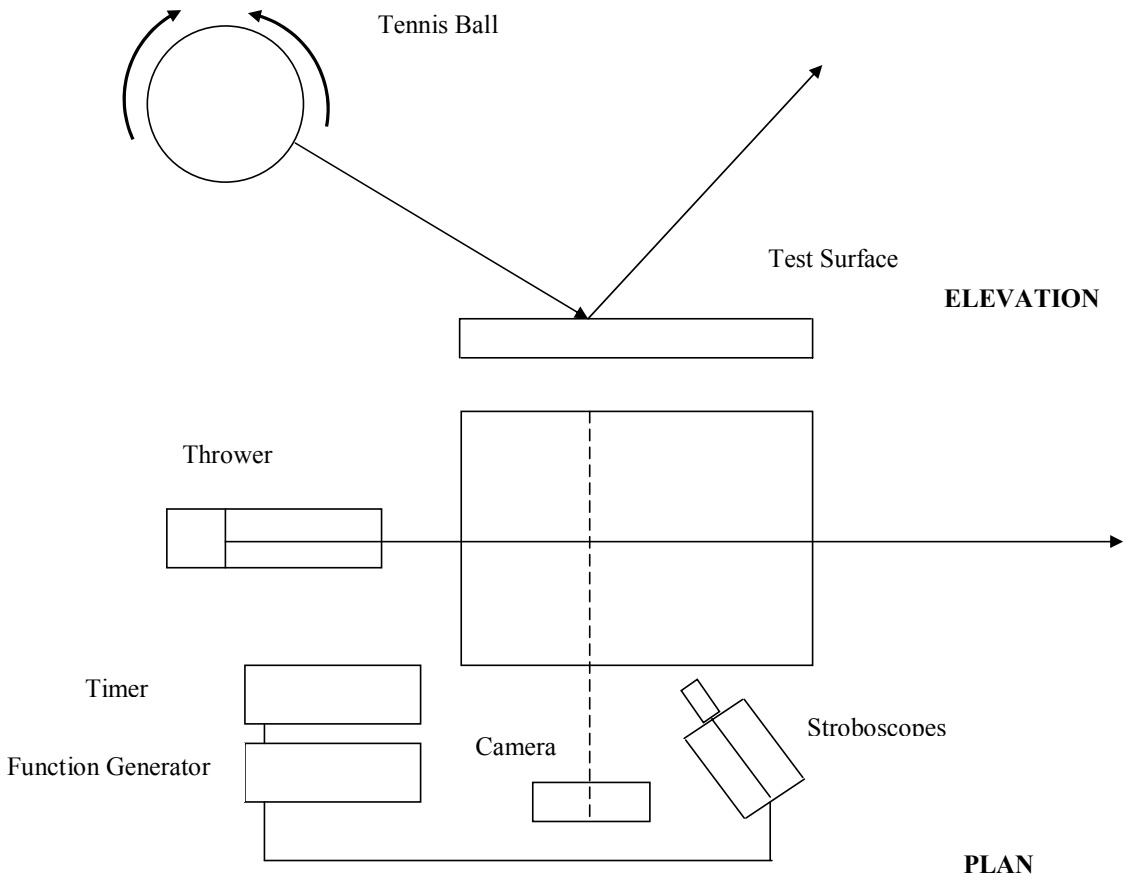

Fig. 29 Schematic drawing of experimental arrangement **[1].**

Wang's data has been used by this author to construct Tables 1 to 6 and Figures 30 to 32. Experimental results for the impact and rebound kinematics are shown in tables 1 through 6. The experimental results are arranged such that the first five columns in each table indicate the incident kinematics, arranged in the order of incidence angle, the horizontal component of velocity at incidence, the vertical component of velocity at incidence, the resultant translational velocity of the center of mass of the ball at incidence, and the angular velocity of the ball at the incidence. The remaining five columns indicate counter-part kinematics parameters at rebound from the ground, in exactly the same order.

All the angles are measured in degrees, the translational velocities and the components are all measured in meters per second, and the angular velocities are measured in radians per second.

For each of the cases of the zero spin, the topspin, and the backspin, there are two tables. The first table has already been described, whereas in the second table, along with the incoming and the rebound kinematics are shown the coefficients of restitution in the vertical and the horizontal directions, and kinetic energies, immediately before and after the impact.

The vertical coefficient of restitution for each angle of incidence is calculated by dividing the negative of the vertical rebound velocity by the vertical incident velocity, whereas the horizontal coefficient is obtained by the ratio of the rebound horizontal velocity to the incident horizontal velocity.

The kinetic energies immediately before and after the impact are determined from the resultant values of the translational velocities of the center of mass of the ball (V_1 and V_2) and the spin speeds (ω_1 and ω_2). The equations used to evaluate the kinetic energies from the given data are:

$$T_1 = \frac{1}{2} M V_1^{\,2} + \frac{1}{2} I \omega_1^{\,2}$$

$$T_2 = \frac{1}{2} M V_2^{\,2} + \frac{1}{2} I \omega_2^{\,2}$$

It will be seen from the experimental data that the calculated values of the kinetic energies indicate there is a loss of kinetic energy associated with each of the impacts. These losses are a result of the friction force acting on the ball as well as the damping associated with the bounce of the ball in the vertical direction.

Figures 30 through 32 show the experimental results on the tennis ball in graphical form.

Table 1 Incidence and rebound kinematics with incident zero spin

θ_i (Degrees)	V_{X1} (m/s)	V_{Y1} (m/s)	V_1 (m/s)	ω_1 (rad/s)	θ_r (Degrees)	V_{X2} (m/s)	V_{Y2} (m/s)	V_2 (m/s)	ω_2 (rad/s)
17.13	15.62	4.81	16.36	-5.34	-20.83	11.09	-4.22	11.73	239.1
22.85	15.62	6.71	17.00	2.61	-32.39	8.84	-5.76	10.55	313.2
34.47	14.49	9.95	17.59	-1.1	-45.04	7.66	-7.66	10.84	293.31
41.1	13.46	11.74	17.87	23.46	-50.33	7.25	-8.73	11.36	239.99
48.55	11.7	13.25	17.70	10.63	-55.37	6.47	-9.37	11.4	213.17
58.94	9.16	15.19	17.74	10.63	-70.42	3.87	-10.87	11.54	144.69
67.84	6.57	16.14	17.44	1.15	-76.12	2.74	-11.09	11.44	96.25

Table 2 Incidence and rebound kinematics for zero spin impact (with restitution coefficients and kinetic energies)

θ_i (Degrees)	V_1 (m/s)	ω_1 (rad/s)	θ_r (Degrees)	V_2 (m/s)	ω_2 (rad/s)	ε_y	ε_x	T_1 (lb-in)	T_2 (lb-in)
17.13	16.36	-5.34	-20.83	11.73	239.1	0.87734	0.70999	68.181	44.823
22.85	17.00	2.61	-32.39	10.55	313.2	0.85842	0.56594	73.62	45.125
34.47	17.59	-1.1	-45.04	10.84	293.31	0.76985	0.52864	78.813	44.642
41.1	17.87	23.46	-50.33	11.36	239.99	0.74361	0.53863	81.436	42.721
48.55	17.70	10.63	-55.37	11.4	213.17	0.70717	0.55299	79.821	40.874
58.94	17.74	10.63	-70.42	11.54	144.69	0.7156	0.42249	80.182	37.501
67.84	17.44	1.15	-76.12	11.44	96.25	0.68711	0.41705	77.475	34.921

Table 3 Incidence and Rebound kinematics for tennis ball with incident topspin

θ_i (Degrees)	V_{X1} (m/s)	V_{Y2} (m/s)	V_1 (m/s)	ω_1 (rad/s)	θ_r (Degrees)	V_{X2} (m/s)	V_{Y2} (m/s)	V_2 (m/s)	ω_2 (rad/s)
18.3	16.13	5.33	16.99	138.2	-23.09	10.98	-4.67	11.94	386.1
22.64	16.19	6.75	17.54	158.06	-30.54	10.36	-6.11	12.03	398.11
33.94	14.83	9.98	17.89	152.53	-40.58	9.65	-8.26	12.71	323.74
42.38	13.76	12.55	18.64	136.32	-43.33	9.67	-9.12	13.3	285.46
47.7	11.98	13.17	17.81	147.58	-51.88	7.75	-9.88	12.56	236.54
61.07	8.45	15.29	17.48	146.74	-62.41	5.51	-10.53	11.89	163.87
70.91	5.67	16.39	17.36	145.88	-67.6	4.55	-11.05	11.95	119.09

Table 4 Incidence and rebound kinematics for topspin impact (with restitution coefficients and kinetic energies)

θ_i (Degrees)	V_1 (m/s)	ω_1 (rad/s)	θ_r (Degrees)	V_2 (m/s)	ω_2 (rad/s)	ε_y	ε_x	T_1 (lb-in)	T_2 (lb-in)
18.3	16.99	138.2	-23.09	11.94	386.1	0.8761726	0.680719	76.794	61.806
22.64	17.54	158.06	-30.54	12.03	398.11	0.9051852	0.639901	82.638	63.965
33.94	17.89	152.53	-40.58	12.71	323.74	0.8276553	0.650708	85.503	59.071
42.38	18.64	136.32	-43.33	13.3	285.46	0.7266932	0.702762	91.681	58.992
47.7	17.81	147.58	-51.88	12.56	236.54	0.7501898	0.646912	84.521	49.751
61.07	17.48	146.74	-62.41	11.89	163.87	0.6886854	0.652071	81.513	40.603
70.91	17.36	145.88	-67.6	11.95	119.09	0.6741916	0.802469	80.405	38.800

Table 5 Incidence and Rebound kinematics for tennis ball with incident backspin

θ_i (Degrees)	V_{X1} (m/s)	V_{Y2} (m/s)	V_1 (m/s)	ω_1 (rad/s)	θ_r (Degrees)	V_{X2} (m/s)	V_{Y2} (m/s)	V_2 (m/s)	ω_2 (rad/s)
17.42	16.18	5.08	16.96	-168.32	-20.31	10.56	-3.91	11.26	105.5
22.44	15.95	6.59	17.26	-148.05	-28.25	9.82	-5.27	11.14	170.35
34.79	14.35	9.97	17.48	-157.58	-49.78	6	-7.09	9.29	261.54
40.48	13.8	11.78	18.15	-179.12	-58.19	5.36	-8.64	10.17	208.97
45.21	12.02	12.11	17.07	-164.57	-65.58	4.12	-9.08	9.99	175.12
58.76	9.12	15.04	17.61	-184.04	-74.78	2.81	-10.29	10.68	106.79
67.62	6.57	15.95	17.25	-165.53	-81.72	1.57	-10.84	10.98	71.43

Table 6 Incidence and rebound kinematics for backspin impact (with restitution coefficients and kinetic energies)

θ_i (Degrees)	V_1 (m/s)	ω_1 (rad/s)	θ_r (Degrees)	V_2 (m/s)	ω_2 (rad/s)	ε_y	ε_x	T_1 (lb-in)	T_2 (lb-in)
17.42	16.96	-168.32	-20.31	11.26	105.5	0.769685	0.652658	78.114	34.199
22.44	17.26	-148.05	-28.25	11.14	170.35	0.799697	0.615674	79.632	36.573
34.79	17.48	-157.58	-49.78	9.29	261.54	0.711133	0.418118	82.076	33.681
40.48	18.15	-179.12	-58.19	10.17	208.97	0.733447	0.388406	89.397	33.813
45.21	17.07	-164.57	-65.58	9.99	175.12	0.749794	0.342762	78.854	30.665
58.76	17.61	-184.04	-74.78	10.68	106.79	0.684176	0.308114	84.784	31.004
67.62	17.25	-165.53	-81.72	10.98	71.43	0.679624	0.238965	80.481	31.582

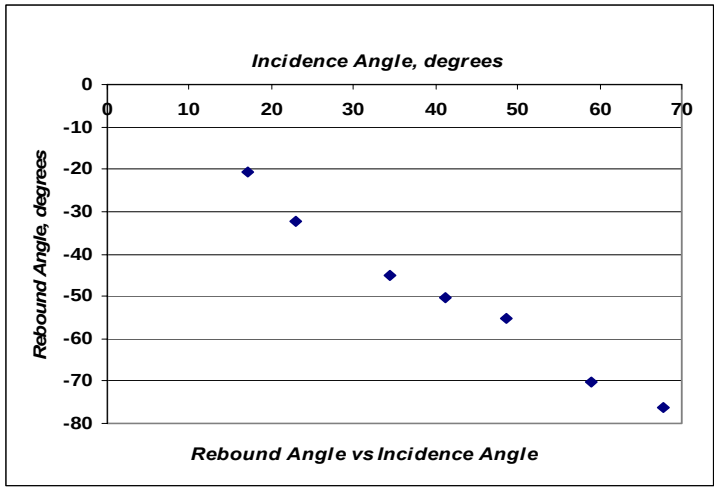

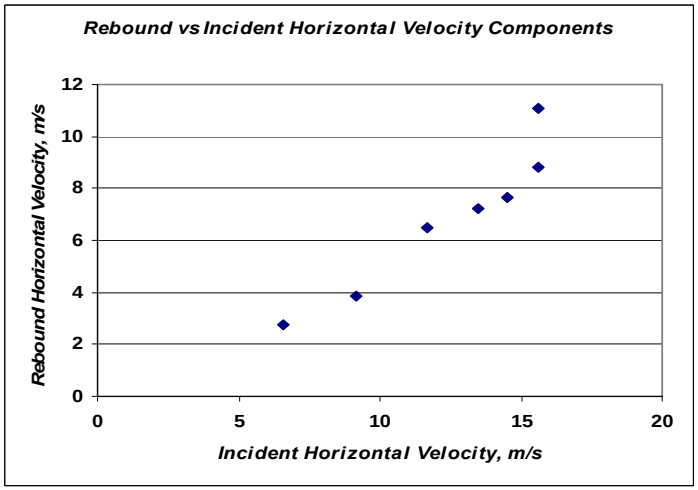

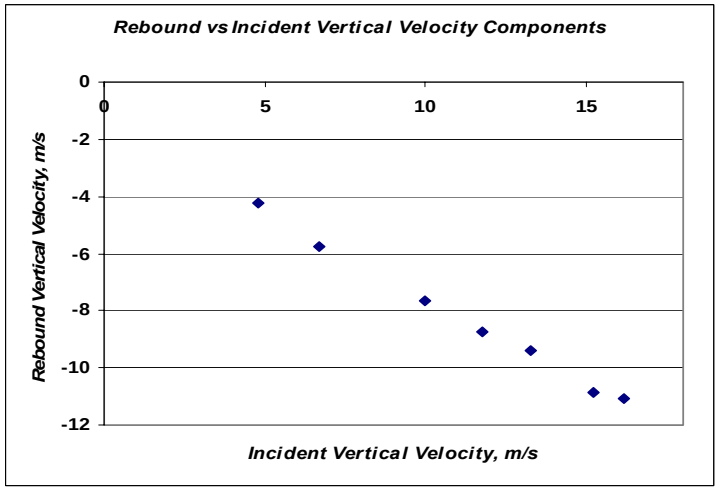

Fig. 30 Incident vs rebound kinematics for zero spin **[1].**

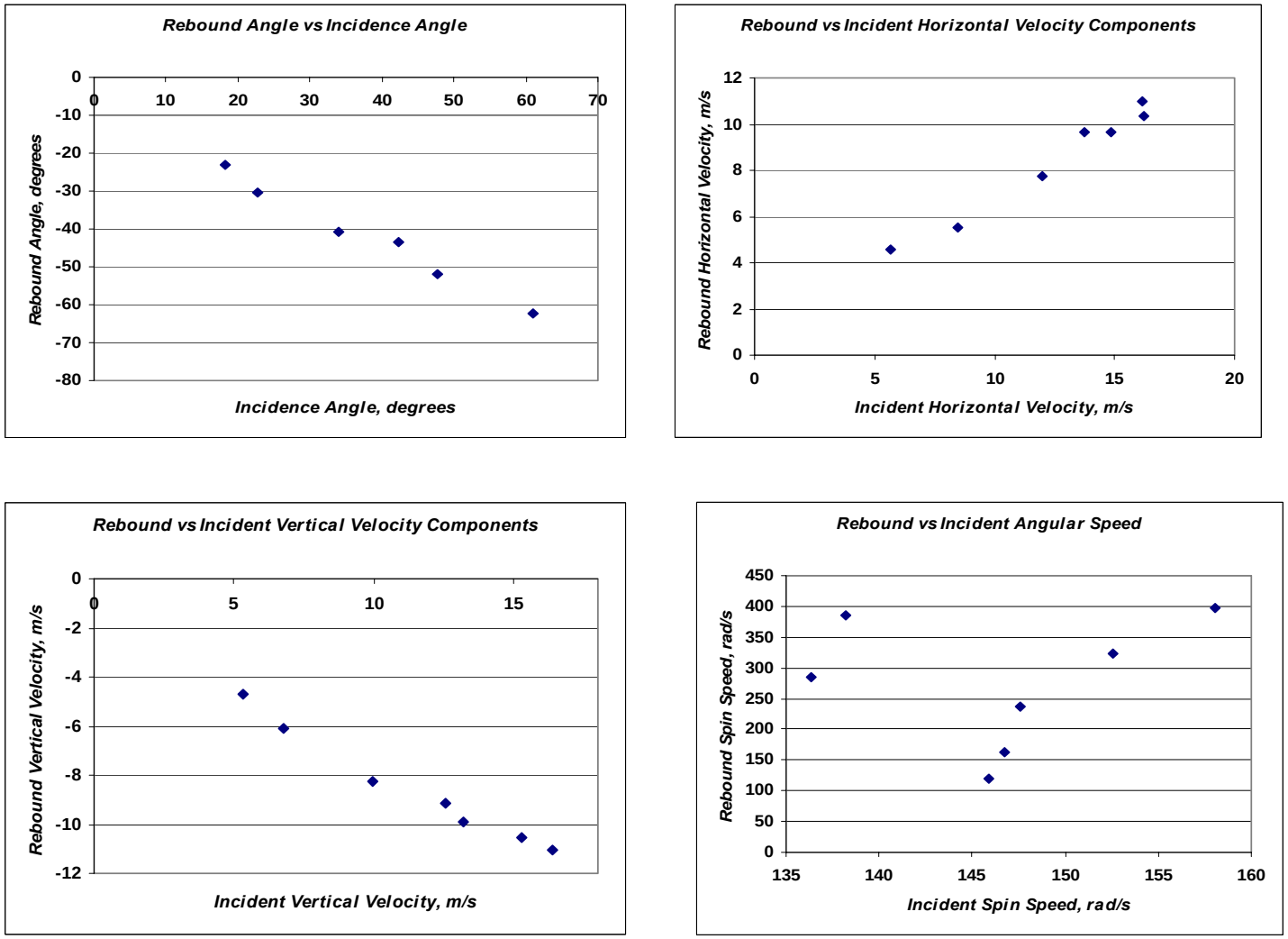

Fig. 31 Incident versus rebound kinematics for topspin **[1].**

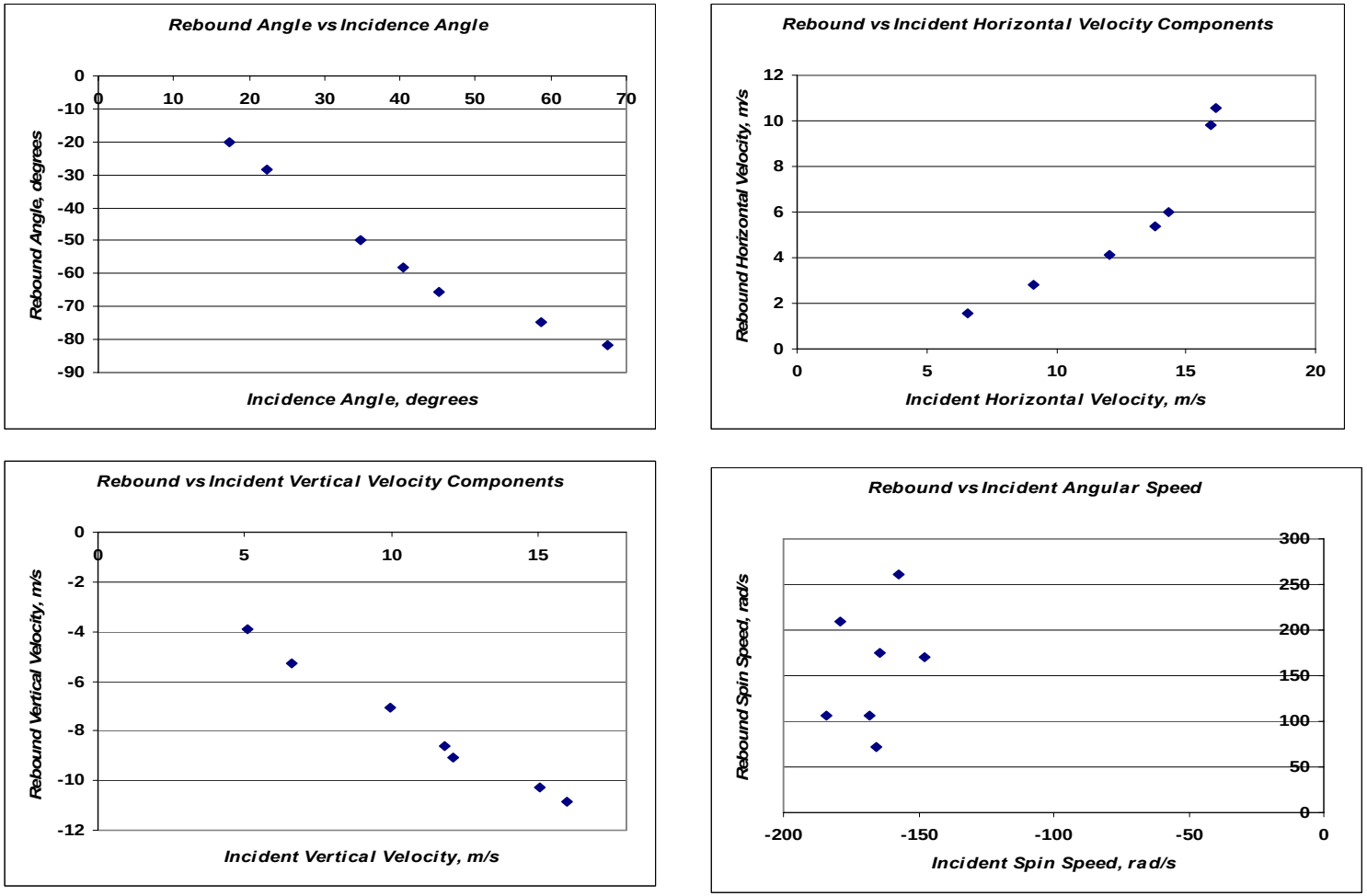

Fig. 32 Incident versus rebound kinematics for backspin **[1].**

From the data presented in Tables 1 through 6, values of the time-averaged coefficient of friction are calculated using equation (63) in Chapter II, and presented in the following table for three cases of zero spin, top spin and back spin.

Table 7. Time-averaged coefficient of friction values for experimental data

Incidence Angles (Degrees)	**Zero Spin**	**Top Spin**	**Back Spin**
18	0.502	0.515	0.625
23	0.543	0.453	0.516
34	0.388	0.284	0.489
42	0.303	0.188	0.413
48	0.231	0.184	0.373
60	0.203	0.114	0.249
70	0.141	0.04	0.186

From the values presented in Table 7 for the time-averaged friction factors, it can be seen that for zero spin incidence, the first three incidences, starting roughly from 18 degrees to 35 degrees, the friction factor is near the value of 0.55. However, after this, the value of the friction factor decreases gradually with each incidence until it reaches the value of 0.141 at an angle approximately equal to 70 degrees, at which there is not only sliding during motion but also pure rolling.

For top spin incidences at same angles as zero spin, the values of the friction factors are seen to be decreasing more with increasing incidence angle. This shows that for top spin, rolling during contact occurs earlier as compared to zero spin. Note the last two values for top spin in Table 7, which are appreciably less than 0.55, thus proving that the ball changes its motion from sliding to rolling during these cases.

For back spin, the friction factor is higher as compared to both top spin and zero spin, thus showing that the ball incident with back spin undergoes rolling only at high angles of incidence. For zero and top spin incidence, transition of motion from sliding to rolling will start as early when angle of incidence reaches around 35 to 40 degrees, but for the ball incident with strong back spin, like in the experimental data presented, the transition will start only at around 55 to 60 degrees angle of incidence.

The results of the experimental measurements on the tennis ball as shown in the previous graphs in figures 31 to 33 show that the angle of rebound is greater than the angle of incidence in case of the backspin impact. In case of the topspin, its trend is the same as the backspin case. For the zero spin impact, the angles of rebound are very close to those for the topspin impacts.

The vertical coefficient of restitution varies for each case of the zero spin, the top spin and the backspin, but trend still follows nearly a straight line, which indicates that the vertical coefficient of restitution for each spin case can be taken, on an average, as a constant. The average vertical coefficient of restitution for all cases comes in a range of 0.74 to 0.78, which is a normally accepted range for this parameter **[1].**

The horizontal coefficient of restitution which is calculated and presented in the tables and can be directly deduced from the graphs of the rebound and the incident horizontal velocities, does show some scatter. It is not as constant as the vertical coefficient of restitution, but for zero spin and topspin impacts, values for this parameter are not as scattered as is the case with the backspin impact.

MEASUREMENT OF THE MASS MOMENT OF INERTIA OF A TENNIS BALL

The mass moment of inertia of a tennis ball is determined experimentally as a part of this thesis to obtain a numerical value of this important rotational parameter of the tennis ball which is used in the impact simulations (Chapter V).

Theoretical background of measurement for mass moment of inertia

The mass moment of inertia of an object can be determined by performing a twisting test on the object. A twisting test is basically a torsional vibration of the object so that it is hung or supported vertically downwards from a ceiling with two or more strings of any appropriate material that can withstand the weight of the object. The torsional vibration is induced by giving an angular twist of a small amplitude about the vertical axis of the object that passes through its center of mass of it and then measuring the period of the ensuing vibrations. In order to develop an analytical expression for the torsional natural frequency as a function of the mass moment of inertia, first of all, the following two linear equivalent systems are considered and their equations of motion are derived in order to establish an expression for the horizontal equivalent stiffness of a pendulum.

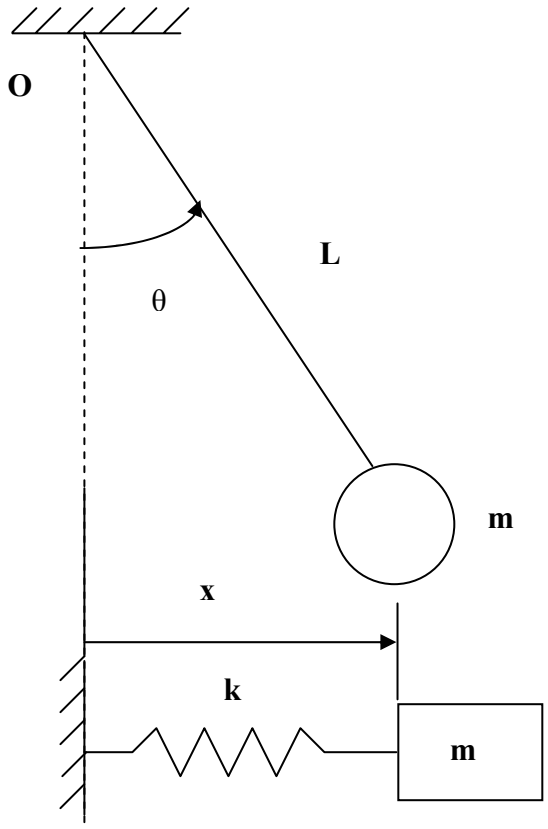

Fig. 33 Equivalent linear vibrating systems.

It can be seen from figure 33 that the two systems are equivalent and given the frequency of vibration of one, the frequency of vibration of the other can be deduced. The governing equations of motion and the kinematics for the above systems are presented as follows:

$$\sum M_O = I_O \ddot{\theta}$$

$$mL^2 \ddot{\theta} + mgL\theta = 0$$

$$\ddot{\theta} + \frac{g}{L}\theta = 0 \qquad (76)$$

For small amplitudes ‘θ’, the kinematics of two systems are related as:

$$x = L\theta$$

Substituting this relation in the differential equation for ‘θ’, the following equation of motion for an equivalent spring-mass system is obtained:

$$\ddot{x} + \frac{g}{L}x = 0$$

$$m\ddot{x} + \frac{mg}{L}x = 0$$

If the equivalent system is considered separately, its governing differential equation of motion is(neglecting damping):

$$m\ddot{x} + kx = 0$$

Thus the equivalent stiffness coefficient for the system is:

$$k = \frac{mg}{L} \qquad (77)$$

This expression provides the stiffness of an equivalent spring-mass system to that of a mass hanging by a rod or a taut and an inflexible string.

Based on the same principle of an equivalent system, consider now a disk shaped object suspended by two strings, which is subjected to a twisting test (torsional vibration about its center of mass) and an equivalent system supported tangentially by equivalent springs. This is illustrated in figure 34 below:

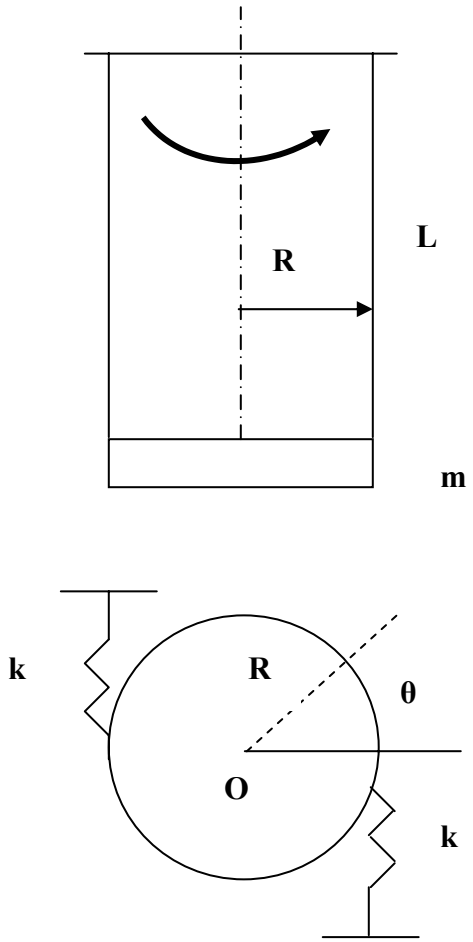

Fig. 34 Equivalent torsional vibrating systems.

In this set of vibrating systems, the above system is subjected to an angular twist about the center of mass of the object supported by two strings of equal length. As a result, the system starts vibrating about its vertical centroidal axis which is shown as a dotted line in figure 34. An equivalent system is obtained if, instead of being supported on strings, the object is supported by the two equivalent springs connected tangentially to it. When the object is given a small twist about its vertical centroidal axis, it will start vibrating. The following equations of motion are derived to determine the mass moment

of inertia of the object about its mass center in terms of the other system parameters with the help of the equivalent system:

$$\sum M_O = I_O \ddot{\theta}$$

Now the external moment acting on the vibrating object (neglecting damping) can be expressed as follows:

$$\sum M_O = -2FR = I_O \ddot{\theta}$$

where 'F' is the tangential force exerted on the object by a spring and the two supporting springs are assumed to be identical. Furthermore, 'F' can be expressed as follows:

$$F = kR\theta = \frac{mg}{2L} R\theta$$

where the value of the equivalent stiffness coefficient is obtained from the consideration of the previous equivalent systems. The factor of 2 comes from the presence of the two strings to support the object instead of a single string.

Thus the differential equation of motion of the equivalent system is obtained by combining the above equations as follows:

$$I_O \ddot{\theta} + \frac{mg}{L} R^2\theta = 0$$

Equivalently, this equation can be written as:

$$\ddot{\theta} + \frac{mgR^2}{I_O L}\theta = 0 \qquad (78)$$

Comparing equation (78) above to the standard second-order linear differential equation describing a vibrating system, the natural frequency can be expressed as follows:

$$\omega_n{}^2 = \frac{mgR^2}{I_O L}$$

From above equation, the mass moment of inertia of the object about its centroidal axis can be obtained as:

$$I_O = \frac{mgR^2}{L\omega_n{}^2} \qquad (79)$$

Thus in the experimental setup for a twisting test, if the torsional period of vibration 'T' of the object is measured, its mass moment of inertia can be determined, since $\omega_n = \frac{2\pi}{T}$

Experimental setup

A simple experimental setup based on the idea of a twisting test is used to determine the mass moment of inertia of the tennis ball. The setup consists of a tennis ball hung from the ceiling by two strings, each about 1m (39.37 in.) long. A meter stick and a foot-scale are required for the measurements of string length. A stopwatch is needed to measure the rotational period of vibration of the tennis ball. This is depicted in figure 35.

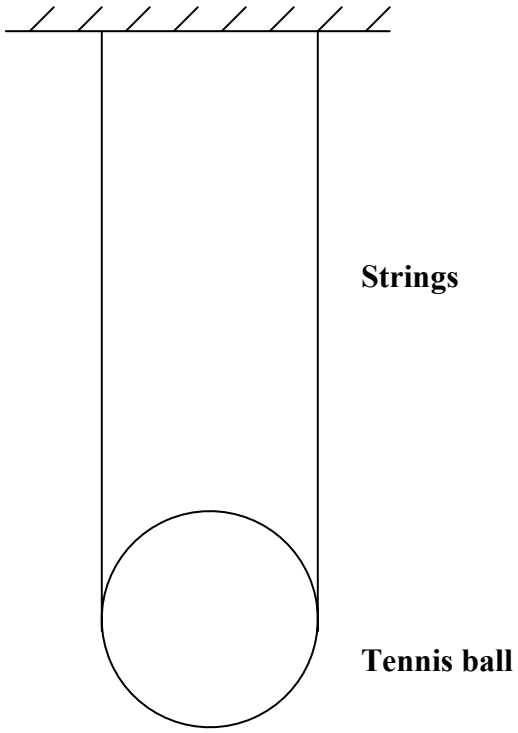

Fig. 35 Experimental setup to measure the mass moment of inertia.

The strings are taped to the ball at the points on the surface so that it becomes very nearly tangent to the surface when the upper ends are joined to the ceiling by the tape as well. To make the two supporting strings parallel and of equal length is not very easy and it took several trials and measurements of the string lengths until they became equal and parallel. Then the twisting test was performed on the ball and the readings were obtained.

Results of the experiment

Several tests, with each one recording the time for 10 complete vibrations were performed and then the average was taken to determine the time period of torsional vibrations. Results are listed in the following table:

Table 8. Experimental results of the twisting test on the tennis ball

Test Number	Number of Cycles	Time for Cycles(seconds)
1	10	15.2
2	10	15.1
3	10	15.2
4	10	15.1
5	10	15.3
6	10	15.1
7	10	15.1
8	10	15.2
9	10	15.1
10	10	15.2
Total	**100**	**151.6**

The average time period of the torsional oscillations is calculated from the above experimental results as:

$$T = \frac{151.6}{100} = 1.516 \text{ seconds}$$

Based on this value of the time period, the circular natural frequency of the torsional oscillations is calculated as:

$$\omega_n = \frac{2\pi}{T} = 4.144 \text{ rad/s}$$

The values of the other physical parameters of the system are as follows:

m = 0.127 lb = 0.000329 lb-s^2/in
g = 386.4 in/s^2
R = 1.25 in.
L = 101.6 cm = 39.99 in.

Substituting these values in equation (79), the mass moment of inertia of the tennis ball about its centroidal axis is calculated as:

$$I_O = \frac{(0.000329)(386.4)(1.25)^2}{(39.99)(4.144)^2} = 0.00028 \text{ lb-s}^2\text{-in}$$

This value of the mass moment of inertia will be used as a benchmark for the simulations of the tennis ball (Chapter V).

CHAPTER V

BEST RESULTS COMPARISONS WITH THE MEASUREMENTS

From the simulation results as presented in Appendix C, there are some parameters of the two-mass elastic systems that consistently seem to produce reasonable results for the rebound motion of the tennis ball as compared against the experimental measurements of the same parameters. These results seem to produce reasonable results for the incident zero spin, top spin and back spin cases for varying angles of incidences. Therefore, the results of the rebound kinematics developed by those selected parameters of the two-mass elastic systems are described in the following pages. In order to get the damping coefficient in the vertical direction, c_y, for each of the cases of the zero spin, the top spin and the back spin, the average vertical coefficient of restitution for each case is calculated as follows:

$$COR = \frac{\sum_{i=1}^{7} COR_i}{7}$$

Based on the value obtained above for that particular case, and having the spring constant and the mass ratios fixed, equation (6) is utilized to vary the coefficient for different values of the damping coefficients until the theoretical value of the coefficient of restitution, as given by equation (6), matches with the experimental value above.

Three cases for the parameters that yield reasonable agreements with the experiments are described in the following table:

Table 9. Dynamic ratios for all cases of incident angles and spins giving best results

Cases	M_1	M_2	K_y	I_1	I_2	k_θ
	Lb-s^2/in	**Lb-s^2/in**	**Lb/in**	**Lb-in-s^2**	**Lb-in-s^2**	**Lb-in/rad**
1	2M/3	M/3	80	0.532I	0.468I	1000
2	2M/3	M/3	90	0.532I	0.468I	1000
3	M/2	M/2	72	0.353I	0.647I	1000

For the zero spin impact, it can be seen from the simulation results and from the simulated kinematic graphs during the contact that above an incident angle of 20 degrees, the ball enters into the rolling mode. The time of contact, t_c, predicted by the simulations agrees very well with the experimental determinations of the contact times of tennis balls [4]. The contact duration usually spans from 4.5 ms to 5.5 ms. The predicted contact times vary in the same range for the different angles of incidence. Thus the contact duration is in close agreement with the experimental values.

For the topspin impacts, the simulations show that the rolling mode occurs during contact as angle of incidence is increased from 17 degrees to 23 degrees. Due to rolling, the horizontal velocity at the rebound is higher as compared to what it would be if it were sliding throughout the contact. This causes the simulated angles of rebound to be smaller than the angles of incidence. This agrees well with the experimental observations (Figs.30-32) in that the rebounds from the topspin impact are usually at smaller angles than incident and relatively less loss of horizontal component of incident velocity. The simulated rebound angles for the topspin impacts agree well with this observation.

The results achieved for the rebound spins for the three cases of the zero spin, the topspin and the backspin are encouraging and agreement with the experiments seems reasonable (Figs.36-44). In almost all case, the spin values are slightly higher than the experimental values. This might be attributed to some complicated effects of stick-slip

occurring at the interface of the tennis ball and the ground, which have not been taken into account in this model.

For the backspin impacts, the simulations show that the rolling mode occurs later than for the corresponding cases of the zero spin or the topspin impacts. Due to occurrence of rolling at later instant of contact in case of backspin as compared to either zero spin or topspin, the rebound horizontal velocity is smaller as compared to either of zero spin or topspin incidence (since most of the contact time of the ball is in sliding motion for the backspin impact, and a small percentage of the contact time is in rolling mode). This causes the simulated angles of rebound to be higher than the angles of incidence. This simulation prediction agrees very well with the experimental observations (Figs.40-42) which reveal that the backspin impacts on the tennis court surfaces generate large angles of rebound, which are always higher than the corresponding angles of incidences.

The simulated horizontal velocities at the rebound are generally higher than the experimental values (Figs.36-44) and the reason again might be the presence of some tangential flexibility, or in other words, elasticity in the X direction, that has not been accommodated in this model.

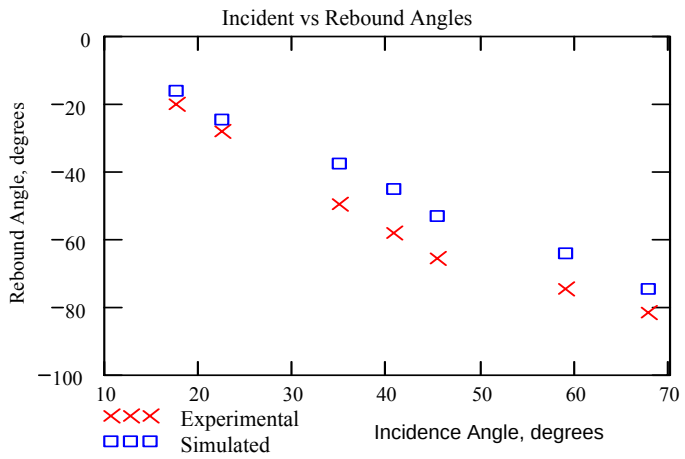

Incident vs. rebound angles

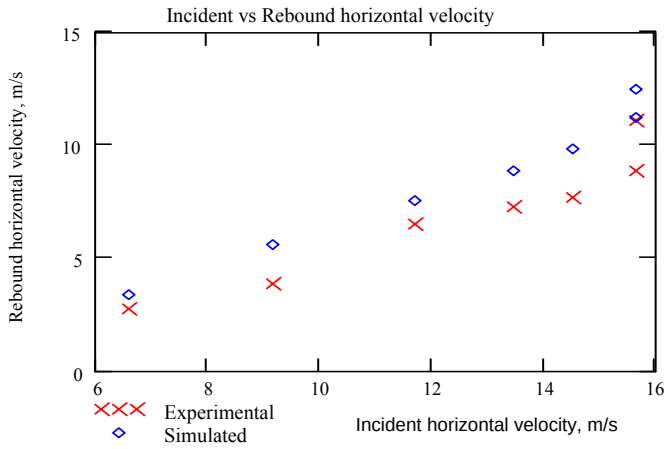

Incident vs. rebound horizontal velocities

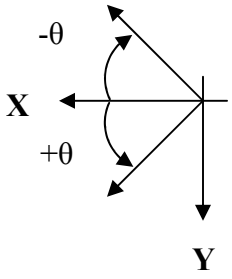

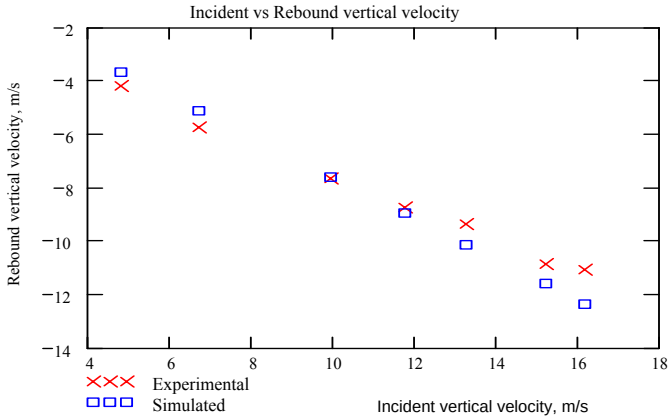

Incident vs. rebound vertical velocity

Fig. 36 Incident vs rebound parameters for the zero spin (average COR = 0.765), case 1. (c_y = 0.0225 lb-s/in)

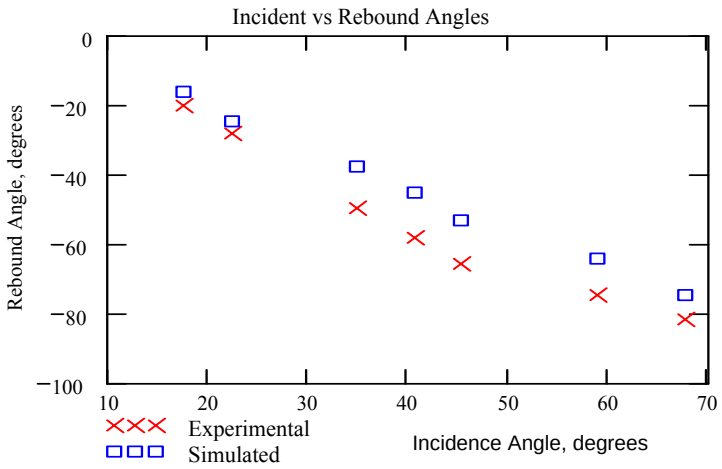

Incident vs. rebound angles

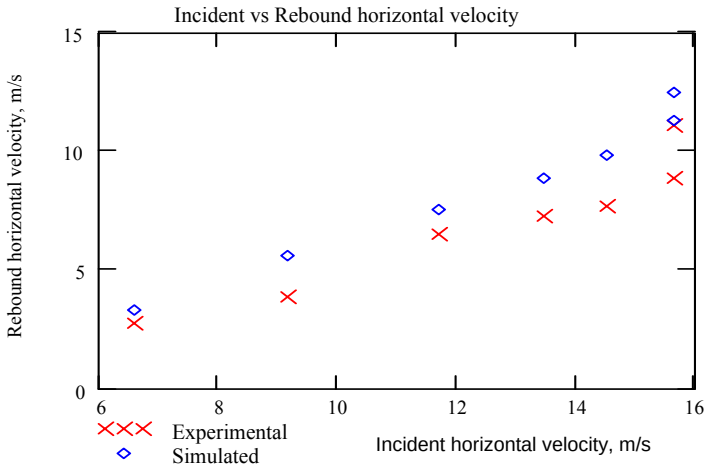

Incident vs. rebound horizontal velocities

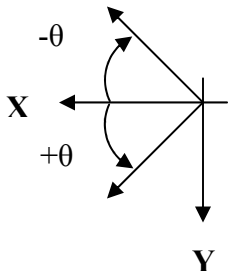

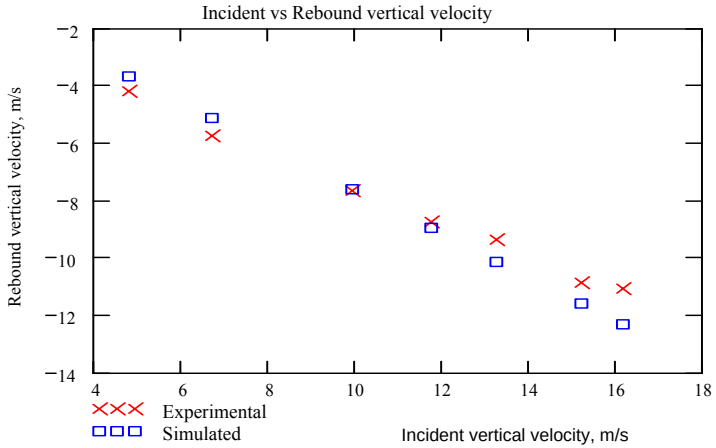

Incident vs. rebound vertical velocity

Fig. 37 Incident vs rebound parameters for the zero spin (average COR = 0.765), case 2. (c_y = 0.0239 lb-s/in)

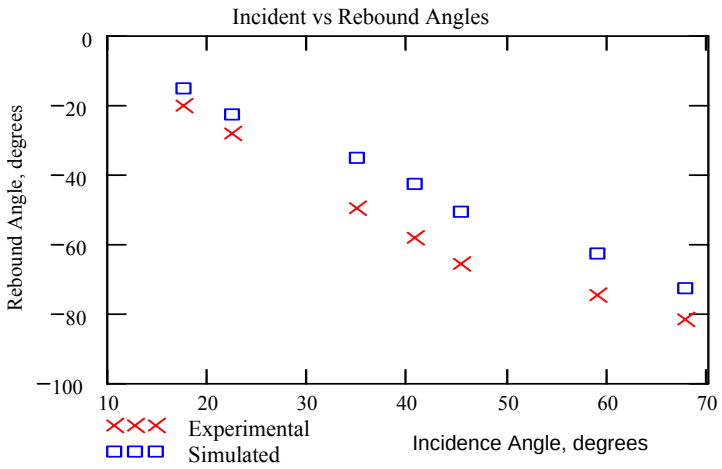

Incident vs. rebound angles

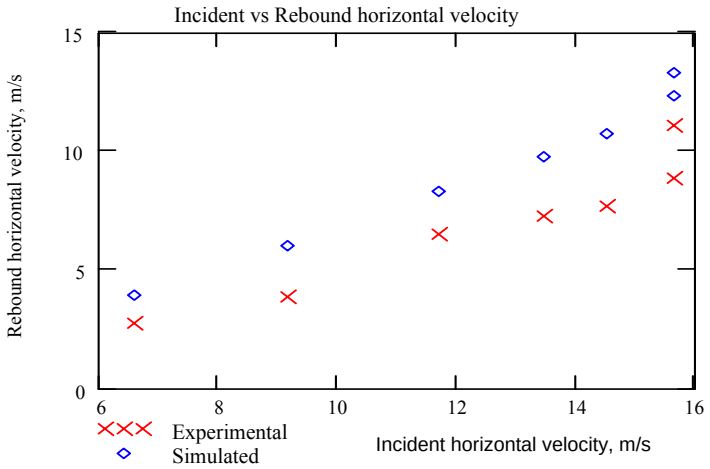

Incident vs. rebound horizontal velocities

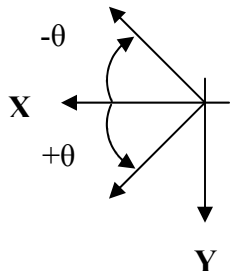

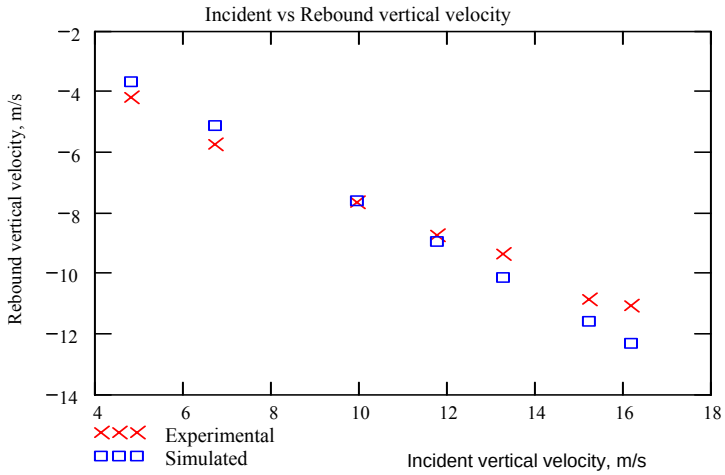

Incident vs. rebound vertical velocity

Fig. 38 Incident vs rebound parameters for the zero spin (average COR = 0.765), case 3. (c_y = 0.0185 lb-s/in)

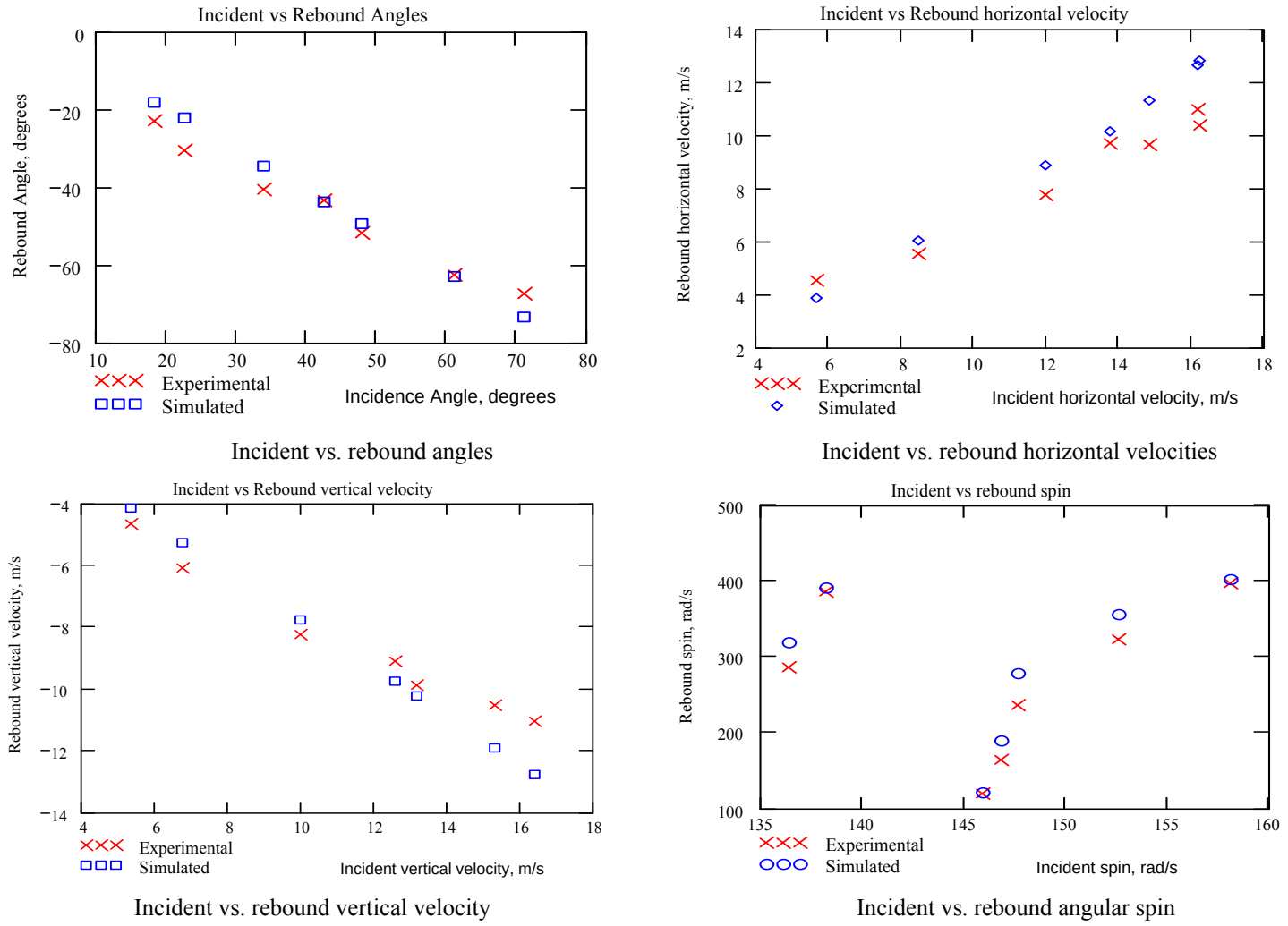

Fig. 39 Incident vs rebound parameters for the top spin (average COR = 0.778), case 1. (c_y = 0.0211 lb-s/in)

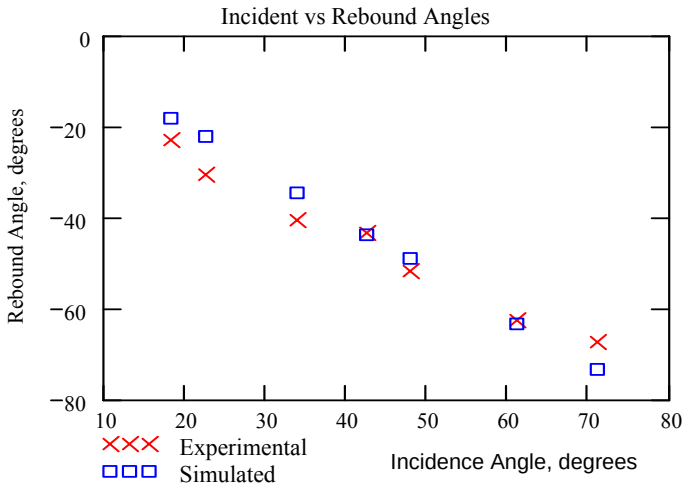

Incident vs. rebound angles

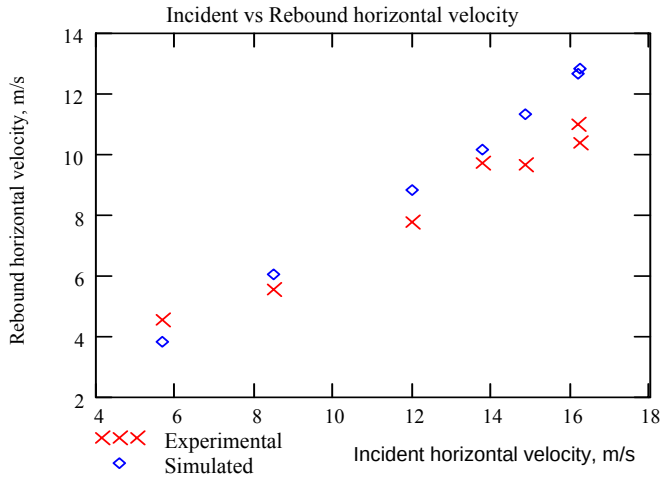

Incident vs. rebound horizontal velocities

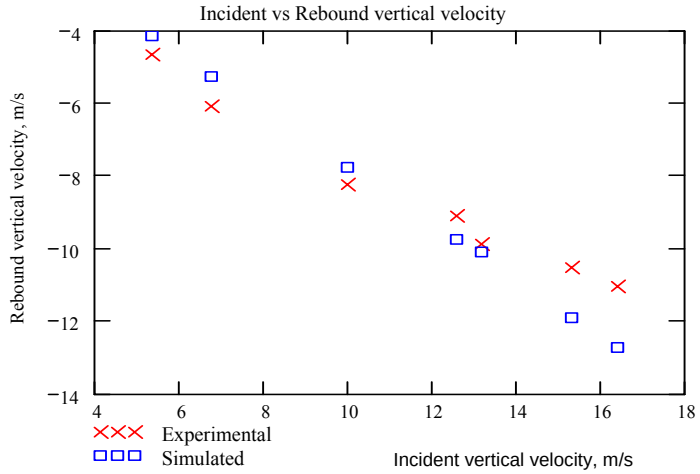

Incident vs. rebound vertical velocity

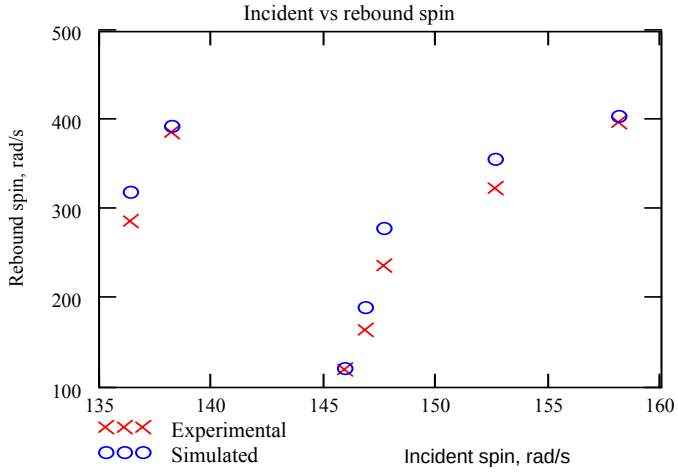

Incident vs. rebound angular spin

Fig. 40 Incident vs rebound parameters for the top spin (average COR = 0.778), case 2. (c_y = 0.0224 lb-s/in)

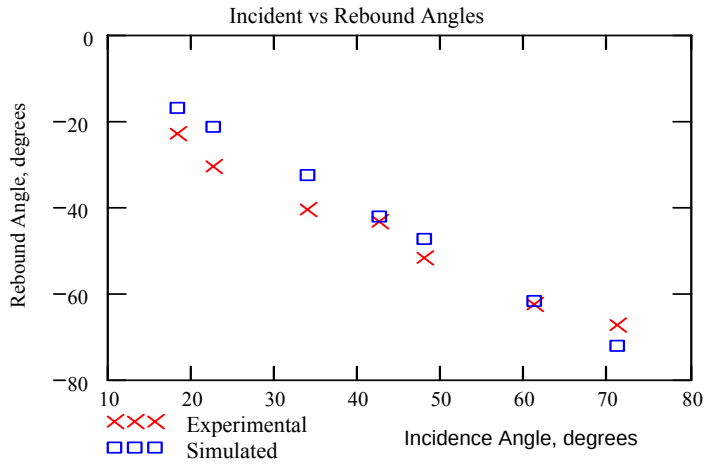

Incident vs. rebound angles

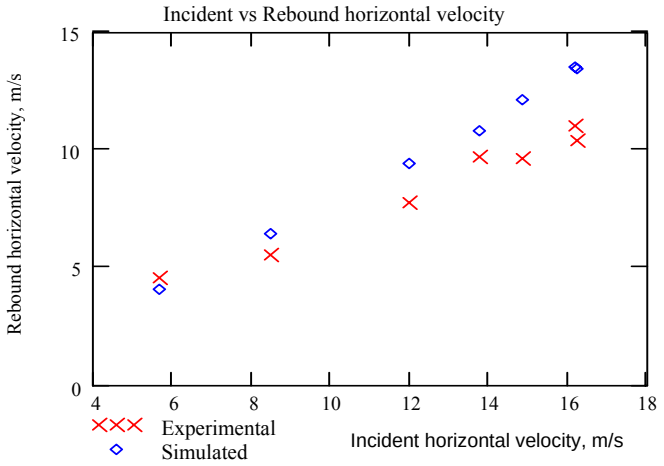

Incident vs. rebound horizontal velocities

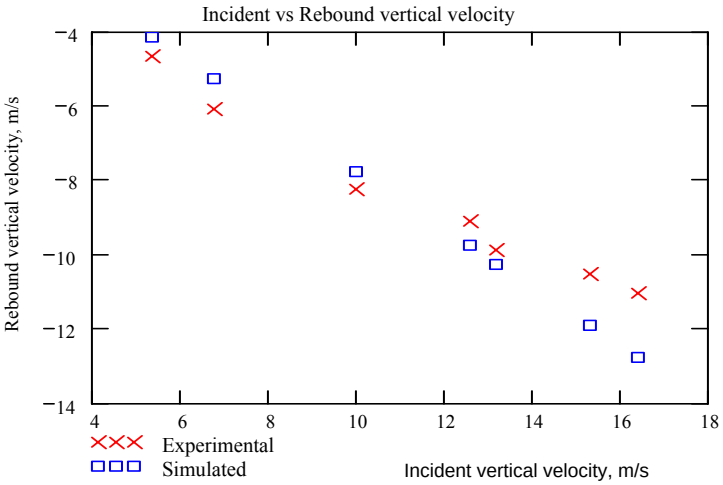

Incident vs. rebound vertical velocity

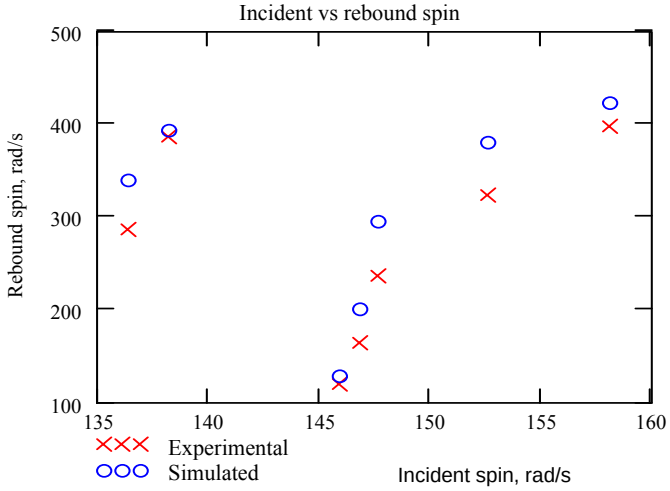

Incident vs. rebound angular spin

Fig. 41 Incident vs rebound parameters for the top spin (average COR = 0.778), case 3. (c_y = 0.0173 lb-s/in)

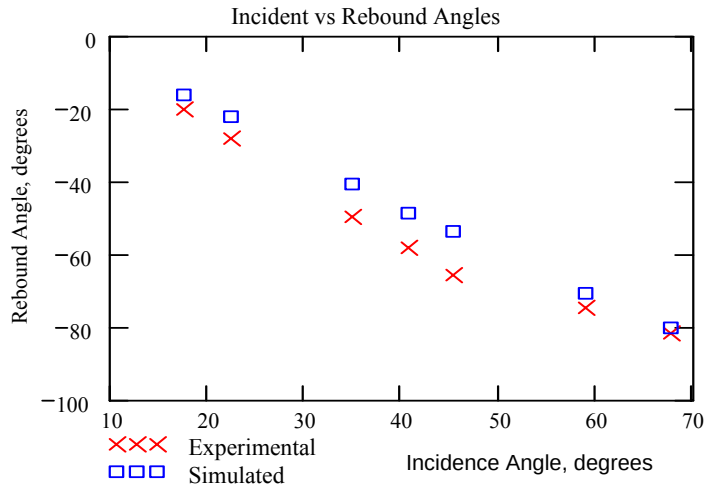

Incident vs. rebound angles

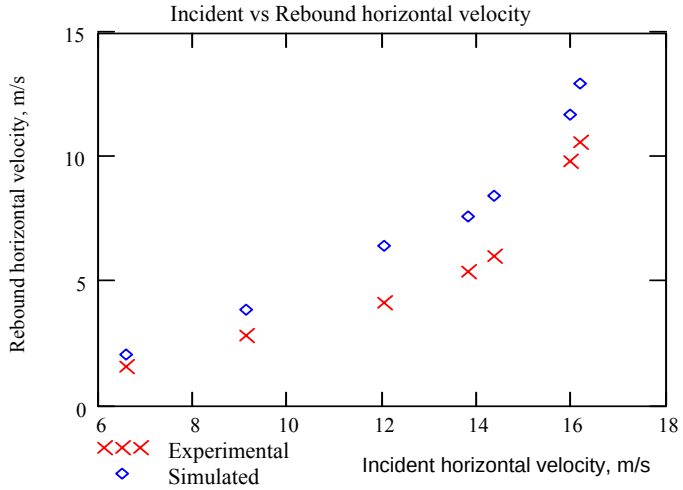

Incident vs. rebound horizontal velocities

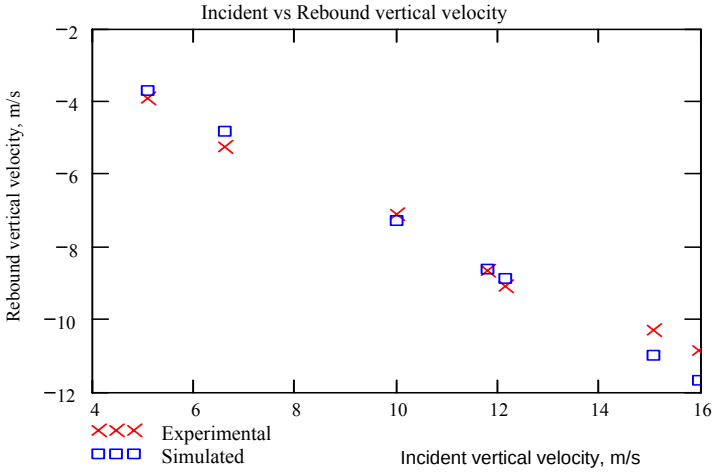

Incident vs. rebound vertical velocity

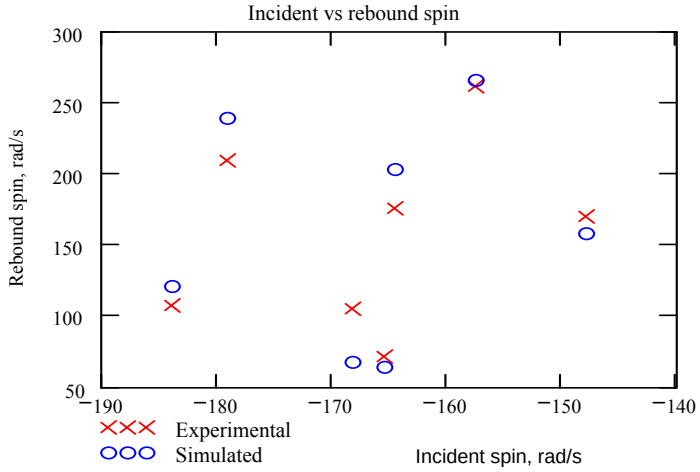

Incident vs. rebound angular spin

Fig. 42 Incident vs. rebound parameters for the back spin (average COR = 0.732), case 1. (c_y = 0.0262 lb-s/in)

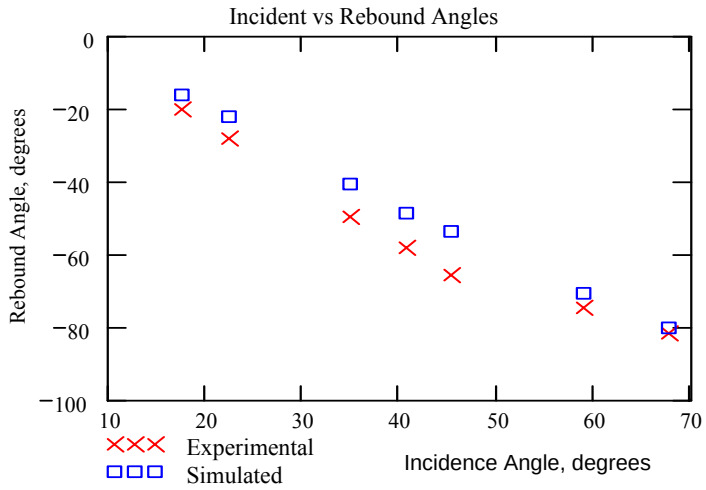

Incident vs. rebound angles

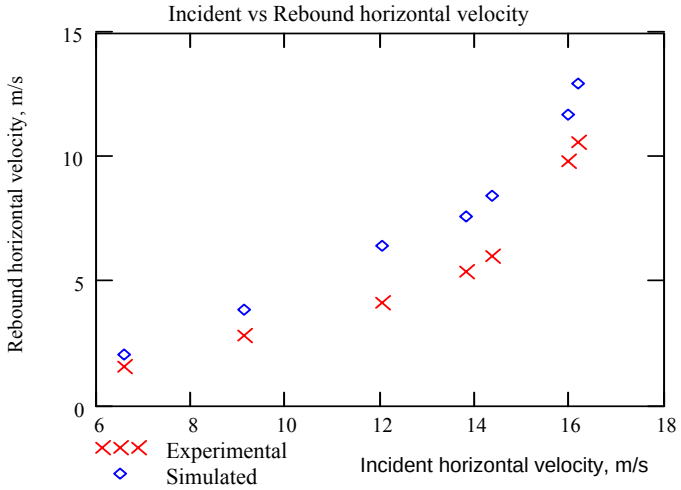

Incident vs. rebound horizontal velocities

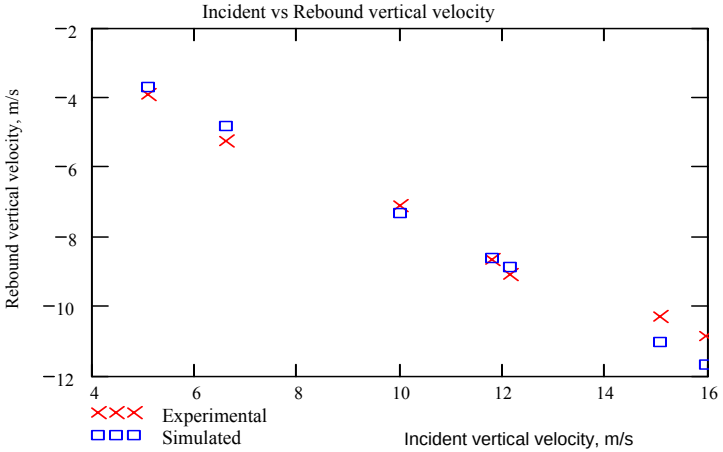

Incident vs. rebound vertical velocity

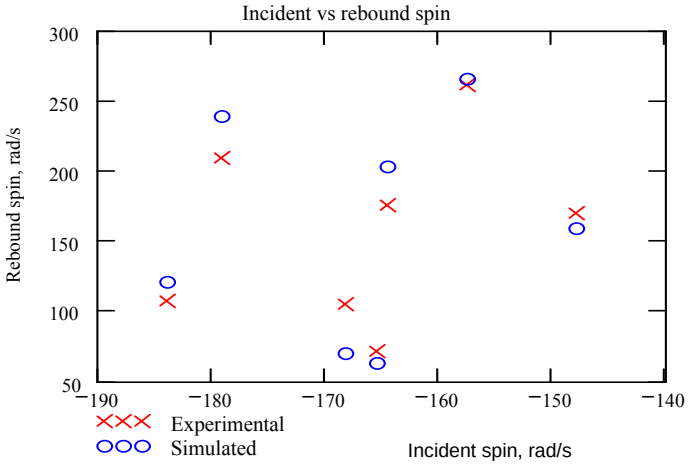

Incident vs. rebound angular spin

Fig. 43 Incident vs. rebound parameters for the back spin (average COR = 0.732), case 2. (c_y = 0.0277 lb-s/in)

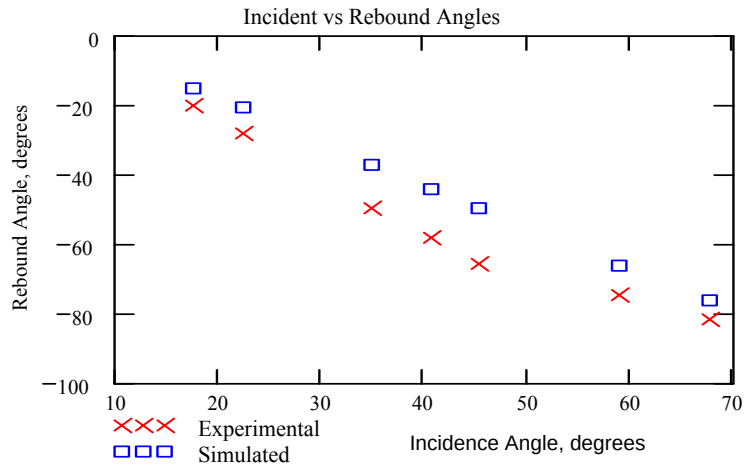

Incident vs. rebound angles

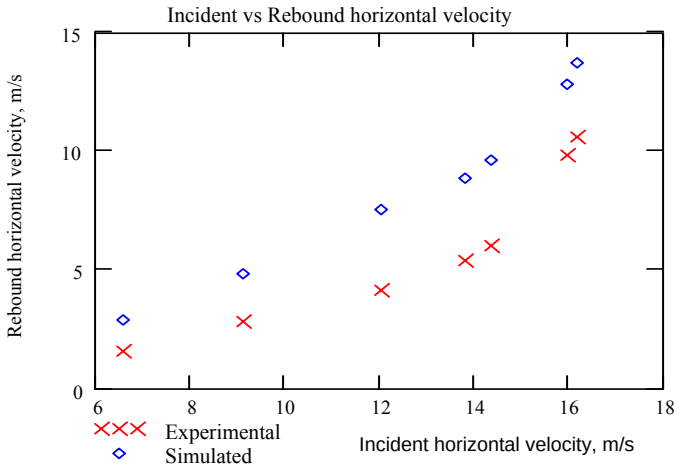

Incident vs. rebound horizontal velocities

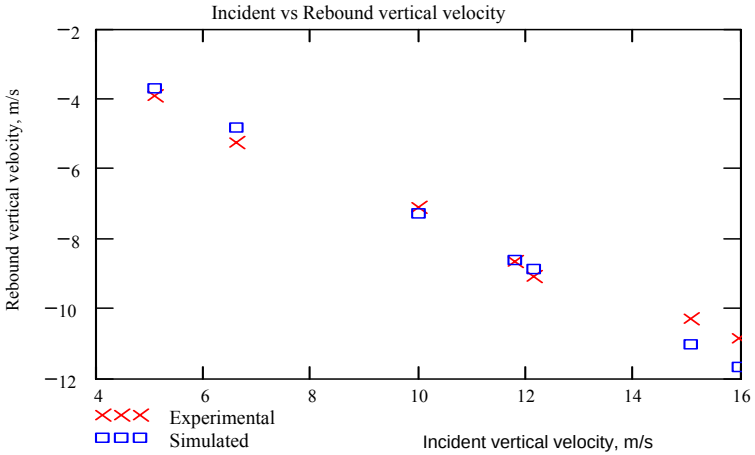

Incident vs. rebound vertical velocity

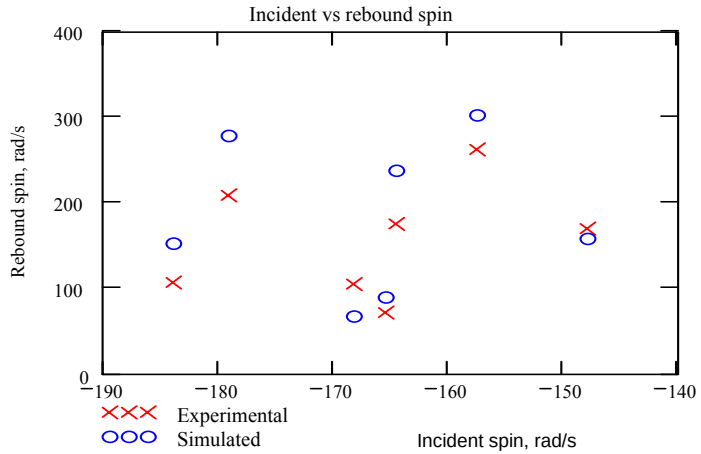

Incident vs. rebound angular spin

Fig. 44 Incident vs. rebound parameters for the back spin (average COR = 0.732), case 3. (c_y = 0.0215 lb-s/in)

CHAPTER VI

CONCLUSIONS

Simulation results of the experimental measurements on the tennis balls with selected parameters were presented in Chapter V. The results show that in general, the two mass model gives a fairly reasonable approximation of the rebound kinematics of the tennis ball.

From the simulations, it can be concluded that the offset parameter 'ε' (rolling friction) plays an important and a crucial part for the success of most of the simulations where there is a transition from the sliding to the rolling mode. This will always occur when the angle of incidence gets larger, which in turn implies a large vertical velocity component. The larger the vertical velocity component, the greater is the effect of the moment about the center of mass of the system produced by the normal contact force.

The application of linear vibrations theory and impact dynamics to the simulation of tennis ball using a two-mass model predicts the kinematics of the rebound, especially the rather challenging parameter of the spin of rebound reasonably well. The model is efficient from the point of view of computation time and effort, and it is simple to understand, since it is a linear model. The results indicate that the linear theory can be used to predict the impact phenomena with good success.

Incorporating the vertical stiffness and the torsional stiffness as well as the damping in the model, which can be deduced by the simple bounce height experiments, the model can be used to predict the rebound velocities, the spins and the angles of rebounds. Also the model can be used to successfully predict the time of contact of the

tennis ball with the ground, the onset of rolling or no-slip motion and the contact forces acting on the ball.

The simulations of the experimental results as presented in tables C-7 to tables C-27 present the time of contact (duration of contact). As can be found from references [3] and [5], the average time of contact that has been measured for the tennis balls is somewhere around 4.5 ms to 5 ms. From the simulation results, the average contact time varies very much in the same range, with 4.5ms to 5ms as the most frequent occurrence. This indicates that the model indeed predicts the time of contact very well.

Finally, the selected three cases of the dynamic parameters that gave the best agreements with the measurements indicate that the inner core mass is always slightly higher in both the mass and the mass moment of inertia to give the best fit with the measurements.

REFERENCES

[1] Wang, J.C., 1989, *The Impact Dynamics of a Tennis Ball Striking a Hard Surface,* PhD Dissertation, Oregon State University

[2] Smith III, J.F., 1987, *The Effect of Angle, Velocity and Rotation of Incidence on the Angle Deviation of Rebounding Tennis Balls,* PhD Dissertation, Texas A&M University

[3] Cross, R., 1999, "The Bounce of a Ball," American Journal of Physics, **67** (3), pp. 222-227

[4] Cross, R., 2002, "Measurements of the Horizontal Coefficient of Restitution for a Superball and a Tennis Ball", American Journal of Physics, **70** (5), pp. 482-489

[5] Brody, H., 1984, "That's How the Ball Bounces," The Physics Teacher, pp. 494-497

[6] Hubbard, M., and Stronge, W.J., 2001, "Bounce of Hollow Balls on Flat Surfaces," Sports Engineering, **1**, pp.94-102

[7] Stronge, W.J., 2000, *Impact Mechanics*, Cambridge University Press

[8] Stevenson, B., Bacon, M.E., and Baines, C.G.S., 1998, "Impulse and Momentum Experiments Using Piezo Disks," American Journal of Physics, **66**(5), pp. 445-448

[9] Malcolm, R.E., 1989, "A Measurement Using the Piezoelectric Effect," The Physics Teacher, pp. 637-639

[10] Minnix, R.B., and Carpenter,D.R., 1985, "Piezoelectric Film Reveals F vs t of Bounce Ball," The Physics Teacher, pp. 180-181

[11] International Tennis Federation Rules and Regulations, ITF, UK, Year 2002

[12] Lankarani,H.M., and Nikravesh, P.E., 1990, " A Contact Force Model With Hysteresis Damping for Impact Analysis of Multibody Systems," Journal of Mechanical Design, **112**, pp.369-376

[13] Stronge, W.J., 1992, "Energy Dissipated in Planar Collisions," ASME Journal of Applied Mechanics, **59**, pp. 681-683

[14] Sondergaard, R., Chaney,K., and Brennen,C.E., 1990, "Measurements of Solid Spheres Bouncing Off Flat Plates," ASME Journal of Applied Mechanics, **57**, pp. 694-699

[15] Keller, J.B., 1986, "Impact With Friction," ASME Journal of Applied Mechanics, **53**, pp. 1-4

[16] Hudnut, K., and Flansburg, L., 1979, "Dynamic Solutions for Linear Elastic Collisions," American Journal of Physics, **47**(10), pp. 911-914

[17] Bayman, B.F., 1976, "Model of the Behaviour of Solid Objects During Collision," American Journal of Physics, **44**(7), pp. 671-676

[18] Johnson, K.L., 1982, "The Bounce of a Superball," International Journal of Engineering Education, pp. 57-63

[19] Hunt, K.H., and Crossley, F.R.E., 1975, "Coefficient of Restitution Interpreted as Damping in Vibroimpact," **42**, pp.440-445

[20] Spradley, J.L., 1987, "Velocity Amplification in Vertical Collisions," American Journal of Physics, **55**(2), pp. 183-184

APPENDIX A

PARTICULAR SOLUTION OF SECOND-ORDER, NON-HOMOGENOUS, ORDINARY LINEAR DIFFERENTIAL EQUATION

Consider the following differential equation:

$$a\frac{d^2\theta}{dt^2} + b\frac{d\theta}{dt} + c\theta = \gamma_1 e^{\alpha t}\sin(\beta t) + \gamma_2 e^{\alpha t}\cos(\beta t) \qquad \text{(A1)}$$

In the above equation, the coefficients of the variables on the left hand side are all constants. In this equation, only θ and t are the variables involved, hence the remaining symbols on the right hand side are all constants as well. The constants γ_1 and γ_2 are non-zero, so equation (A1) is a non-homogenous, second- order, ordinary differential equation with constant coefficients. It is desired to determine the particular solution of the above differential equation.

In order to determine the solution of equation (A1), the method of undetermined coefficients is used. Accordingly, the assumed particular solution of equation (A1) is of the form:

$$\theta(t) = Ae^{\alpha t}\sin(\beta t) + Be^{\alpha t}\cos(\beta t) \qquad \text{(A2)}$$

where ‘A’ and ‘B’ are the constants whose values have to be determined.

The first and second derivatives of the assumed function in equation (A2) are readily evaluated as follows:

$$\frac{d\theta}{dt} = e^{\alpha t}\sin(\beta t)(\alpha A - \beta B) + e^{\alpha t}\cos(\beta t)(\beta A + \alpha B) \quad \text{(A3)}$$

$$\frac{d^2\theta}{dt^2} = e^{\alpha t}\sin(\beta t)[A(\alpha^2 - \beta^2) - 2\alpha\beta B] + e^{\alpha t}\cos(\beta t)[2\alpha\beta A + B(\alpha^2 - \beta^2)] \quad \text{(A4)}$$

Substituting equations (A2), (A3) and (A4) in equation (A1), the following algebraic equation is obtained:

$$a[A(\alpha^2 - \beta^2) - 2\alpha\beta B]e^{\alpha t}\sin(\beta t) + a[2\alpha\beta A + (\alpha^2 - \beta^2)B]e^{\alpha t}\cos(\beta t) + b(\alpha A - \beta B)e^{\alpha t}\sin(\beta t)$$

$$+ b(\beta A + \alpha B)e^{\alpha t}\cos(\beta t) + cAe^{\alpha t}\sin(\beta t) + cBe^{\alpha t}\cos(\beta t) = \gamma_1 e^{\alpha t}\sin(\beta t) + \gamma_2 e^{\alpha t}\cos(\beta t)$$

(A5)

The coefficients for the time functions on the left and the right hand side in equation (A5) can be compared to obtain the following linear simultaneous equations in 'A' and 'B':

$$a[A(\alpha^2 - \beta^2) - 2\alpha\beta B] + b(\alpha A - \beta B) + cA = \gamma_1 \quad \text{(A6)}$$

$$a[2\alpha\beta A + (\alpha^2 - \beta^2)B] + b(\beta A + \alpha B) + cB = \gamma_2 \quad \text{(A7)}$$

Separating the terms involving 'A' and 'B', the above equations can be re-written as:

$$A[a(\alpha^2 - \beta^2) + b\alpha + c] - B(2a\alpha\beta + b\beta) = \gamma_1 \quad \text{(A8)}$$

$$A(2a\alpha\beta + b\beta) + B[a(\alpha^2 - \beta^2) + b\alpha + c] = \gamma_2 \quad \text{(A9)}$$

Solving equations (A8) and (A9) simultaneously, the values of ‘A’ and ‘B’ are determined as:

$$A = \frac{(2a\alpha\beta + b\beta)}{[\{a(\alpha^2 - \beta^2) + b\alpha + c\}^2 + (2a\alpha\beta + b\beta)^2]}[\gamma_2 + \frac{\gamma_1(a\alpha^2 - a\beta^2 + b\alpha + c)}{(2a\alpha\beta + b\beta)}]$$

(A10)

$$B = \frac{A(a\alpha^2 - a\beta^2 + b\alpha + c) - \gamma_1}{(2a\alpha\beta + b\beta)} \qquad \text{(A11)}$$

(‘B’ is expressed in terms of ‘A’. Once ‘A’ is known from equation (A10), ‘B’ is known from equation (A11)).

From equations (A10), (A11) and (A2), it can be seen that the particular solution of equation (A1) is completely established in terms of the constants involved in the differential equation (A1). Thus substituting the values of ‘A’ and ‘B’ from equations (A10) and (A11) into equation (A2), which is the assumed particular solution, the particular integral of equation (A1) is determined.

APPENDIX B

MATHCAD CODES FOR VARIOUS KINEMATICS

Vertical displacement during contact

$$D(n, M1, cy, ky, Vy1) := \left| \begin{array}{l} Vy1i \leftarrow Vy1 \cdot 39.37 \\ W \leftarrow 0.127 \\ g \leftarrow 386.4 \\ R \leftarrow 1.25 \\ \omega y \leftarrow \sqrt{\frac{ky}{M1}} \\ \xi y \leftarrow \frac{cy}{2 \cdot M1 \cdot \omega y} \\ \omega dy \leftarrow \omega y \cdot \sqrt{1 - \xi y^2} \\ \frac{Vy1i}{R \cdot \omega dy} \cdot e^{\frac{-n \cdot \xi y \cdot \pi \cdot \omega y}{\omega dy}} \cdot \sin(n \cdot \pi) \end{array} \right.$$

The code above generates the vertical displacement of the inner core mass M_1, given the stiffness of the spring and the damping coefficient of the damper in the vertical direction, as well as the incident vertical velocity. The code requires, as its arguments, the numerical values of the inner core mass M_1, the damping coefficient, the stiffness coefficient and the incident vertical velocity. The 'n' inside the brackets on the right hand side of the first line of the code indicates that the dimensionless contact time 'n' is also present in the equations. As the equations inside the code indicate, the displacement is plotted as a function of dimensionless contact time 'n'. Given the physical parameters, it calculates the damping ratio, the undamped natural frequency and the damped natural

frequency inside the code and then on the basis of these quantities, the vertical velocity during the contact is determined.

Code for rebound velocity in Y direction

The following code generates the velocity of rebound (in m/s) in Y direction during any instant of contact and at any value of the dynamic parameters (to be inputted in FPS units).

$$
\begin{aligned}
&Vy(M1, ky, cy, n, Vy1) := \left| \begin{array}{l}
Vyi \leftarrow Vy1 \cdot 39.37 \\
\omega y \leftarrow \sqrt{\frac{ky}{M1}} \\
\xi y \leftarrow \frac{cy}{2 \cdot M1 \cdot \omega y} \\
\omega dy \leftarrow \omega y \cdot \sqrt{1 - \xi y^2} \\
\left(\frac{-Vyi \cdot \xi y \cdot \omega y \cdot e^{-\xi y \cdot \omega y \cdot \frac{n \cdot \pi}{\omega dy}}}{\omega dy} \cdot \sin(n \cdot \pi) + Vyi \cdot e^{-\xi y \cdot \omega y \cdot \frac{n \cdot \pi}{\omega dy}} \cdot \cos(n \cdot \pi) \right) \\
\hline
39.37
\end{array} \right.
\end{aligned}
$$

The code for the vertical velocity during the contact is shown above. With the incident vertical velocity input in meters per second, and the remaining physical parameters in FPS units, it gives the vertical velocity during the contact as a function of dimensionless contact time, ‘n’. It gives the final answers in SI units.

Code for X velocity of the ball during sliding

$$
\begin{aligned}
&Vxs(\mu, M1, cy, ky, n, Vx1, Vy1) := \\
&\quad Vyi \leftarrow Vy1 \cdot 39.37 \\
&\quad Vxi \leftarrow Vx1 \cdot 39.37 \\
&\quad \omega y \leftarrow \sqrt{\frac{ky}{M1}} \\
&\quad \xi y \leftarrow \frac{cy}{2 \cdot M1 \cdot \omega y} \\
&\quad \omega dy \leftarrow \omega y \cdot \sqrt{1 - \xi y^2} \\
&\quad y \leftarrow \frac{Vyi}{\omega dy} \cdot e^{\frac{-n \cdot \xi y \cdot \pi \cdot \omega y}{\omega dy}} \cdot \sin(n \cdot \pi) \\
&\quad Vy \leftarrow \left(\frac{-Vyi \cdot \xi y \cdot \omega y \cdot e^{-\xi y \cdot \omega y \cdot \frac{n \cdot \pi}{\omega dy}}}{\omega dy} \cdot \sin(n \cdot \pi) + Vyi \cdot e^{-\xi y \cdot \omega y \cdot \frac{n \cdot \pi}{\omega dy}} \cdot \cos(n \cdot \pi) \right) \\
&\quad ax \leftarrow \frac{-\mu}{M} \cdot (|cy \cdot Vy + ky \cdot y|) \\
&\quad Vx1 \leftarrow cy \cdot \frac{Vyi}{\omega dy} \cdot e^{-\xi y \cdot \omega y \cdot \frac{n \cdot \pi}{\omega dy}} \cdot \sin(n \cdot \pi) \\
&\quad Vx2 \leftarrow \frac{ky \cdot Vyi}{\omega dy} \cdot \left(\frac{-\xi y \cdot \omega y}{\xi y^2 \cdot \omega y^2 + \omega dy^2} \cdot e^{-\xi y \cdot \omega y \cdot \frac{n \cdot \pi}{\omega dy}} \cdot \sin(n \cdot \pi) \right) \\
&\quad Vx3 \leftarrow \frac{ky \cdot Vyi}{\omega dy} \cdot \left(\frac{-\omega dy}{\xi y^2 \cdot \omega y^2 + \omega dy^2} \cdot e^{-\xi y \cdot \omega y \cdot \frac{n \cdot \pi}{\omega dy}} \cdot \cos(n \cdot \pi) + \frac{\omega dy}{\xi y^2 \cdot \omega y^2 + \omega dy^2} \right) \\
&\quad Vxi - \frac{\mu}{M} \cdot (|Vx1| + |Vx2| + |Vx3|)
\end{aligned}
$$

The above code evaluates the horizontal component of velocity of the two-mass system during the sliding contact as a function of the dimensionless contact time, ‘n’. As can be seen form the code, it is a function that is dependent on the vertical parameters of the two-mass system. The results that combine to produce the horizontal velocity during the contact are the integrations of the acceleration function. The code indicates the results for the case in which the friction force goes opposite to the X velocity. In case it goes in the same direction as the X velocity (topspin, in which surface velocity due to spin is higher than incident horizontal velocity), simply the sign if the term following Vxi in the last line should be put positive instead of the negative to give the correct velocity variation.

Code for the angular velocity of the ball during sliding

Vy1:=	(Incident vertical velocity in m/s)
Vx1:=	(Incident horizontal velocity in m/s)
Vyi=Vy1·39.37	(Incident vertical velocity in in/s)
Vxi=Vx1·39.37	(Incident horizontal velocity in in/s)
ω1:=	(Incident angular spin)
I:=0.000342	(Mass moment if inertia of ball (FPS units))
IG:=	(Mass moment of inertia of inner core)
I2:=	(Mass moment of inertia of outer shell)
kθ:=	(Torsional stiffness)

$M := 0.000329$ (Mass of the ball(FPS units))

$M1 :=$ (Mass of inner core)

$M2 :=$ (Mass of outer shell)

$R := 1.25$ (Outer radius of the ball(FPS units))

$cy :=$ (Damping coefficient(FPS units))

$ky :=$ (Stiffness coefficient(FPS units))

$$a1 \leftarrow \frac{1}{\left(\frac{1}{IG} + \frac{1}{I2}\right)}$$

$$\omega y \leftarrow \sqrt{\frac{ky}{M1}}$$

$$\xi y \leftarrow \frac{cy}{2 \cdot M1 \cdot \omega y}$$

$$\omega dy := \omega y \cdot \sqrt{1 - \xi y^2}$$

$$\omega\theta \leftarrow \sqrt{k\theta \cdot \left(\frac{1}{IG} + \frac{1}{I2}\right)}$$

$$b1 := c\theta$$

$$c1 := k\theta$$

$$\omega d\theta := \omega\theta \sqrt{1 - \xi\theta^2}$$

$$\gamma 1 \leftarrow \frac{\mu \cdot R}{I2} \cdot \left(\frac{ky \cdot Vyi}{\omega dy} - \frac{cy \cdot \xi y \cdot Vyi \cdot \omega y}{\omega dy} \right) \cdot \left(\frac{1}{IG} + \frac{1}{I2} \right)^{-1}$$

$$\gamma 2 \leftarrow \frac{\mu \cdot R}{I2} \cdot cy \cdot Vyi \cdot \left(\frac{1}{IG} + \frac{1}{I2} \right)^{-1}$$

$$\alpha 1 := -\xi y \cdot \omega y$$

$$\beta 1 := \omega dy$$

$$A1 \leftarrow \frac{(2 \cdot a1 \cdot \alpha 1 \cdot \beta 1 + b1 \cdot \beta 1)}{\left[\left(a1 \cdot \alpha 1^2 - a1 \cdot \beta 1^2 + b1 \cdot \alpha 1 + c1 \right)^2 + (2 \cdot a1 \cdot \alpha 1 \cdot \beta 1 + b1 \cdot \beta 1)^2 \right]} \cdot \left[\gamma 2 + \frac{\gamma 1 \cdot \left(a1 \cdot \alpha 1^2 - a1 \cdot \beta 1^2 + b1 \cdot \alpha 1 + c1 \right)}{(2 \cdot a1 \cdot \alpha 1 \cdot \beta 1 + b1 \cdot \beta 1)} \right]$$

$$B1 \leftarrow \frac{A1 \cdot \left(a1 \cdot \alpha 1^2 - a1 \cdot \beta 1^2 + b1 \cdot \alpha 1 + c1 \right) - \gamma 1}{(2 \cdot a1 \cdot \alpha 1 \cdot \beta 1 + b1 \cdot \beta 1)}$$

$$v\theta os1 := \frac{c\theta}{I2} \cdot \left(A1 \cdot e^{-\xi y \cdot \omega y \cdot \frac{n \cdot \pi}{\omega dy}} \cdot \sin(n \cdot \pi) + B1 \cdot e^{-\xi y \cdot \omega y \cdot \frac{n \cdot \pi}{\omega dy}} \cdot \cos(n \cdot \pi) - B1 \right)$$

$$v\theta os2 := \frac{k\theta}{I2} \cdot \int_0^n \left(A1 \cdot e^{-\xi y \cdot \omega y \cdot \frac{n \cdot \pi}{\omega dy}} \cdot \sin(n \cdot \pi) + B1 \cdot e^{-\xi y \cdot \omega y \cdot \frac{n \cdot \pi}{\omega dy}} \cdot \cos(n \cdot \pi) \right) \cdot \frac{\pi}{\omega dy} \, dn$$

$$v\theta os3 := \int_0^n \left(\gamma 1 \cdot e^{-\xi y \cdot \omega y \cdot \frac{n \cdot \pi}{\omega dy}} \cdot \sin\left(\omega dy \cdot \frac{n \cdot \pi}{\omega dy} \right) + \gamma 2 \cdot e^{-\xi y \cdot \omega y \cdot \frac{n \cdot \pi}{\omega dy}} \cdot \cos\left(\omega dy \cdot \frac{n \cdot \pi}{\omega dy} \right) \right) \cdot \frac{\pi}{\omega dy} \, dn + \omega 1$$

vθos := vθos1 + vθos2 + vθos3 (Angular velocity of outer shell)

Code for the angular velocity of the ball during rolling

Vy1:= (Incident vertical velocity in m/s)

Vx1:= (Incident horizontal velocity in m/s)

Vyi:=Vy1.39.37 (Incident vertical velocity in in/s)

Vxi:=Vx1.39.37 (Incident horizontal velocity in in/s)

ω1:= (Incident angular spin)

I:=0.000342 (Mass moment if inertia of ball (FPS units))

IG:= (Mass moment of inertia of inner core)

I2:= (Mass moment of inertia of outer shell)

kθ:= (Torsional stiffness)

M:=0.000329 (Mass of the ball(FPS units))

M1:= (Mass of inner core)

M2:= (Mass of outer shell)

R:=1.25 (Outer radius of the ball(FPS units))

cy:= (Damping coefficient(FPS units))

ky:= (Stiffness coefficient(FPS units))

ε:= (Eccentricity of normal force)

$$\omega y := \sqrt{\frac{ky}{M1}}$$

$$\xi y := \frac{cy}{2 \cdot M1 \cdot \omega y}$$

$$\omega dy := \omega y \cdot \sqrt{1 - \xi y^2}$$

$$\omega\theta \leftarrow \sqrt{k\theta \cdot \left(\frac{1}{IG} + \frac{1}{I2 + M \cdot R^2} \right)}$$

$$\xi\theta \leftarrow \sqrt{1 - \left(\frac{\omega y}{\omega\theta} \right)^2 \cdot \left(1 - \xi y^2 \right)}$$

$$\omega d\theta \leftarrow \omega\theta \cdot \sqrt{1 - \xi\theta^2}$$

$$a1 \leftarrow \frac{1}{\left(\frac{1}{IG} + \frac{1}{I2 + M \cdot R^2} \right)}$$

$$c\theta \leftarrow 2 \cdot \xi\theta \cdot \sqrt{\frac{k\theta}{\left(\frac{1}{IG} + \frac{1}{I2 + M \cdot R^2} \right)}}$$

$$b1 \leftarrow c\theta$$

$$c1 \leftarrow k\theta$$

$$\gamma 1 \leftarrow \frac{-\varepsilon}{I2 + M \cdot R^2} \cdot \left(\frac{ky \cdot Vyi}{\omega dy} - \frac{cy \cdot \xi y \cdot Vyi \cdot \omega y}{\omega dy} \right) \cdot \left(\frac{1}{IG} + \frac{1}{I2 + M \cdot R^2} \right)^{-1}$$

$$\gamma 2 \leftarrow \frac{-\varepsilon}{I2 + M \cdot R^2} \cdot cy \cdot Vyi \cdot \left(\frac{1}{IG} + \frac{1}{I2 + M \cdot R^2} \right)^{-1}$$

$\alpha 1 := -\xi y \cdot \omega y$

$\beta 1 := \omega d\theta$

$$A1 \leftarrow \frac{(2 \cdot a1 \cdot \alpha 1 \cdot \beta 1 + b1 \cdot \beta 1)}{\left[\left(a1 \cdot \alpha 1^2 - a1 \cdot \beta 1^2 + b1 \cdot \alpha 1 + c1\right)^2 + (2 \cdot a1 \cdot \alpha 1 \cdot \beta 1 + b1 \cdot \beta 1)^2\right]} \cdot \left[\gamma 2 + \frac{\gamma 1 \cdot \left(a1 \cdot \alpha 1^2 - a1 \cdot \beta 1^2 + b1 \cdot \alpha 1 + c1\right)}{(2 \cdot a1 \cdot \alpha 1 \cdot \beta 1 + b1 \cdot \beta 1)}\right]$$

$$B1 \leftarrow \frac{A1 \cdot \left(a1 \cdot \alpha 1^2 - a1 \cdot \beta 1^2 + b1 \cdot \alpha 1 + c1\right) - \gamma 1}{(2 \cdot a1 \cdot \alpha 1 \cdot \beta 1 + b1 \cdot \beta 1)}$$

$$\theta i \leftarrow \sqrt{\frac{M \cdot \left(Vxi^2\right) + I \cdot \omega 1^2 - IG \cdot \omega 1^2}{I2 + M \cdot R^2}}$$

$n := 0, 0.001 \ldots 1$

$$v\theta or1(n) := \frac{k\theta}{I2 + M \cdot R^2} \cdot \int_0^n \left[\frac{(\omega 1 - \theta i)}{\omega d\theta} \cdot e^{-\xi\theta \cdot \omega\theta \cdot \frac{n \cdot \pi}{\omega dy}} \cdot \sin\left(\omega d\theta \cdot \frac{n \cdot \pi}{\omega dy}\right)\right] \cdot \frac{\pi}{\omega dy}\, dn$$

$$v\theta or2(n) := \frac{k\theta}{I2 + M \cdot R^2} \cdot \int_0^n \left(A1 \cdot e^{-\xi y \cdot \omega y \cdot \frac{n \cdot \pi}{\omega dy}} \cdot \sin\left(\omega dy \cdot \frac{n \cdot \pi}{\omega dy}\right) + B1 \cdot e^{-\xi y \cdot \omega y \cdot \frac{n \cdot \pi}{\omega dy}} \cdot \cos\left(\omega dy \cdot \frac{n \cdot \pi}{\omega dy}\right) - B1\right) \cdot \frac{\pi}{\omega dy}\, dn$$

$$v\theta or3(n) := \frac{c\theta}{I2 + M \cdot R^2} \cdot \left[\frac{(\omega 1 - \theta i)}{\omega d\theta} \cdot e^{-\xi\theta \cdot \omega\theta \cdot \frac{n \cdot \pi}{\omega dy}} \cdot \sin\left(\omega d\theta \cdot \frac{n \cdot \pi}{\omega dy}\right)\right]$$

$$v\theta or4(n) := \frac{c\theta}{I2 + M \cdot R^2} \cdot \left(A1 \cdot e^{-\xi y \cdot \omega y \cdot \frac{n \cdot \pi}{\omega dy}} \cdot \sin\left(\omega dy \cdot \frac{n \cdot \pi}{\omega dy}\right) + B1 \cdot e^{-\xi y \cdot \omega y \cdot \frac{n \cdot \pi}{\omega dy}} \cdot \cos\left(\omega dy \cdot \frac{n \cdot \pi}{\omega dy}\right) - B1\right)$$

$$v\theta or5(n) := \int_0^n \left(\gamma 1 \cdot e^{-\xi y \cdot \omega y \cdot \frac{n \cdot \pi}{\omega dy}} \cdot \sin\left(\omega dy \cdot \frac{n \cdot \pi}{\omega dy} \right) + \gamma 2 \cdot e^{-\xi y \cdot \omega y \cdot \frac{n \cdot \pi}{\omega dy}} \cdot \cos\left(\omega dy \cdot \frac{n \cdot \pi}{\omega dy} \right) \right) \cdot \frac{\pi}{\omega dy} \, dn + \theta i$$

$$v\theta or(n) = v\theta or1(n) + v\theta or2(n) + v\theta or3(n) + v\theta or4(n) + v\theta or5(n)$$

$$Vx(n) = R \cdot v\theta or(n)$$

<u>Code for the transition point during contact (sliding to rolling transition)</u>

n= ▪

sol:=root(Vx(n) – R·vθos(n), n)

sol=▪

Vx(sol) =▪

$$\frac{Vx(sol)}{R} = \blacksquare$$

vθos(sol) =▪

ω2:=vθos(sol)

APPENDIX C

COMPARISON OF THEORY WITH EXPERIMENT

SIMULATION RESULTS

Some simulation results for the tennis ball dynamics are shown on the following pages. For each incident angle and for the major cases of zero spin, topspin and backspin, there are several possibilities of varying the mass, the stiffness, the damping, the mass moment of inertias and the torsional stiffness parameters and then obtaining the rebound kinematics. Accordingly, first of all, three cases for the impact have been categorized as zero spin, topspin and backspin. Then, for each of those major categories, sub-categories have been formed based on the angles of incidence of the ball with the ground. For the experimental data available **[1]**, the angles of incidence vary from 17 degrees to 70 degrees. For each angle of incidence, the cases column on the extreme left of the Tables indicates that the dynamic input parameters of the tennis ball model are varied i.e., the inner core mass, the torsional stiffness, the moments of inertia etc. and these variations produce the simulated values in the columns for the rebound velocities, the rebound angle and the time of contact of the ball with the ground, which are the last five columns.

The fixed inputs are the parameters that are constant for each incidence angle. These include the horizontal and the vertical components of the incident velocity, with the values being input the same as those found out from the experimental results for each of these angles. Another important fixed parameter to be used in order to generate the simulated values of the kinematics includes the vertical coefficient of restitution, with the value being input same as that obtained from the corresponding experimental result. The first four columns in the table are ones that directly affect the value of the vertical coefficient of restitution (equation (6), Chapter 1) and these input parameter values are

adjusted for each simulation such that the theoretical value of the coefficient of restitution is equal to the one input, which in turn is equal to the experimental value for that particular case. Another fixed input parameter is coefficient of sliding friction. All simulations are based on an assumption that the damped period of vibration in relative rotation is equal to the period of vibration in vertical motion. This ensures that the rotational vibrations complete their one cycle during the impact and that the cycle is not incomplete when the contact finally ends. Equating these two periods also provides with an estimation of the damping ratio in the rotation. The value of 1000 lb-in/rad has been used for torsional stiffness, since it produces the best agreements with the experiments, and also that it fits the description of a tennis ball as a relatively stiff torsional spring [1]. The solutions of the differential equations derived in chapter II have been coded in the MathCAD software and all the results have been obtained from there.

The actual experiments [1] were performed on an acrylic surface, for which the average sliding coefficient of friction is 0.55. This same value is used throughout the simulations for this parameter.

It is helpful to ascertain some fixed physical parameters of the whole system.

Mass of tennis ball

According to [1], the tennis ball weight is around 0.0576 kg or 0.127 lb. From the International Tennis Federation (ITF) standards, the weight should be between 56.0 grams and 59.4 grams. For the simulations, the weight of 0.127 lb has been selected.

The mass can be calculated as follows:

$$M = \frac{W}{g} = \frac{0.127}{386.4} = 0.000329 lb - \frac{s^2}{in}$$

SELECTED CASES

The selected cases for comparison with the experiment are presented in tables 7 to 27 and figures 35 to 51.

ZERO SPIN IMPACT

17 degrees angle of incidence

Fixed Inputs:

Incident horizontal velocity = V_{x1} =15.62 m/s

Incident vertical velocity = V_{y1} = 4.81 m/s

Incident spin velocity = ω_1 = 0 rad/s

Vertical coefficient of restitution = 0.877

Coefficient of sliding friction = μ = 0.55

Torsional stiffness coefficient = k_θ = 1000 lb-in/rad

Table C1. Dynamic parameters and simulation results

Cases	M_1	M_2	k_y	c_y	I_1	I_2	I	V_{y2}	V_{x2}	ω_2	θ_2	t_c
	Lb-s^2/in	Lb-s^2/in	Lb/in	Lb-s/in	Lb-in-s^2	Lb-in-s^2	Lb-in-s^2	m/s	m/s	Rad/s	Degrees	msec
1	M/2	M/2	72	0.029	0.352I	0.647I	0.00028	-4.217	13.399	73.846	-15.356	4.791
2	M/2	M/2	80	0.031	0.352I	0.647I	0.00028	-4.217	13.403	73.901	-15.352	4.546
3	M/2	M/2	90	0.0338	0.352I	0.647I	0.00028	-4.217	13.394	74.527	-15.362	4.288
4	2M/3	M/3	72	0.0107	0.532I	0.468I	0.00026	-4.217	12.308	244.57	-16.645	5.488
5	2M/3	M/3	80	0.0113	0.532I	0.468I	0.00026	-4.22	12.309	245.44	-16.645	5.206
6	2M/3	M/3	90	0.0119	0.532I	0.468I	0.00026	-4.219	12.307	245.86	-16.646	4.908
7	3M/4	M/4	90	0.00187	0.634I	0.366I	0.00025	-4.219	11.691	298.83	-17.471	5.202

2. 23 degrees angle of incidence
Fixed Inputs:

Incident horizontal velocity = V_{x1} =15.62 m/s

Incident vertical velocity = V_{y1} = 6.71 m/s

Incident spin velocity = ω_1 = 0 rad/s

Vertical coefficient of restitution = 0.858

Coefficient of sliding friction = μ = 0.55

Torsional stiffness coefficient = k_θ = 1000 lb-in/rad

Table C2. Dynamic parameters and simulation results

Cases	M_1	M_2	k_y	c_y	I_1	I_2	I	V_{y2}	V_{x2}	ω_2	θ_2	t_c
	Lb-s^2/in	Lb-s^2/in	Lb/in	Lb-s/in	Lb-in-s^2	Lb-in-s^2	Lb-in-s^2	m/s	m/s	Rad/s	Degrees	msec
1	M/2	M/2	72	0.029	0.352I	0.647I	0.00028	-5.757	12.521	104.24	-22.292	4.791
2	M/2	M/2	80	0.031	0.352I	0.647I	0.00028	-5.757	12.528	103.09	-24.669	4.546
3	M/2	M/2	90	0.0338	0.352I	0.647I	0.00028	-5.754	12.54	104.57	-24.671	4.288
4	2M/3	M/3	72	0.0107	0.532I	0.468I	0.00026	-5.76	11.08	335.56	-27.468	5.488
5	2M/3	M/3	80	0.0113	0.532I	0.468I	0.00026	-5.76	11.087	335.76	-27.441	5.206
6	2M/3	M/3	90	0.0119	0.532I	0.468I	0.00026	-5.757	11.095	336.01	-27.444	4.908
7	3M/4	M/4	90	0.00187	0.634I	0.366I	0.00025	-5.762	11.47	361.26	-26.649	5.202

3. 35 degrees angle of incidence

Fixed Inputs:

Incident horizontal velocity = V_{x1} =14.49 m/s

Incident vertical velocity = V_{y1} = 9.95 m/s

Incident spin velocity = ω_1 = 0 rad/s

Vertical coefficient of restitution = 0.7698

Coefficient of sliding friction = μ = 0.55

Torsional stiffness coefficient = k_θ = 1000 lb-in/rad

Table C3. Dynamic parameters and simulation results

Cases	M_1	M_2	k_y	c_y	I_1	I_2	I	V_{y2}	V_{x2}	ω_2	θ_2	t_c
	Lb-s^2/in	Lb-s^2/in	Lb/in	Lb-s/in	Lb-in-s^2	Lb-in-s^2	Lb-in- s^2	m/s	m/s	Rad/s	Degrees	msec
1	M/2	M/2	72	0.029	0.352I	0.647I	0.00028	-7.654	9.895	152.47	-37.569	4.791
2	M/2	M/2	80	0.031	0.352I	0.647I	0.00028	-7.654	9.904	152.87	-37.730	4.546
3	M/2	M/2	90	0.0338	0.352I	0.647I	0.00028	-7.663	9.923	152.74	-37.622	4.288
4	2M/3	M/3	72	0.0107	0.532I	0.468I	0.00026	-7.648	9.97	301.94	-37.714	5.488
5	2M/3	M/3	80	0.0113	0.532I	0.468I	0.00026	-7.654	10.144	307.20	-37.014	5.206
6	2M/3	M/3	90	0.0119	0.532I	0.468I	0.00026	-7.648	10.148	307.32	-37.018	4.908
7	3M/4	M/4	90	0.00187	0.634I	0.366I	0.00025	-7.652	11.089	335.82	-34.608	5.202

4. 41 degrees angle of incidence

Fixed Inputs:

Incident horizontal velocity = V_{x1} =13.46 m/s

Incident vertical velocity = V_{y1} = 11.74 m/s

Incident spin velocity = ω_1 = 0 rad/s

Vertical coefficient of restitution = 0.7436

Coefficient of sliding friction = μ = 0.55

Torsional stiffness coefficient = k_θ = 1000 lb-in/rad

Table C4. Dynamic parameters and simulation results

Cases	M_1	M_2	k_y	c_y	I_1	I_2	I	V_{y2}	V_{x2}	ω_2	θ_2	t_c
	Lb-s^2/in	Lb-s^2/in	Lb/in	Lb-s/in	Lb-in-s^2	Lb-in-s^2	Lb-in- s^2	m/s	m/s	Rad/s	Degrees	msec
1	M/2	M/2	72	0.029	0.352I	0.647I	0.00028	-8.733	8.038	180.24	-48.172	4.791
2	M/2	M/2	80	0.031	0.352I	0.647I	0.00028	-8.733	8.049	180.37	-47.334	4.546
3	M/2	M/2	90	0.0338	0.352I	0.647I	0.00028	-8.733	8.071	180.21	-47.259	4.288
4	2M/3	M/3	72	0.0107	0.532I	0.468I	0.00026	-8.734	9.269	280.70	-43.278	5.488
5	2M/3	M/3	80	0.0113	0.532I	0.468I	0.00026	-8.728	9.169	277.67	-43.582	5.206
6	2M/3	M/3	90	0.0119	0.532I	0.468I	0.00026	-8.726	9.273	280.83	-43.263	4.908
7	3M/4	M/4	90	0.00187	0.634I	0.366I	0.00025	-8.727	9.219	279.18	-42.429	5.202

5. <u>48 degrees angle of incidence</u>

Fixed Inputs:

Incident horizontal velocity = V_{x1} =11.7 m/s

Incident vertical velocity = V_{y1} = 13.25 m/s

Incident spin velocity = ω_1 = 0 rad/s

Vertical coefficient of restitution = 0.7072

Coefficient of sliding friction = μ = 0.55

Torsional stiffness coefficient = k_θ = 1000 lb-in/rad

Table C5. Dynamic parameters and simulation results

Cases	M_1	M_2	k_y	c_y	I_1	I_2	k_θ	V_{y2}	V_{x2}	ω_2	θ_2	t_c
	Lb-s^2/in	Lb-s^2/in	Lb/in	Lb-s/in	Lb-in-s^2	Lb-in-s^2	Lb-in- s^2	m/s	m/s	Rad/s	Degrees	msec
1	M/2	M/2	72	0.029	0.352I	0.647I	0.00028	-9.363	6.14	185.95	-58.795	4.791
2	M/2	M/2	80	0.031	0.352I	0.647I	0.00028	-9.363	6.149	186.21	-56.703	4.546
3	M/2	M/2	90	0.0338	0.352I	0.647I	0.00028	-9.362	6.16	186.55	-56.667	4.288
4	2M/3	M/3	72	0.0107	0.532I	0.468I	0.00026	-9.366	7.891	238.98	-49.876	5.488
5	2M/3	M/3	80	0.0113	0.532I	0.468I	0.00026	-9.363	7.894	239.06	-49.896	5.206
6	2M/3	M/3	90	0.0119	0.532I	0.468I	0.00026	-9.373	7.894	239.07	-49.884	4.908
7	3M/4	M/4	90	0.00187	0.634I	0.366I	0.00025	-9.369	7.795	245.5	-50.239	5.202

6. <u>59 degrees angle of incidence</u>

Fixed Inputs:

Incident horizontal velocity = V_{x1} =9.16 m/s

Incident vertical velocity = V_{y1} = 15.19 m/s

Incident spin velocity = ω_1 = 0 rad/s

Vertical coefficient of restitution = 0.7156

Coefficient of sliding friction = μ = 0.55

Torsional stiffness coefficient = k_θ = 1000 lb-in/rad

Table C6. Dynamic parameters and simulation results

Cases	M_1	M_2	k_y	c_y	I_1	I_2	I	V_{y2}	V_{x2}	ω_2	θ_2	t_c
	Lb-s^2/in	Lb-s^2/in	Lb/in	Lb-s/in	Lb-in-s^2	Lb-in-s^2	Lb-in- s^2	m/s	m/s	Rad/s	Degrees	msec
1	M/2	M/2	72	0.029	0.352I	0.647I	0.00028	-10.87	4.702	142.39	-67.970	4.791
2	M/2	M/2	80	0.031	0.352I	0.647I	0.00028	-10.87	4.672	141.49	-66.766	4.546
3	M/2	M/2	90	0.0338	0.352I	0.647I	0.00028	-10.88	4.68	141.47	-66.723	4.288
4	2M/3	M/3	72	0.0107	0.532I	0.468I	0.00026	-10.88	5.747	174.05	-62.136	5.488
5	2M/3	M/3	80	0.0113	0.532I	0.468I	0.00026	-10.87	5.745	173.99	-62.155	5.206
6	2M/3	M/3	90	0.0119	0.532I	0.468I	0.00026	-10.87	5.742	173.90	-62.168	4.908
7	3M/4	M/4	90	0.00187	0.634I	0.366I	0.00025	-10.87	5.185	163.30	-64.511	5.202

7. <u>68 degrees angle of incidence</u>

Fixed Inputs:

Incident horizontal velocity = V_{x1} =6.57 m/s

Incident vertical velocity = V_{y1} = 16.14 m/s

Incident spin velocity = ω_1 = 0 rad/s

Vertical coefficient of restitution = 0.6871

Coefficient of sliding friction = μ = 0.55

Torsional stiffness coefficient = k_θ = 1000 lb-in/rad

Table C7. Dynamic parameters and simulation results

Cases	M_1	M_2	k_y	c_y	I_1	I_2	I	V_{y2}	V_{x2}	ω_2	θ_2	t_c
	Lb-s^2/in	Lb-s^2/in	Lb/in	Lb-s/in	Lb-in-s^2	Lb-in-s^2	Lb-in- s^2	m/s	m/s	Rad/s	Degrees	msec
1	M/2	M/2	72	0.029	0.352I	0.647I	0.00028	-11.14	3.179	96.283	-75.562	4.791
2	M/2	M/2	80	0.031	0.352I	0.647I	0.00028	-11.14	3.183	96.389	-74.049	4.546
3	M/2	M/2	90	0.0338	0.352I	0.647I	0.00028	-11.13	3.188	96.55	-74.032	4.288
4	2M/3	M/3	72	0.0107	0.532I	0.468I	0.00026	-11.14	3.701	112.09	-71.543	5.488
5	2M/3	M/3	80	0.0113	0.532I	0.468I	0.00026	-11.09	3.698	111.99	-71.561	5.206
6	2M/3	M/3	90	0.0119	0.532I	0.468I	0.00026	-11.13	3.693	111.84	-71.644	4.908
7	3M/4	M/4	90	0.00187	0.634I	0.366I	0.00025	-11.13	0.554	16.78	-87.151	5.202

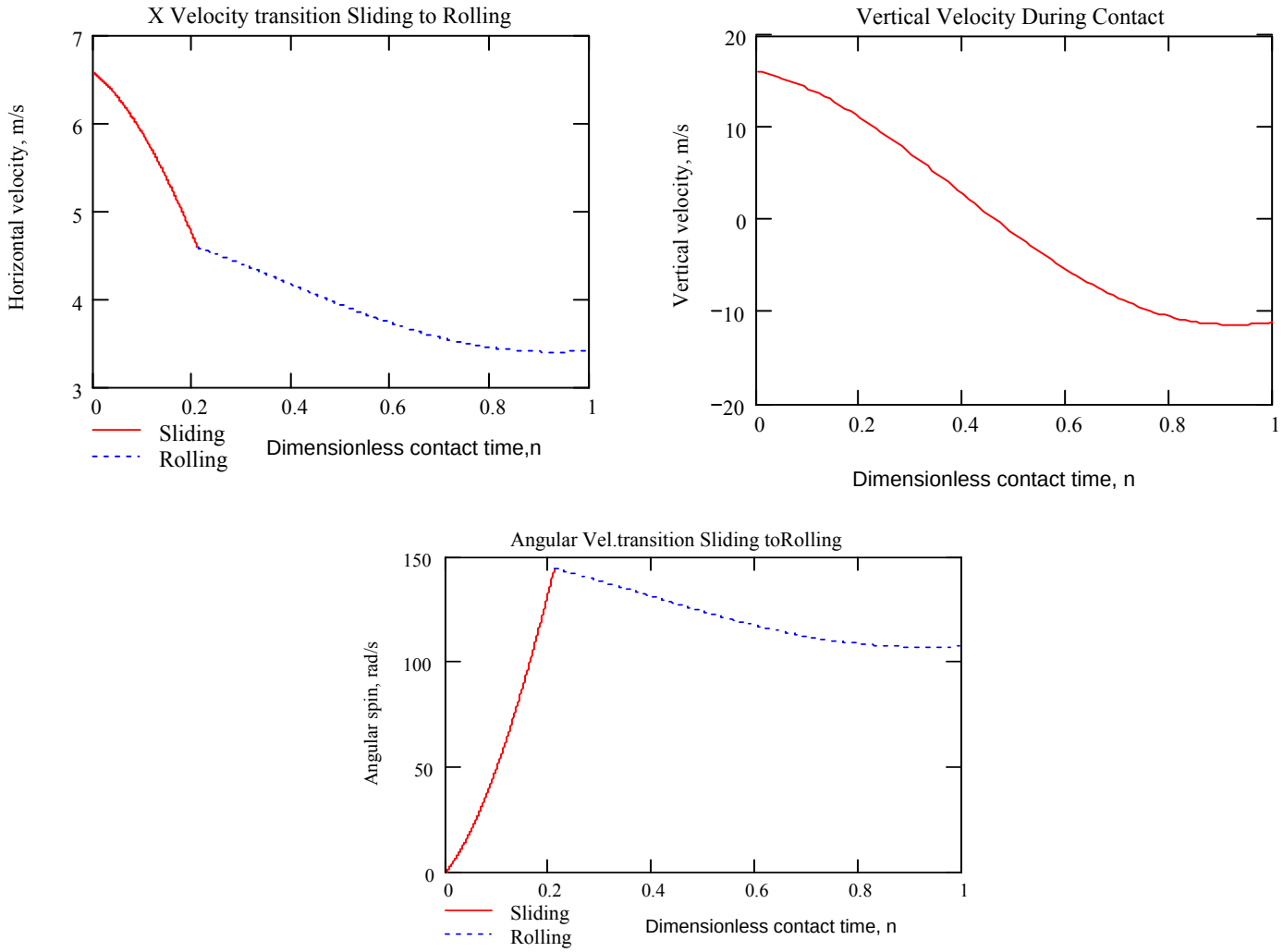

Fig.C1 Kinematic parameters and their variation with time during contact, case 1

TOPSPIN IMPACT

18 degrees angle of incidence

Fixed Inputs:

Incident horizontal velocity = V_{x1} =16.13 m/s

Incident vertical velocity = V_{y1} = 5.33 m/s

Incident spin velocity = ω_1 = 138.20 rad/s

Vertical coefficient of restitution = 0.876

Coefficient of sliding friction = μ = 0.55

Torsional stiffness coefficient = k_θ = 1000 lb-in/rad

Table C8. Dynamic parameters and simulation results

Cases	M_1	M_2	k_y	c_y	I_1	I_2	I	V_{y2}	V_{x2}	ω_2	θ_2	t_c
	Lb-s^2/in	Lb-s^2/in	Lb/in	Lb-s/in	Lb-in-s^2	Lb-in-s^2	Lb-in- s^2	m/s	m/s	Rad/s	Degrees	msec
1	M/2	M/2	72	0.03	0.352I	0.647I	0.00028	-4.67	13.681	219.55	-18.847	4.794
2	M/2	M/2	80	0.0318	0.352I	0.647I	0.00028	-4.67	13.683	217.01	-18.841	4.548
3	M/2	M/2	90	0.0338	0.352I	0.647I	0.00028	-4.669	13.683	220.02	-18.852	4.288
4	2M/3	M/3	72	0.0123	0.532I	0.468I	0.00026	-4.672	12.766	386.62	-20.085	5.489
5	2M/3	M/3	80	0.0129	0.532I	0.468I	0.00026	-4.668	12.771	386.76	-20.082	5.208
6	2M/3	M/3	90	0.0137	0.532I	0.468I	0.00026	-4.669	12.777	386.93	-20.077	4.910
7	3M/4	M/4	90	0.00345	0.634I	0.366I	0.00025	-4.67	12.762	386.48	-20.099	5.517

2. <u>23 degrees angle of incidence</u>

Fixed Inputs:

Incident horizontal velocity = V_{x1} =16.19 m/s

Incident vertical velocity = V_{y1} = 6.75 m/s

Incident spin velocity = ω_1 = 158.06 rad/s

Vertical coefficient of restitution = 0.905

Coefficient of sliding friction = μ = 0.55

Torsional stiffness coefficient = k_θ = 1000 lb-in/rad

Table C9. Dynamic parameters and simulation results

Cases	M_1	M_2	k_y	c_y	I_1	I_2	I	V_{y2}	V_{x2}	ω_2	θ_2	t_c
	Lb-s^2/in	Lb-s^2/in	Lb/in	Lb-s/in	Lb-in-s^2	Lb-in-s^2	Lb-in- s^2	m/s	m/s	Rad/s	Degrees	msec
1	M/2	M/2	72	0.03	0.352I	0.647I	0.00028	-6.11	13.088	261.08	-25.025	4.794
2	M/2	M/2	80	0.0318	0.352I	0.647I	0.00028	-6.11	13.091	260.02	-25.009	4.548
3	M/2	M/2	90	0.0338	0.352I	0.647I	0.00028	-6.107	13.092	259.25	-25.022	4.288
4	2M/3	M/3	72	0.0123	0.532I	0.468I	0.00026	-6.111	12.968	392.72	-25.217	5.489
5	2M/3	M/3	80	0.0129	0.532I	0.468I	0.00026	-6.107	12.971	392.83	-25.248	5.208
6	2M/3	M/3	90	0.0137	0.532I	0.468I	0.00026	-6.117	12.975	392.95	-25.216	4.910
7	3M/4	M/4	90	0.00345	0.634I	0.366I	0.00025	-6.11	13.821	418.55	-23.849	5.517

3. <u>34 degrees angle of incidence</u>

Fixed Inputs:

Incident horizontal velocity = V_{x1} =14.83m/s

Incident vertical velocity = V_{y1} = 9.98 m/s

Incident spin velocity = ω_1 = 152.53 rad/s

Vertical coefficient of restitution = 0.827

Coefficient of sliding friction = μ = 0.55

Torsional stiffness coefficient = k_θ = 1000 lb-in/rad

Table C10. Dynamic parameters and simulation results

Cases	M_1	M_2	k_y	c_y	I_1	I_2	k_θ	V_{y2}	V_{x2}	ω_2	θ_2	t_c
	Lb-s^2/in	Lb-s^2/in	Lb/in	Lb-s/in	Lb-in-s^2	Lb-in-s^2	Lb-in- s^2	m/s	m/s	Rad/s	Degrees	msec
1	M/2	M/2	72	0.03	0.352I	0.647I	0.00028	-8.257	10.244	304.86	-38.87	4.794
2	M/2	M/2	80	0.0318	0.352I	0.647I	0.00028	-8.257	10.248	305.18	-38.862	4.548
3	M/2	M/2	90	0.0338	0.352I	0.647I	0.00028	-8.258	10.249	305.73	-38.836	4.288
4	2M/3	M/3	72	0.0123	0.532I	0.468I	0.00026	-8.251	11.78	356.76	-35.002	5.489
5	2M/3	M/3	80	0.0129	0.532I	0.468I	0.00026	-8.249	11.737	355.44	-35.110	5.208
6	2M/3	M/3	90	0.0137	0.532I	0.468I	0.00026	-8.252	11.783	356.86	-34.995	4.910
7	3M/4	M/4	90	0.00345	0.634I	0.366I	0.00025	-8.249	12.414	375.96	-33.604	5.517

4. <u>42 degrees angle of incidence</u>

Fixed Inputs:

Incident horizontal velocity = V_{x1} =13.76m/s

Incident vertical velocity = V_{y1} = 12.55 m/s

Incident spin velocity = ω_1 = 136.32 rad/s

Vertical coefficient of restitution = 0.726

Coefficient of sliding friction = μ = 0.55

Torsional stiffness coefficient = k_θ = 1000 lb-in/rad

Table C11. Dynamic parameters and simulation results

Cases	M_1	M_2	k_y	c_y	I_1	I_2	I	V_{y2}	V_{x2}	ω_2	θ_2	t_c
	Lb-s^2/in	Lb-s^2/in	Lb/in	Lb-s/in	Lb-in-s^2	Lb-in-s^2	Lb-in- s^2	m/s	m/s	Rad/s	Degrees	msec
1	M/2	M/2	72	0.03	0.352I	0.647I	0.00028	-9.119	9.318	282.18	-44.382	4.794
2	M/2	M/2	80	0.0318	0.352I	0.647I	0.00028	-9.119	9.324	282.36	-44.319	4.548
3	M/2	M/2	90	0.0338	0.352I	0.647I	0.00028	-9.105	9.33	282.56	-44.307	4.288
4	2M/3	M/3	72	0.0123	0.532I	0.468I	0.00026	-9.107	10.803	327.16	-40.134	5.489
5	2M/3	M/3	80	0.0129	0.532I	0.468I	0.00026	-9.108	9.813	297.18	-42.859	5.208
6	2M/3	M/3	90	0.0137	0.532I	0.468I	0.00026	-9.106	10.638	322.16	-40.573	4.910
7	3M/4	M/4	90	0.00345	0.634I	0.366I	0.00025	-9.109	11.096	336.04	-39.384	5.517

5. <u>48 degrees angle of incidence</u>

Fixed Inputs:

Incident horizontal velocity = V_{x1} =11.98m/s

Incident vertical velocity = V_{y1} = 13.17 m/s

Incident spin velocity = ω_1 = 147.58 rad/s

Vertical coefficient of restitution = 0.750

Coefficient of sliding friction = μ = 0.55

Torsional stiffness coefficient = k_θ = 1000 lb-in/rad

Table C12. Dynamic parameters and simulation results

Cases	M_1	M_2	k_y	c_y	I_1	I_2	I	V_{y2}	V_{x2}	ω_2	θ_2	t_c
	Lb-s^2/in	Lb-s^2/in	Lb/in	Lb-s/in	Lb-in-s^2	Lb-in-s^2	Lb-in- s^2	m/s	m/s	Rad/s	Degrees	msec
1	M/2	M/2	72	0.03	0.352I	0.647I	0.00028	-9.883	8.487	257.04	-49.346	4.794
2	M/2	M/2	80	0.0318	0.352I	0.647I	0.00028	-9.883	8.491	257.15	-49.321	4.548
3	M/2	M/2	90	0.0338	0.352I	0.647I	0.00028	-9.879	8.496	257.28	-49.293	4.288
4	2M/3	M/3	72	0.0123	0.532I	0.468I	0.00026	-9.875	9.373	283.85	-46.503	5.489
5	2M/3	M/3	80	0.0129	0.532I	0.468I	0.00026	-9.878	9.371	283.80	-46.523	5.208
6	2M/3	M/3	90	0.0137	0.532I	0.468I	0.00026	-9.883	9.369	283.75	-46.549	4.910
7	3M/4	M/4	90	0.00345	0.634I	0.366I	0.00025	-9.89	9.622	291.38	-45.755	5.517

6. <u>61 degrees angle of incidence</u>

Fixed Inputs:

Incident horizontal velocity = V_{x1} =8.45 m/s

Incident vertical velocity = V_{y1} = 15.29 m/s

Incident spin velocity = ω_1 = 146.74 rad/s

Vertical coefficient of restitution = 0.688

Coefficient of sliding friction = μ = 0.55

Torsional stiffness coefficient = k_θ = 1000 lb-in/rad

Table C13. Dynamic parameters and simulation results

Cases	M_1	M_2	k_y	c_y	I_1	I_2	I	V_{y2}	V_{x2}	ω_2	θ_2	t_c
	Lb-s^2/in	Lb-s^2/in	Lb/in	Lb-s/in	Lb-in-s^2	Lb-in-s^2	Lb-in- s^2	m/s	m/s	Rad/s	Degrees	msec
1	M/2	M/2	72	0.03	0.352I	0.647I	0.00028	-10.52	6.425	194.56	-58.591	4.794
2	M/2	M/2	80	0.0318	0.352I	0.647I	0.00028	-10.52	6.425	194.59	-58.586	4.548
3	M/2	M/2	90	0.0338	0.352I	0.647I	0.00028	-10.52	6.798	205.88	-57.112	4.288
4	2M/3	M/3	72	0.0123	0.532I	0.468I	0.00026	-10.51	6.500	196.84	-58.287	5.489
5	2M/3	M/3	80	0.0129	0.532I	0.468I	0.00026	-10.52	6.496	196.72	-58.303	5.208
6	2M/3	M/3	90	0.0137	0.532I	0.468I	0.00026	-10.52	6.491	196.58	-58.322	4.910
7	3M/4	M/4	90	0.00345	0.634I	0.366I	0.00025	-10.52	6.328	191.65	-58.69	5.517

7. <u>71 degrees angle of incidence</u>

Fixed Inputs:

Incident horizontal velocity = V_{x1} =5.67 m/s

Incident vertical velocity = V_{y1} = 16.39 m/s

Incident spin velocity = ω_1 = 145.88 rad/s

Vertical coefficient of restitution = 0.674

Coefficient of sliding friction = μ = 0.55

Torsional stiffness coefficient = k_θ = 1000 lb-in/rad

Table C14. Dynamic parameters and simulation results

Cases	M_1	M_2	k_y	c_y	I_1	I_2	I	V_{y2}	V_{x2}	ω_2	θ_2	t_c
	Lb-s^2/in	Lb-s^2/in	Lb/in	Lb-s/in	Lb-in-s^2	Lb-in-s^2	Lb-in- s^2	m/s	m/s	Rad/s	Degrees	msec
1	M/2	M/2	72	0.03	0.352I	0.647I	0.00028	-11.05	4.795	145.21	-66.538	4.794
2	M/2	M/2	80	0.0318	0.352I	0.647I	0.00028	-11.05	4.794	145.17	-66.533	4.548
3	M/2	M/2	90	0.0338	0.352I	0.647I	0.00028	-11.04	4.791	145.11	-66.556	4.288
4	2M/3	M/3	72	0.0123	0.532I	0.468I	0.00026	-11.05	4.27	129.32	-68.867	5.489
5	2M/3	M/3	80	0.0129	0.532I	0.468I	0.00026	-11.05	4.265	129.16	-68.888	5.208
6	2M/3	M/3	90	0.0137	0.532I	0.468I	0.00026	-11.05	4.259	128.99	-68.915	4.910
7	3M/4	M/4	90	0.00345	0.634I	0.366I	0.00025	-11.05	3.799	115.06	-71.021	5.517

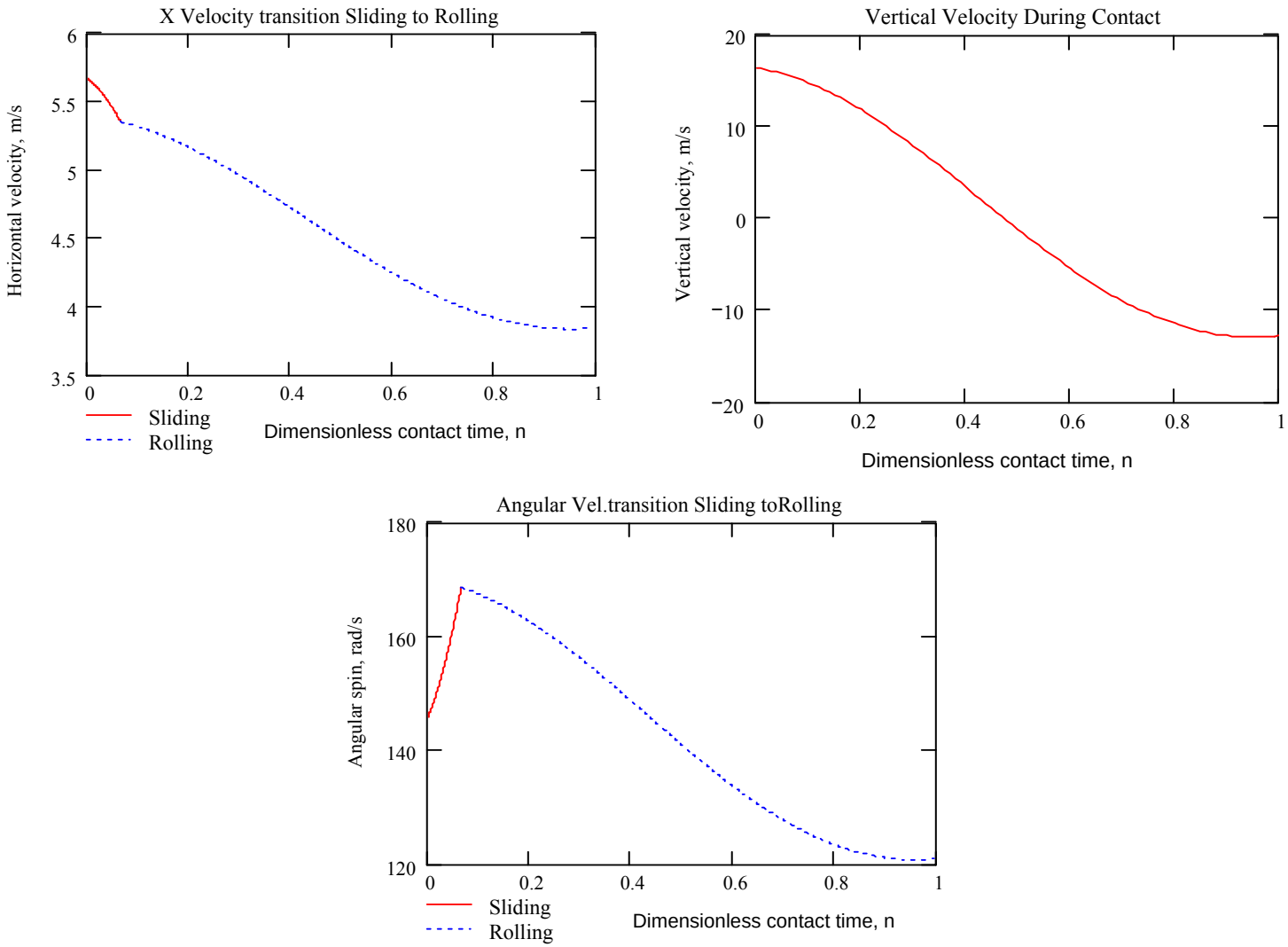

Fig.C2 Kinematic parameters and their variation with time during contact, case 6.

BACKSPIN IMPACT

1. 17 degrees angle of incidence

Fixed Inputs:

Incident horizontal velocity = V_{x1} =16.18 m/s

Incident vertical velocity = V_{y1} = 5.08 m/s

Incident spin velocity = ω_1 = -168.32 rad/s

Vertical coefficient of restitution = 0.769

Coefficient of sliding friction = μ = 0.55

Torsional stiffness coefficient = k_θ = 1000 lb-in/rad

Table C15. Dynamic parameters and simulation results

Cases	M_1	M_2	k_y	c_y	I_1	I_2	k_θ	V_{y2}	V_{x2}	ω_2	θ_2	t_c
	Lb-s^2/in	Lb-s^2/in	Lb/in	Lb-s/in	Lb-in-s^2	Lb-in-s^2	Lb-in/rad	m/s	m/s	Rad/s	Degrees	msec
1	M/2	M/2	72	0.026	0.352I	0.647I	0.00028	-5.265	13.798	-88.94	-15.814	4.783
2	M/2	M/2	80	0.0275	0.352I	0.647I	0.00028	-5.265	13.799	-88.74	-15.808	4.537
3	M/2	M/2	90	0.00633	0.352I	0.647I	0.00028	-5.268	13.494	-100.6	-16.139	4.248
4	2M/3	M/3	72	0.00728	0.532I	0.468I	0.00026	-5.267	12.614	95.18	-17.214	5.485
5	2M/3	M/3	80	0.00768	0.532I	0.468I	0.00026	-5.265	12.622	95.76	-17.191	5.204
6	2M/3	M/3	90	0.00815	0.532I	0.468I	0.00026	-5.263	12.614	96.46	-17.209	4.906
7	3M/4	M/4	90	0.00230	0.634I	0.366I	0.00025	-5.266	5.302	166.99	-36.386	5.517

2. 22 degrees angle of incidence

Fixed Inputs:

Incident horizontal velocity = V_{x1} =15.95 m/s

Incident vertical velocity = V_{y1} = 6.95 m/s

Incident spin velocity = ω_1 = -148.05 rad/s

Vertical coefficient of restitution = 0.799

Coefficient of sliding friction = μ = 0.55

Torsional stiffness coefficient = k_θ = 1000 lb-in/rad

Table C16. Dynamic parameters and simulation results

Cases	M_1	M_2	k_y	c_y	I_1	I_2	k_θ	V_{y2}	V_{x2}	ω_2	θ_2	t_c
	Lb-s^2/in	Lb-s^2/in	Lb/in	Lb-s/in	Lb-in-s^2	Lb-in-s^2	Lb-in/rad	m/s	m/s	Rad/s	Degrees	msec
1	M/2	M/2	72	0.026	0.352I	0.647I	0.00028	-3.908	12.86	-45.07	-22.264	4.783
2	M/2	M/2	80	0.0275	0.352I	0.647I	0.00028	-3.908	12.861	-44.81	-22.275	4.537
3	M/2	M/2	90	0.00633	0.352I	0.647I	0.00028	-3.907	12.466	-30.09	-22.905	4.248
4	2M/3	M/3	72	0.00728	0.532I	0.468I	0.00026	-3.905	11.324	194.01	-24.936	5.485
5	2M/3	M/3	80	0.00768	0.532I	0.468I	0.00026	-3.908	11.335	193.25	-24.906	5.204
6	2M/3	M/3	90	0.00815	0.532I	0.468I	0.00026	-3.905	11.324	195.44	-24.939	4.906
7	3M/4	M/4	90	0.00230	0.634I	0.366I	0.00025	-3.907	11.558	350.03	-24.495	5.517

3. 35 degrees angle of incidence

Fixed Inputs:

Incident horizontal velocity = V_{x1} =14.35 m/s

Incident vertical velocity = V_{y1} = 9.97 m/s

Incident spin velocity = ω_1 = -157.58 rad/s

Vertical coefficient of restitution = 0.711

Coefficient of sliding friction = μ = 0.55

Torsional stiffness coefficient = k_θ = 1000 lb-in/rad

Table C17. Dynamic parameters and simulation results

Cases	M_1	M_2	k_y	c_y	I_1	I_2	k_θ	V_{y2}	V_{x2}	ω_2	θ_2	t_c
	Lb-s^2/in	Lb-s^2/in	Lb/in	Lb-s/in	Lb-in-s^2	Lb-in-s^2	Lb-in/rad	m/s	m/s	Rad/s	Degrees	msec
1	M/2	M/2	72	0.026	0.352I	0.647I	0.00028	-7.087	9.675	-1.783	-36.223	4.783
2	M/2	M/2	80	0.0275	0.352I	0.647I	0.00028	-7.087	9.677	-1.386	-36.206	4.537
3	M/2	M/2	90	0.00633	0.352I	0.647I	0.00028	-7.084	9.611	20.875	-36.432	4.248
4	2M/3	M/3	72	0.00728	0.532I	0.468I	0.00026	-7.094	8.594	260.26	-39.523	5.485
5	2M/3	M/3	80	0.00768	0.532I	0.468I	0.00026	-7.09	8.595	260.29	-39.507	5.204
6	2M/3	M/3	90	0.00815	0.532I	0.468I	0.00026	-7.087	8.607	260.68	-39.48	4.906
7	3M/4	M/4	90	0.00230	0.634I	0.366I	0.00025	-7.09	10.027	303.65	-35.264	5.517

4. 40.5 degrees angle of incidence

Fixed Inputs:

Incident horizontal velocity = V_{x1} =13.8 m/s

Incident vertical velocity = V_{y1} = 11.78 m/s

Incident spin velocity = ω_1 = -179.12 rad/s

Vertical coefficient of restitution = 0.733

Coefficient of sliding friction = μ = 0.55

Torsional stiffness coefficient = k_θ = 1000 lb-in/rad

Table C18. Dynamic parameters and simulation results

Cases	M_1	M_2	k_y	c_y	I_1	I_2	I	V_{y2}	V_{x2}	ω_2	θ_2	t_c
	Lb-s^2/in	Lb-s^2/in	Lb/in	Lb-s/in	Lb-in-s^2	Lb-in-s^2	Lb-in- s^2	m/s	m/s	Rad/s	Degrees	msec
1	M/2	M/2	72	0.026	0.352I	0.647I	0.00028	-8.635	8.276	4.962	-46.216	4.783
2	M/2	M/2	80	0.0275	0.352I	0.647I	0.00028	-8.635	8.279	5.43	-46.189	4.537
3	M/2	M/2	90	0.00633	0.352I	0.647I	0.00028	-8.63	7.572	31.65	-48.763	4.248
4	2M/3	M/3	72	0.00728	0.532I	0.468I	0.00026	-8.638	7.893	239.05	-47.577	5.485
5	2M/3	M/3	80	0.00768	0.532I	0.468I	0.00026	-8.637	7.895	239.09	-47.579	5.204
6	2M/3	M/3	90	0.00815	0.532I	0.468I	0.00026	-8.64	7.838	237.37	-47.779	4.906
7	3M/4	M/4	90	0.00230	0.634I	0.366I	0.00025	-8.638	9.073	274.76	-43.593	5.517

5. 45 degrees angle of incidence

Fixed Inputs:

Incident horizontal velocity = V_{x1} =12.02 m/s

Incident vertical velocity = V_{y1} = 12.11 m/s

Incident spin velocity = ω_1 = -164.57 rad/s

Vertical coefficient of restitution = 0.749

Coefficient of sliding friction = μ = 0.55

Torsional stiffness coefficient = k_θ = 1000 lb-in/rad

Table C19. Dynamic parameters and simulation results

Cases	M_1	M_2	k_y	c_y	I_1	I_2	I	V_{y2}	V_{x2}	ω_2	θ_2	t_c
	Lb-s^2/in	Lb-s^2/in	Lb/in	Lb-s/in	Lb-in-s^2	Lb-in-s^2	Lb-in- s^2	m/s	m/s	Rad/s	Degrees	msec
1	M/2	M/2	72	0.026	0.352I	0.647I	0.00028	-9.074	6.342	24.668	-55.049	4.783
2	M/2	M/2	80	0.0275	0.352I	0.647I	0.00028	-9.074	6.344	25.15	-55.032	4.537
3	M/2	M/2	90	0.00633	0.352I	0.647I	0.00028	-9.071	5.617	52.104	-58.225	4.248
4	2M/3	M/3	72	0.00728	0.532I	0.468I	0.00026	-9.068	6.701	202.94	-53.548	5.485
5	2M/3	M/3	80	0.00768	0.532I	0.468I	0.00026	-9.072	6.704	203.04	-53.518	5.204
6	2M/3	M/3	90	0.00815	0.532I	0.468I	0.00026	-9.066	6.708	203.16	-53.523	4.906
7	3M/4	M/4	90	0.00230	0.634I	0.366I	0.00025	-9.073	7.853	237.82	-49.123	5.517

6. 59 degrees angle of incidence

Fixed Inputs:

Incident horizontal velocity = V_{x1} =9.12 m/s

Incident vertical velocity = V_{y1} = 15.04 m/s

Incident spin velocity = ω_1 = -184.04 rad/s

Vertical coefficient of restitution = 0.684

Coefficient of sliding friction = μ = 0.55

Torsional stiffness coefficient = k_θ = 1000 lb-in/rad

Table C20. Dynamic parameters and simulation results

Cases	M_1	M_2	k_y	c_y	I_1	I_2	I	V_{y2}	V_{x2}	ω_2	θ_2	t_c
	Lb-s^2/in	Lb-s^2/in	Lb/in	Lb-s/in	Lb-in-s^2	Lb-in-s^2	Lb-in- s^2	m/s	m/s	Rad/s	Degrees	msec
1	M/2	M/2	72	0.026	0.352I	0.647I	0.00028	-10.29	2.068	50.984	-78.635	4.783
2	M/2	M/2	80	0.0275	0.352I	0.647I	0.00028	-10.29	2.071	51.583	-78.622	4.537
3	M/2	M/2	90	0.00633	0.352I	0.647I	0.00028	-10.29	1.708	53.797	-80.572	4.248
4	2M/3	M/3	72	0.00728	0.532I	0.468I	0.00026	-10.29	4.111	124.51	-68.205	5.485
5	2M/3	M/3	80	0.00768	0.532I	0.468I	0.00026	-10.28	4.112	124.52	-68.208	5.204
6	2M/3	M/3	90	0.00815	0.532I	0.468I	0.00026	-10.29	4.112	124.52	-68.214	4.906
7	3M/4	M/4	90	0.00230	0.634I	0.366I	0.00025	-10.29	4.891	148.11	-64.573	5.517

7. 68 degrees angle of incidence

Fixed Inputs:

Incident horizontal velocity = V_{x1} =6.57 m/s

Incident vertical velocity = V_{y1} = 15.95 m/s

Incident spin velocity = ω_1 = -165.53 rad/s

Vertical coefficient of restitution = 0.679

Coefficient of sliding friction = μ = 0

Torsional stiffness coefficient = k_θ = 1000 lb-in/rad

Table C21. Dynamic parameters and simulation results

Cases	M_1	M_2	k_y	c_y	I_1	I_2	k_θ	V_{y2}	V_{x2}	ω_2	θ_2	t_c
	Lb-s^2/in	Lb-s^2/in	Lb/in	Lb-s/in	Lb-in-s^2	Lb-in-s^2	Lb-in/rad	m/s	m/s	Rad/s	Degrees	msec
1	M/2	M/2	72	0.026	0.352I	0.647I	0.00028	-10.83	0.76	23.02	-85.986	4.783
2	M/2	M/2	80	0.0275	0.352I	0.647I	0.00028	-10.83	0.767	23.226	-85.952	4.537
3	M/2	M/2	90	0.00633	0.352I	0.647I	0.00028	-10.84	0.685	20.748	-86.378	4.248
4	2M/3	M/3	72	0.00728	0.532I	0.468I	0.00026	-10.82	2.273	68.844	-78.150	5.485
5	2M/3	M/3	80	0.00768	0.532I	0.468I	0.00026	-10.83	2.272	68.8	-78.149	5.204
6	2M/3	M/3	90	0.00815	0.532I	0.468I	0.00026	-10.83	2.269	68.728	-78.161	4.906
7	3M/4	M/4	90	0.00230	0.634I	0.366I	0.00025	-10.82	2.734	82.803	-75.824	5.517

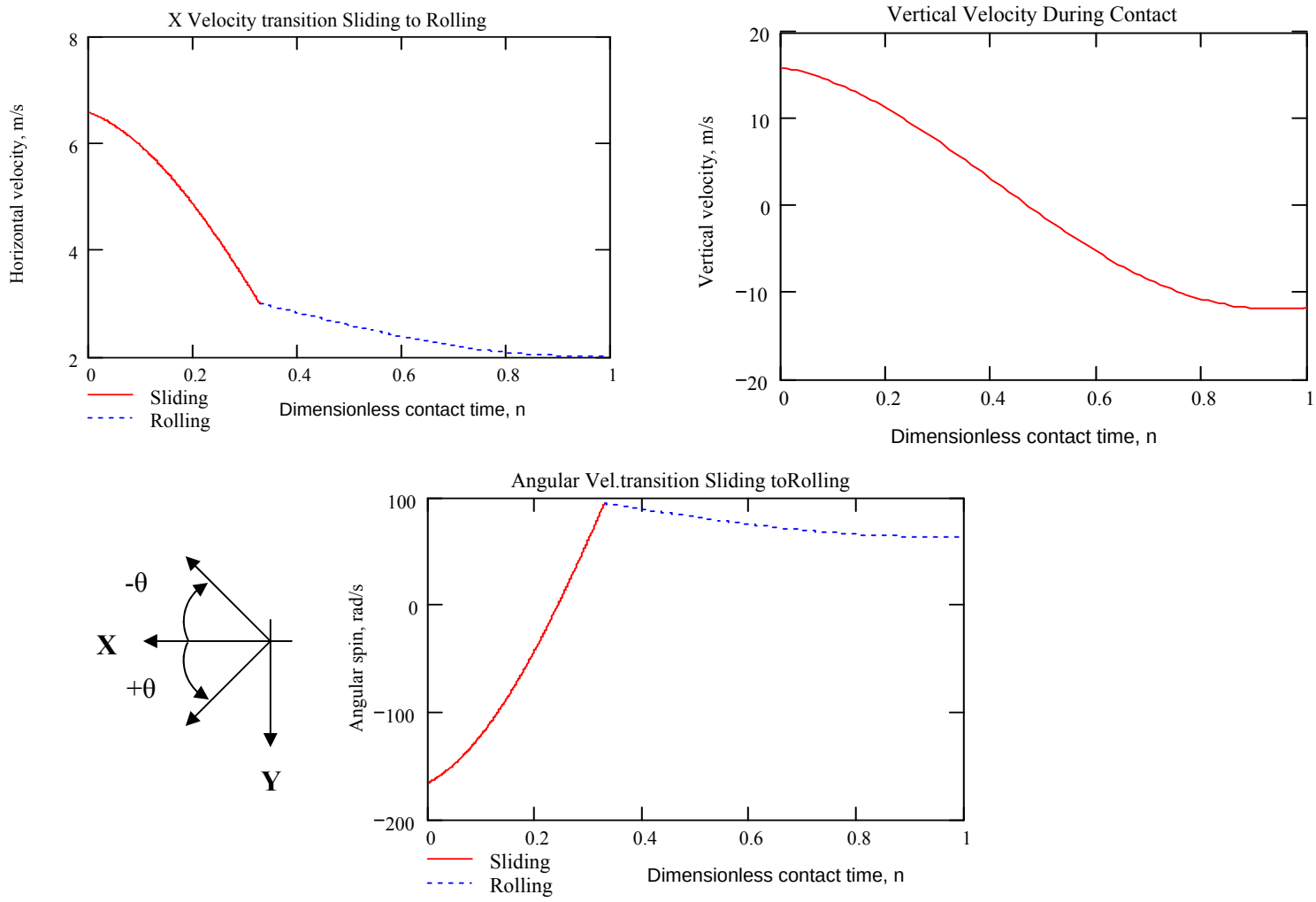

Fig.C3 Kinematic parameters and their variation with time during contact, case 6

APPENDIX D

ERROR ANALYSIS

A simple error analysis can be performed for each of the cases of zero spin, top spin and back spin whereby the percentage difference between the theoretically predicted rebound parameters and experimentally determined values of these parameters are obtained. These percentage differences, with experimental values as reference, are obtained for all three sets of dynamic parameters used to perform the simulations of the tennis ball, namely Case 1, Case 2, and Case 3, as presented in Chapter V. The comparison of percentage differences will also give an idea of how the selection of varying dynamic parameters in Cases 1, 2 and 3 affects the rebound parameters.

1. Zero Spin

Case 1

Table D1. Percentage error for different incident angles

Rebound Horizontal Velocity	**Rebound Angle**	**Rebound Angular Spin**
10.992	19.476	2.655
25.418	23.300	7.205
32.428	18.107	4.736
27.876	12.398	16.992
20.108	5.141	10.404
48.449	9.554	20.254
34.963	3.669	16.357

Case 2

Table D2. Percentage error for different incident angles

Rebound Horizontal Velocity	Rebound Angle	Rebound Angular Spin
10.974	19.464	2.829
24.423	22.762	9.509
32.480	18.132	4.778
27.903	12.411	17.017
22.009	5.927	12.151
48.372	9.537	20.189
34.781	3.642	16.196

Case 3

Table D3. Percentage error for different incident angles

Rebound Horizontal Velocity	Rebound Angle	Rebound Angular Spin
20.821	25.699	-69.115
41.380	31.064	-66.717
29.177	16.585	-48.017
10.869	4.288	-24.897
-5.100	6.184	-12.767
21.498	3.479	-1.583
14.635	0.516	0.034

2. Top Spin

Case 1

Table D4. Percentage error for different incident angles

Rebound Horizontal Velocity	Rebound Angle	Rebound Angular Spin
16.348	22.116	0.202
25.203	27.828	-1.327
21.627	17.481	9.791
10.010	1.807	12.860
20.916	8.337	19.980
17.895	1.679	20.044
-6.264	5.778	8.457

Case 2

Table D5. Percentage error for different incident angles

Rebound Horizontal Velocity	Rebound Angle	Rebound Angular Spin
16.348	22.116	-0.026
25.241	27.848	-1.295
22.104	17.735	10.229
10.010	1.807	12.857
20.890	8.325	19.958
17.804	1.649	19.959
-6.396	5.815	8.312

Case 3

Table D6. Percentage error for different incident angles

Rebound Horizontal Velocity	Rebound Angle	Rebound Angular Spin
24.918	27.147	-43.135
26.100	28.293	-34.418
6.155	8.426	-5.832
-3.640	6.944	-1.148
9.509	2.920	8.664
16.606	1.256	18.733
5.385	2.651	21.932

3. Back Spin

Case 1

Table D7. Percentage error for different incident angles

Rebound Horizontal Velocity	Rebound Angle	Rebound Angular Spin
19.526	19.175	-10.165
15.427	18.395	13.443
43.25	18.974	-0.474
47.295	18.331	14.416
62.718	19.334	15.943
46.335	7.035	16.601
44.713	3.343	-3.682

Case 2

Table D8. Percentage error for different incident angles

Rebound Horizontal Velocity	Rebound Angle	Rebound Angular Spin
19.451	19.127	-8.566
15.315	18.324	14.726
43.450	19.054	-0.331
46.231	17.975	13.590
62.815	19.359	16.015
46.335	7.035	16.605
44.522	3.326	-3.783

Case 3

Table D9. Percentage error for different incident angles

Rebound Horizontal Velocity	Rebound Angle	Rebound Angular Spin
30.663	25.736	-184.300
30.957	27.216	-126.457
61.250	25.616	-100.682
54.403	20.646	-97.625
53.932	17.019	-85.914
-26.406	6.126	-52.257
-51.592	5.574	-67.773

These results are presented in graphical form on next pages for each of the three incidences of zero spin, top spin and back spin.

Zero Spin

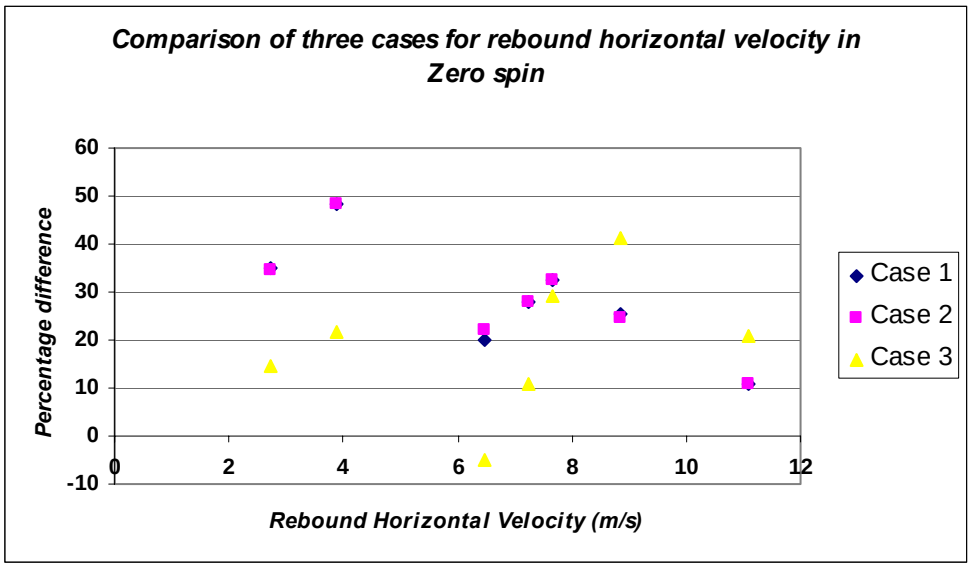
Comparison of three cases for rebound horizontal velocity in Zero spin
Percentage difference
60
50
40
30
20
10
0
-10
0
2
4
6
8
10
12
Rebound Horizontal Velocity (m/s)
Case 1
Case 2
Case 3

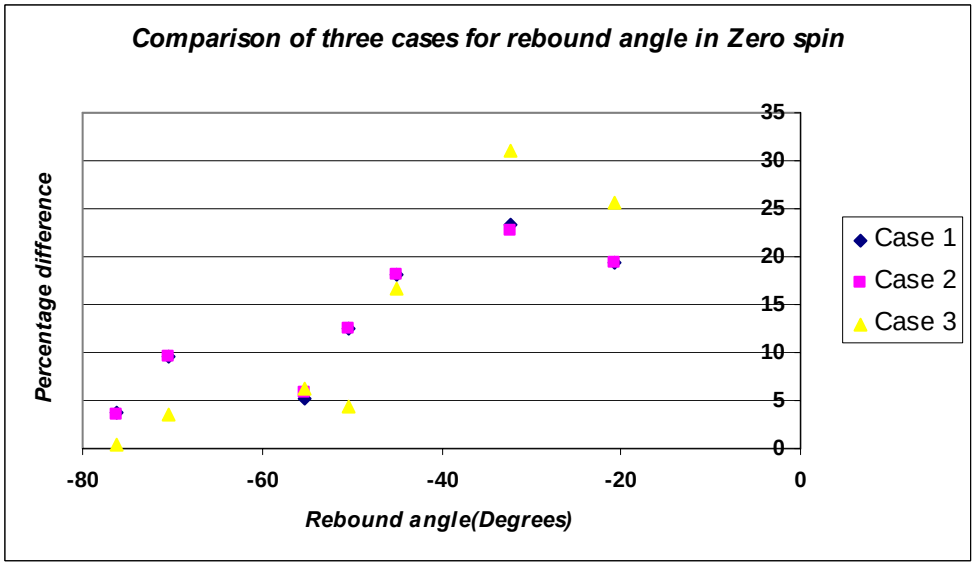
Comparison of three cases for rebound angle in Zero spin
Percentage difference
35
30
25
20
15
10
5
0
-80
-60
-40
-20
0
Rebound angle(Degrees)
Case 1
Case 2
Case 3

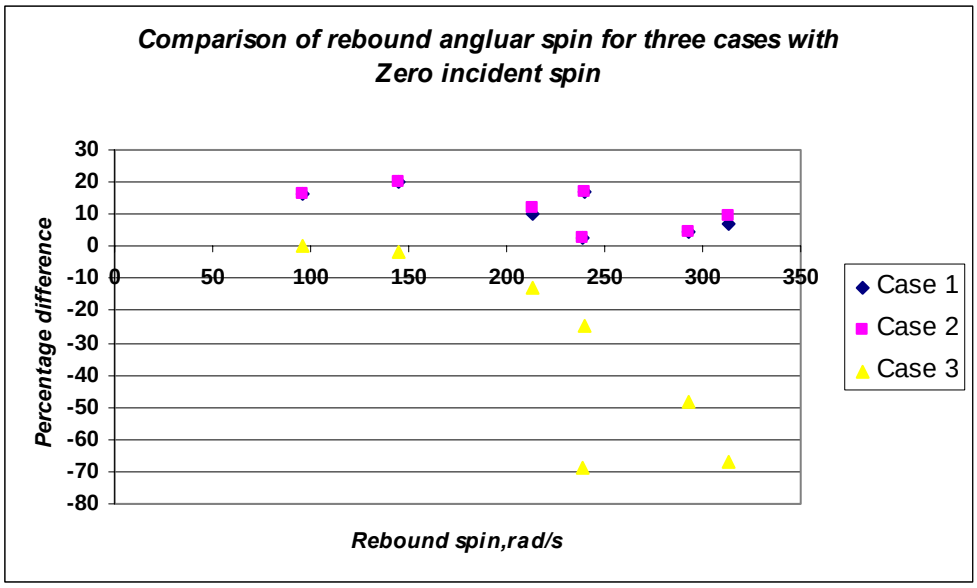
Comparison of rebound angluar spin for three cases with Zero incident spin
Percentage difference
30
20
10
0
-10
-20
-30
-40
-50
-60
-70
-80
0
50
100
150
200
250
300
350
Rebound spin,rad/s
Case 1
Case 2
Case 3

Top Spin

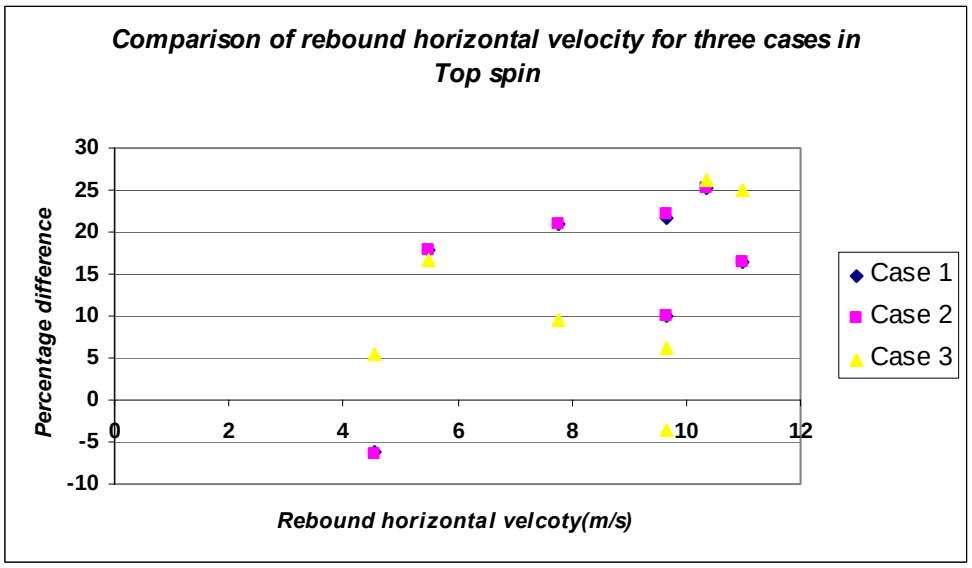
Comparison of rebound horizontal velocity for three cases in Top spin
Percentage difference
30
25
20
15
10
5
0
-5
-10
0
2
4
6
8
10
12
Rebound horizontal velcoty(m/s)
Case 1
Case 2
Case 3

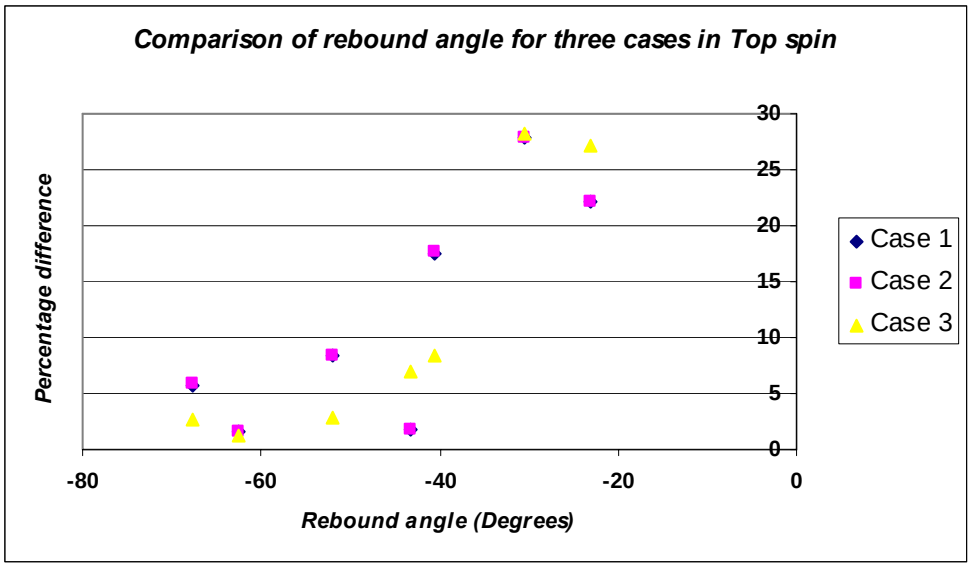
Comparison of rebound angle for three cases in Top spin
Percentage difference
30
25
20
15
10
5
0
-80
-60
-40
-20
0
Rebound angle (Degrees)
Case 1
Case 2
Case 3

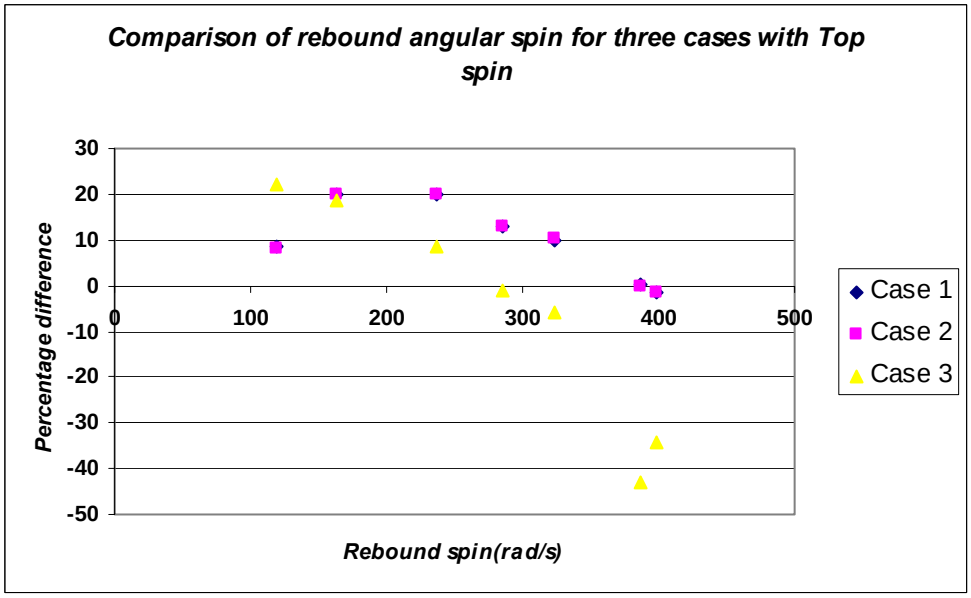
Comparison of rebound angular spin for three cases with Top spin
Percentage difference
30
20
10
0
-10
-20
-30
-40
-50
0
100
200
300
400
500
Rebound spin(rad/s)
Case 1
Case 2
Case 3

Back Spin

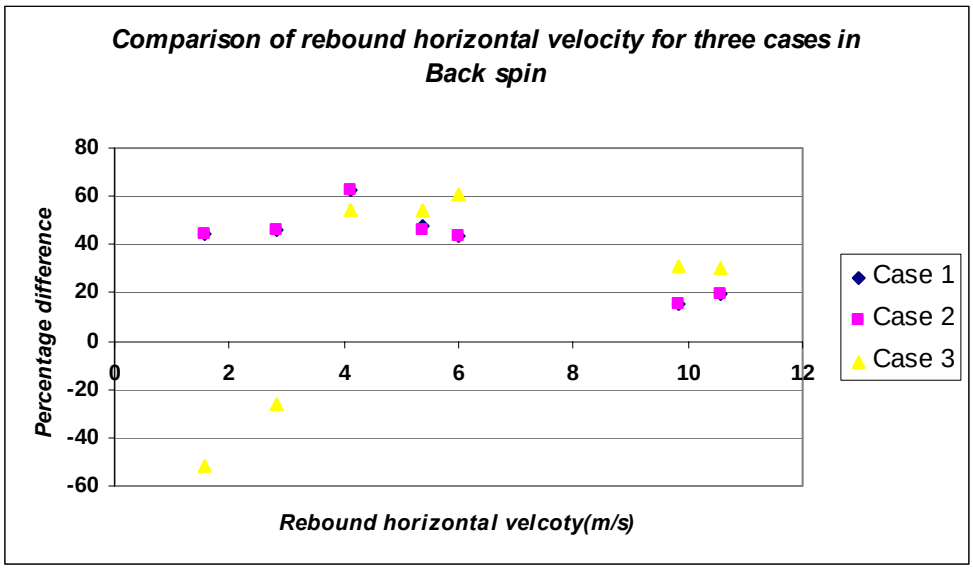
Comparison of rebound horizontal velocity for three cases in Back spin
Percentage difference
80
60
40
20
0
-20
-40
-60
0
2
4
6
8
10
12
Rebound horizontal velcoty(m/s)
Case 1
Case 2
Case 3

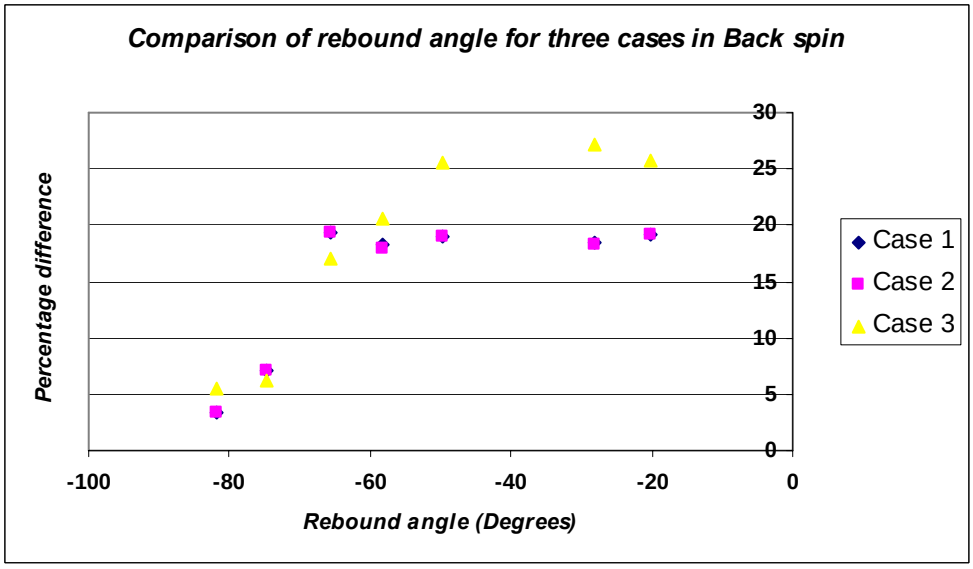
Comparison of rebound angle for three cases in Back spin
Percentage difference
30
25
20
15
10
5
0
-100
-80
-60
-40
-20
0
Rebound angle (Degrees)
Case 1
Case 2
Case 3

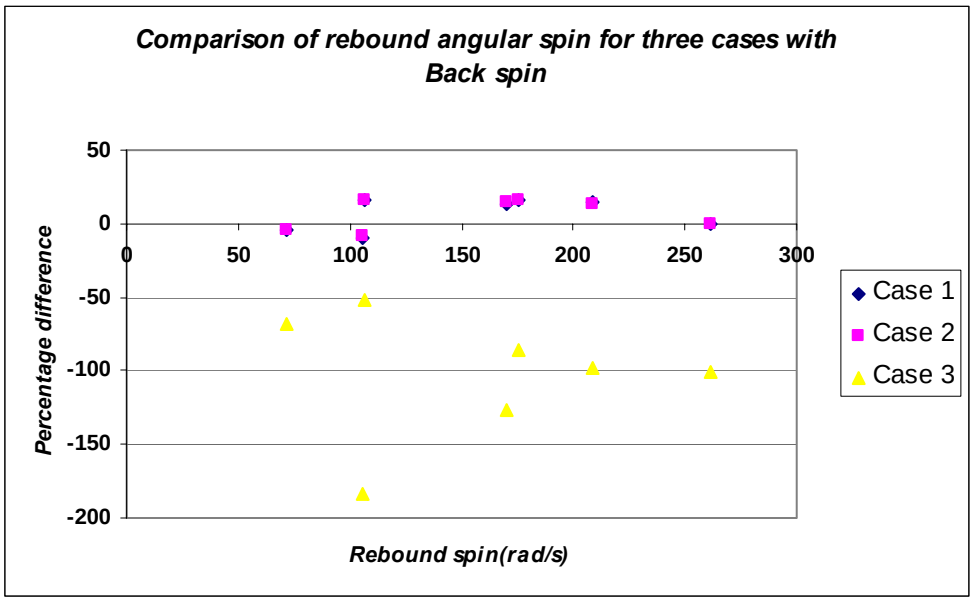
Comparison of rebound angular spin for three cases with Back spin
Percentage difference
50
0
-50
-100
-150
-200
0
50
100
150
200
250
300
Rebound spin(rad/s)
Case 1
Case 2
Case 3

VITA

Syed Muhammad Mohsin Jafri
B-311, Block-10, F.B. Area, Karachi, Pakistan

EDUCATION

Master of Science in Mechanical Engineering from Texas A&M University, College Station,USA(August 2000-May 2004)

Area of interest

Vibrations, Dynamics and Rotordynamics

Relevant courses

Engineering dynamics, Mechanical vibrations, Vibration measurements in rotating machinery and machine structures, Dynamics of rotating machinery, Methods of partial differential equations

Bachelor of Mechanical Engineering from NED University of Engineering & Technology, Karachi (February 1995-May 1999)

Final year design project

Design of liquified petroleum storage facility

Relevant courses

Engineering mechanics, Solid mechanics, Fluid mechanics, Stress analysis, Vibrations

PROFESSIONAL AFFILIATIONS

Member of Pakistan Engineering Council

CONTACT INFORMATION

E-mail: mjafri@neo.tamu.edu
Phone: (979)739-2220
Local Address: 4302 College Main, Apt.114
Bryan, TX 77801